T2R2 東京科学大学 リサーチリポジトリ
Science Tokyo Research Repository

論文 / 著書情報
Article / Book Information

題目(和文)	粉末X線結晶構造解析による有機結晶溶媒和/溶媒脱離転移挙動の解明
Title(English)	Solid-state solvation & desolvation process of organic crystals investigated by ab initio powder crystal structure analysis
著者(和文)	藤井孝太郎
Author(English)	Kotaro Fujii
出典(和文)	学位:博士(理学), 学位授与機関:東京工業大学, 報告番号:甲第7500号, 授与年月日:2009年3月31日, 学位の種別:課程博士, 審査員:
Citation(English)	Degree:Doctor (Science), Conferring organization: Tokyo Institute of Technology, Report number:甲第7500号, Conferred date:2009/3/31, Degree Type:Course doctor, Examiner:
学位種別(和文)	博士論文
Type(English)	Doctoral Thesis

Powered by T2R2 (Science Tokyo Research Repository)

2009 Doctoral Dissertation

Solid-State Solvation & Desolvation Process of Organic Crystals Investigated by *ab initio* Powder Crystal Structure Analysis

Kotaro Fujii

Department of Chemistry and Materials Science, Tokyo Institute of Technology

Acknowledgement

The author wishes to express his gratitude to Associate Professor Hidehiro Uekusa for his valuable guidance, helpful suggestion and continual discussion throughout the course of this study. The author also thanks to Emeritus Professor Yuji Ohashi, Associate Professor Tomoji Ozeki, Dr. Akiko Sekine, and the colleagues of research groups for their suggestions and encouragements. The author wishes to thank Professor Kenneth D. M. Harris, Professor Katsuhide Terada, and Associate Professor Etsuo Yonemochi for appropriate advises and suggestive discussions.

Finally, the author wishes to give a huge thanks to his parents for their affectionate encouragement.

December 2008
Kotaro FUJII

2009 DOCTORAL DISSERTATION

SOLID-STATE SOLVATION & DESOLVATION PROCESS OF ORGANIC CRYSTALS INVESTIGATED BY *AB INITIO* POWDER CRYSTAL STRUCTURE ANALYSIS

Chapter 1

General Introduction

1.1. Polymorph and Pseudopolymorph

1.1.1. Polymorphism and Properties

Many organic crystals are known to have alternative crystalline phases, polymorph and pseudopolymorph crystal, in which same compound has different crystal packing and molecular conformations. When the difference is only in the crystal packing and/or molecular conformations, it is called polymorph[(1)], and if the difference is due to the existence of solvent molecule in the crystal lattice, it is called solvates or pseudopolymorph[(2)]. The polymorphs and pseudopolymorphs attract a lot of interest, because they exhibit different solid-state properties, such as electric conductivity, magnetic property, photovoltaicity, photoconductivity, nonlinear optical activity, photochromic and thermochromic property, and photoreactivity.

For example, Moorthy and Venkatesan reported the different photoreactivity between two polymorphs of the 4-styrylcoumarin[(3)]. They found that the compound crystallize into two polymorphic forms, needles and prisms, and, interestingly, while the monoclinic form (needle, $P2_1/c$) undergoes stereospecific photodimerization producing *anti*-head-to-tail dimer across pyrone double bond, the triclinic form (prism, $P\bar{1}$) dimerizes to the *anti*-head-to-tail dimer across styrenic double bond(Figure 1-1). In addition, the reaction efficiencies are different between these two forms (almost 100% for needle form and 45-50% for prism form). The different photoreactivities can be explained by the crystal structures. In needle form crystal, as shown in Figure 1-1b, the nearest neighbor molecules are arranged in opposite direction and the pyrone double bonds are

the nearest reactive position. On the other hands, in prism form, there are two independent molecules in the asymmetric unit. One molecule is also arranged in opposite direction each other with the nearest double bonds of not pyrone but styrenic double bond (Figure 1-1c). However, there is no sufficiently near reactive double bonds for the other molecule and this can be considered as the reason of lower reaction efficiencies of prism form.

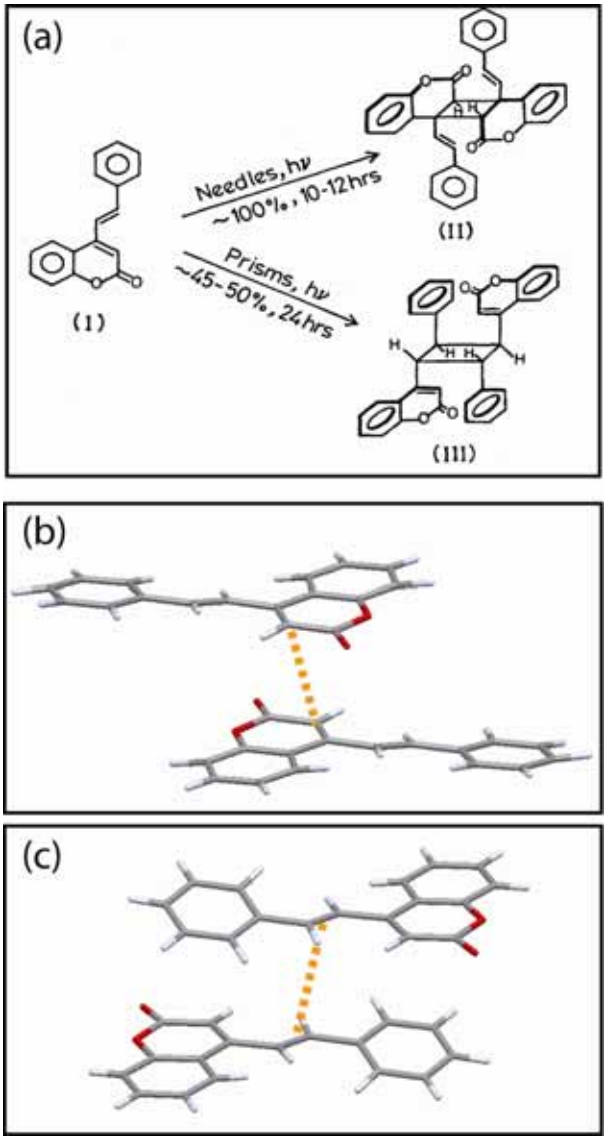

Figure 1-1 : (a) Different photoreactivities of two polymorphic forms of 4-styrylcoumarin. Nearest neighbor molecules which exist in the (b) needle form and (c) prism form. The orange dash lines show the reactive positions. [3]

Another good example can be seen in the field of pharmaceuticals. Shinzer *et al.* investigated the properties for polymorph form I and form III of premafloxacin which is well known quinolone antibiotic[4]. In this report, there are large difference on the moisture sorption property and the solubility. As shown in Figure 1-2, form I was found to absorb a water and transform to hydrate form at RH80%, whereas form III is stable for the moisture and it doesn't transform to hydrate form. In addition, the solubility of form I is measured as 3.23mg/ml which is about 23 times larger than that of form III (0.14 mg/ml). As can be seen in this example, polymorphs show large difference in their properties and these results show the importance of investigation of the polymorphs.

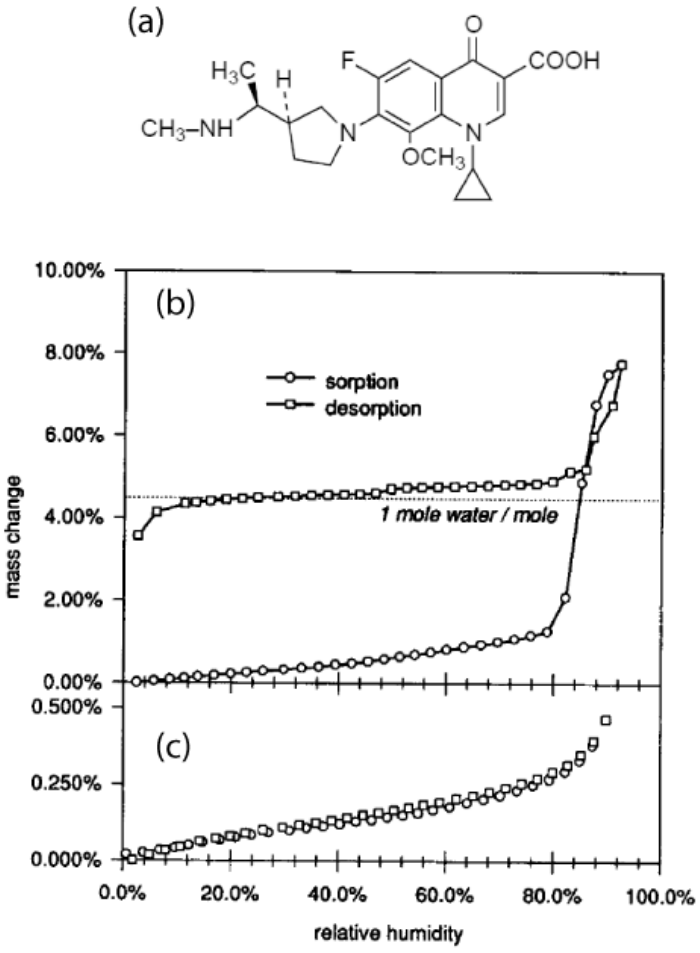

Figure 1-2 : (a) molecular structure of premafloxacin. Dynamic moisture sorption gravimetry of premafloxacin at 25.0 °C of (b) Form I and (c) Form III.[4]

As shown in the second example, the considerable awareness of polymorphism and/or pseudopolymorphism (mostly about the hydrates), is seen in the field of pharmaceuticals. Further examples which focused on the pharmaceutical polymorphism and/or pseudopolymorphism and the interests are summarized in the books and reviews[1), 5)-7)].

1.1.2. Polymorphic Transformation and Pseudopolymorphic Transformation

Another important feature of the polymorphism and pseudopolymorphism is a transformation between them. Generally, these alternative crystalline phases (polymorphs and pseudopolymorphs) are often known to undergo transformations among these phases induced by the change of environment. For example, thermal phase transformation[8)-12)], which usually accompanied by the changes of the molecular conformations and/or molecular packing arrangement, mechanically induced phase transformation[13)], thermal desolvation[14)-16)], solvent (guest) exchanges or solvation induced by the change of humidity condition[17)-23)] are known. Because the resultant crystalline phase by the transformations usually possesses the different solid-state properties, as described above, there are several reports which focused on the relationship between the transform and the properties. For example, Bashkirava *et al.* found the color change was caused by the transformation from β form (orange) to γ form (yellow) of N-(4'-methoxy-phenyl)-3-bromothiobenzamide polymorphs and they concluded that the color difference was comes from the conformational change in the transformation[24)]. Yamamura showed the dielectric property change caused by the transformation for tetramethylammonium and *o*-phenylenebis organic salt[25)]. Interestingly, the low temperature form does not exhibit the dielectric response, the high temperature form exhibits the extensive dielectric response.

The recent interesting example is that the racemic crystal transforms to the conglomerate crystals. The phenomena was first reported by Yoshizawa *et al.*[26)]. They found that the racemic complex of binaphtol and tetramethylammonium chloride undergoes the spontaneous chiral separation and gave the mixture of chiral crystals which is so-called conglomerate by heating or by exposure to the methanol vapor(Figure 1-3a). After his repot, Van Eupen *et al.* reported the similar racemic to conglomerate transformation by heating for

venlafaxine[27](Figure 1-3b). As can be seen in these examples, such a racemic to conglomerate transformation is noteworthy because it has a potential for an application to the chiral separation technique.

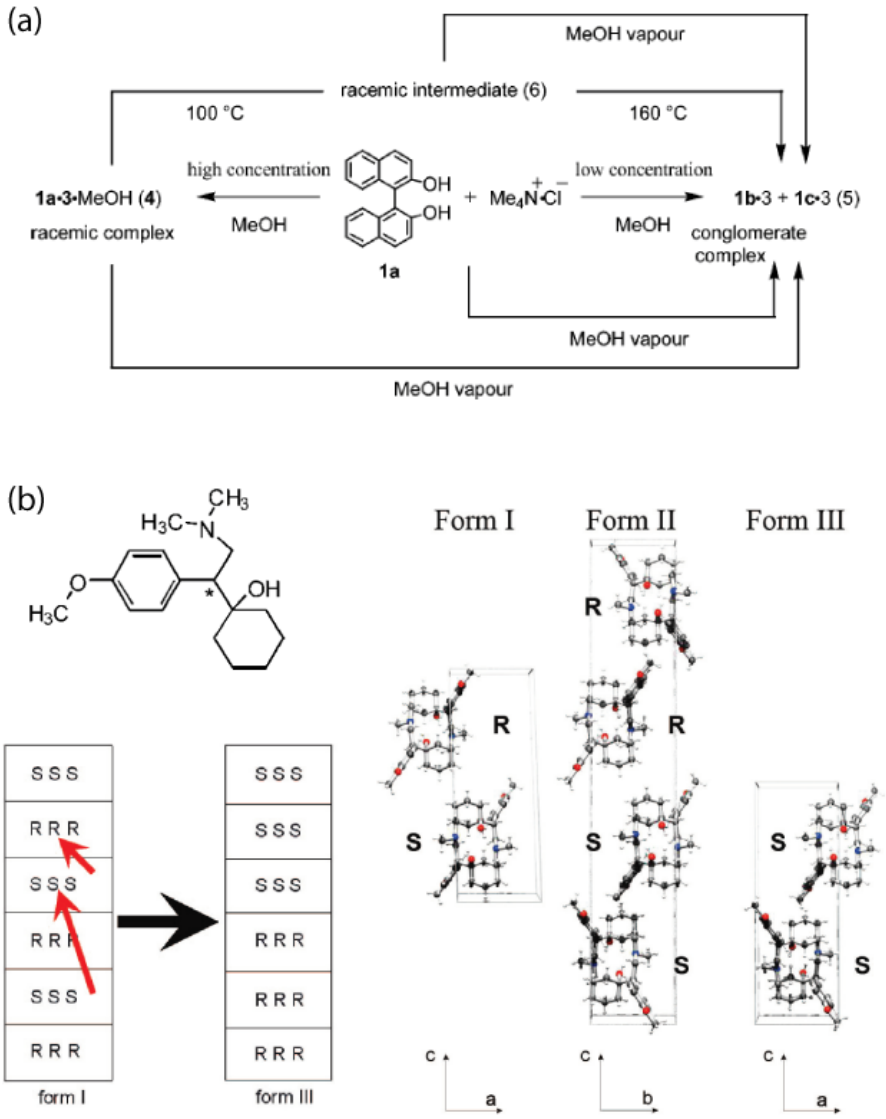

Figure 1-3 : The examples of the transformation from racemic crystal to conglomerate crystals. (a) The racemic inclusion crystal **4** of binaphtol and tetramethylammonium chloride undergoes the transformation by heating or methanol vapor and gave the conglomerate crystal **5**. [26] (b) The racemic venlafaxine form I undergoes the racemic to conglomerate tranfromation which give chiral form III. [27]

Other examples of the polymorph transformations are well reported in the field of pharmaceuticals, such as physical transformations of active pharmaceutical ingredients during manufacturing processes[7], solution-mediated polymorphic phase transformation[28], pressure and thermal effect on the pharmaceutical hydrates[29] and dehydration process studied by IR spectra[30][31], X-ray powder diffraction[32]-[35] and single crystal structure analyses[36]-[40].

1.1.3. Problem in Study of Polymorphic Transformation and Pseudopolymorphic Transformation

Many techniques were used for understanding the transformation mechanism and/or the properties of the resultant forms. Among them, single crystal structure analysis acted very important role in such studies. The technique to determine the crystal structures from single crystal diffraction data provides the three dimensional information (molecular structure and molecular arrangement), thus the technique acted an important role in several literatures shown above. However, unfortunately, most transformations accompanied by disintegration of single crystal, and in such cases, the technique to solve the crystal structures from single crystal diffraction cannot be applied. Especially, the pseudopolymorphic transformations (desolvation and solvation) are not sufficiently studied because it generally accompanied by large structural changes which caused by the solvent release and/or sorption (Figure 1-4). Thus, systematic studies of the pseudopolymorphic transformations have not sufficiently been achieved until today. In this context, the technique to determine the crystal structures of polycrystalline forms is the key problem for understanding the pseudopolymorphic transformations. Recently, the technique to determine the crystal structures from powder diffraction data has been dramatically developed and it has a potential to solve the problem that *" the difficulty to determine the crystal structures of transformed phases "*.

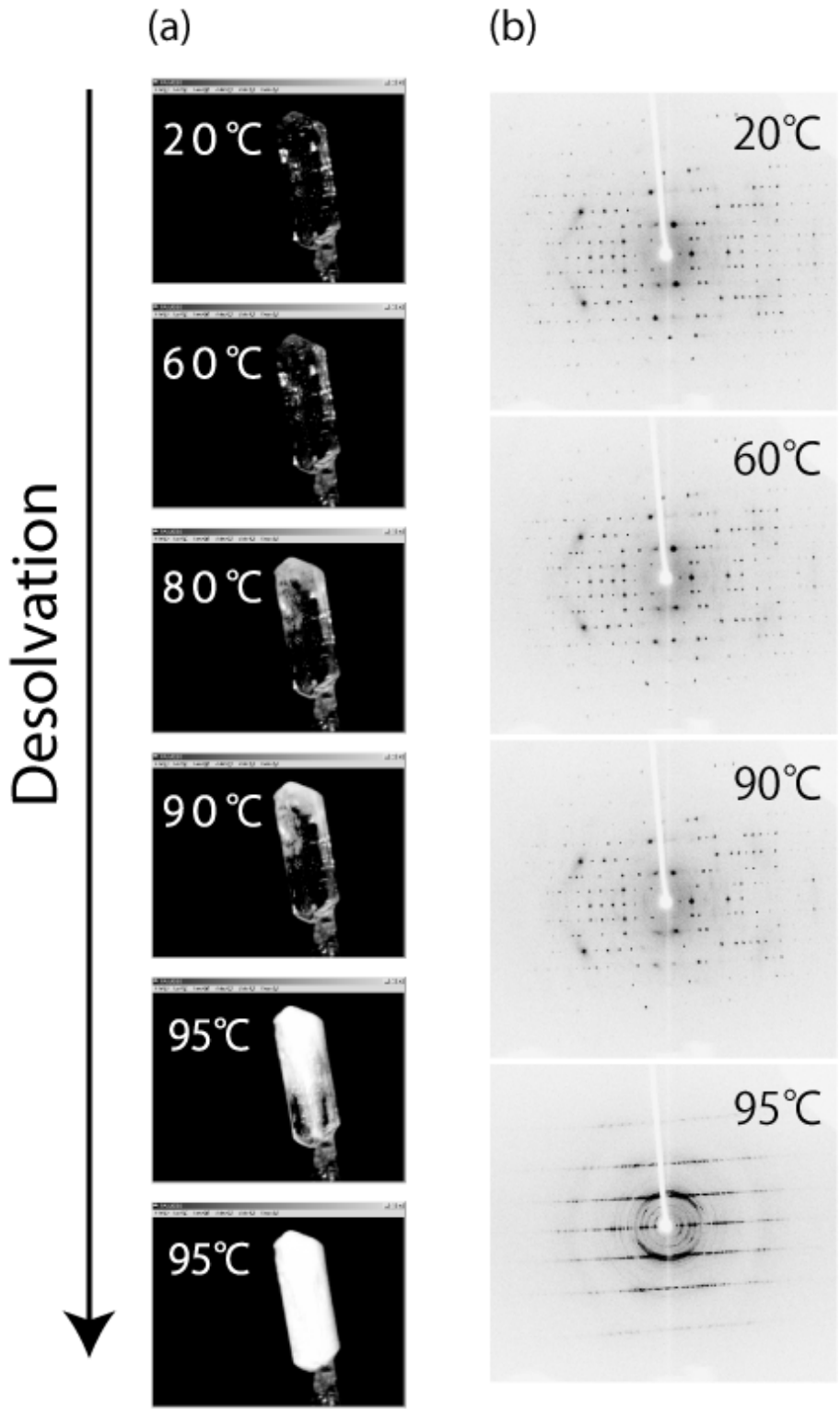

Figure 1-4 : The example of desolvation accompanied the disintegration of single crystal. (a) shows the disintegration by desolvation induced by temperature increasing, and (b) shows the diffraction pattern change.

1.2. Crystal structure analysis from powder X-ray diffraction data

1.2.1. Powder X-ray diffraction

The powder diffraction measurements are traditionally widely used in many fields. It can be easily measured and can use for phase characterization. For some inorganic materials, the powder diffraction data were used to analyze the crystal structures by using direct method and/or Rietveld structural refinement, however, traditionally, it was not applied to the organic crystals. Because, generally, organic crystalline materials have worse crystallinity and lower symmetry than those of inorganic materials, the powder diffraction patterns of organic crystalline materials have broad and extremely overlapped peaks and, thus, it is difficult to extract accurate intensity data for the crystal structure analysis.

On the other hands, recently, several techniques to determine the organic crystal structures from powder X-ray diffraction are developed. The key technology which enable to solve the organic crystal structures are the improvement of the X-ray source, the calculation ability of computers and the development of the crystal structure determination calculation methodology. Because the powder diffraction data have only one dimensional diffraction information which is considered as the collapse of the three dimensional crystallographic information such as the single crystal diffraction data(see Figure 1-5). Thus the structure determination from powder diffraction data is much more difficult than from single crystal data and the same techniques of single crystal analysis are usually failed in the powder diffraction analysis. Therefore, the unique techniques to analyze the powder diffraction data have long been developed.

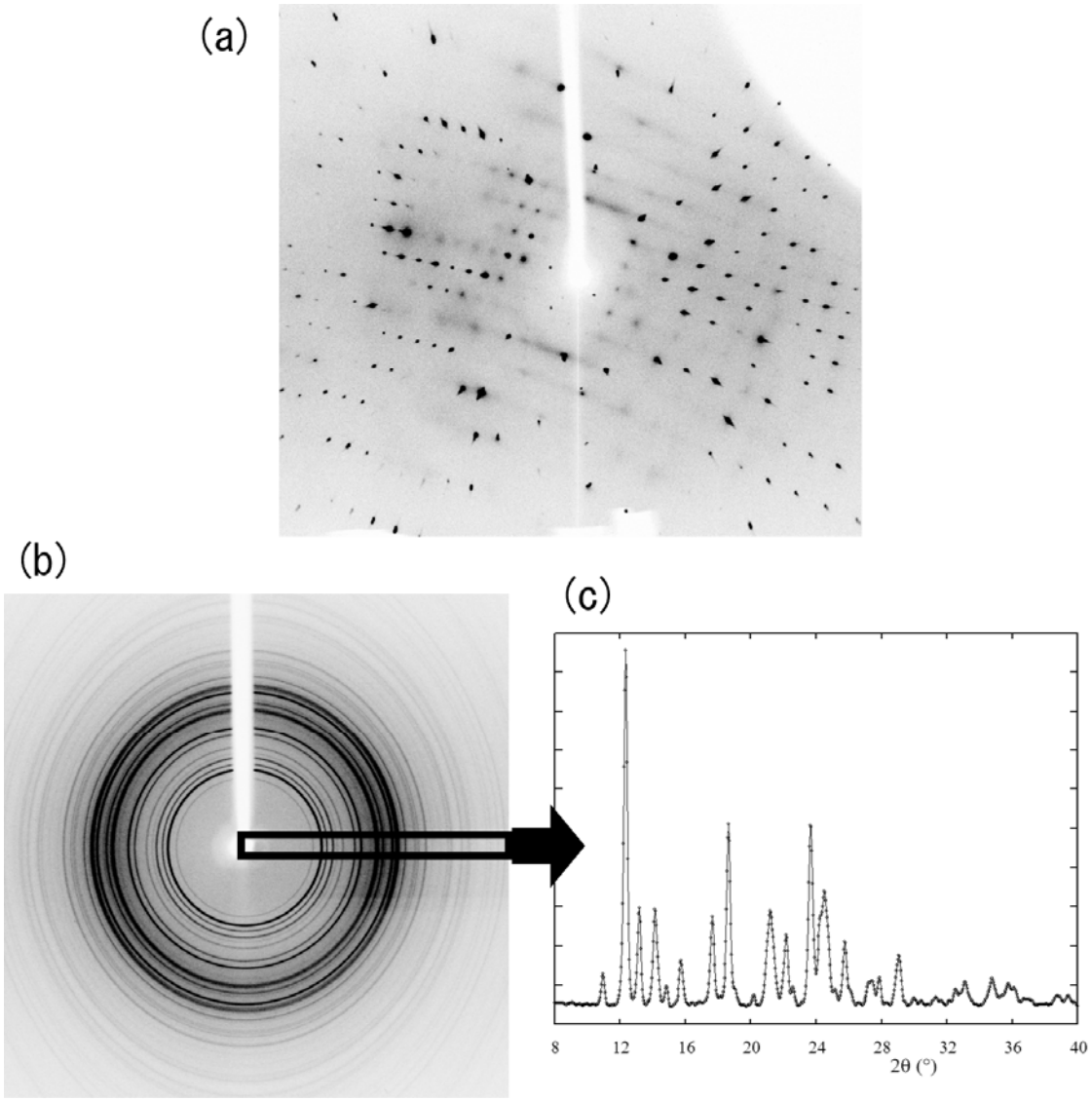

Figure 1-5 : Diffraction Images from (a) Single Crystal and (b) Crystalline Powder. (c) Powder X-ray Diffraction pattern.

1.2.2. Indexing

The most important procedure is the indexing, because the determined unit cell parameters are most important crystallographic information and are necessary for the subsequent structure analysis procedures. Generally, the indexing of powder diffraction data is carried out using peak positions which were detected from the experimental powder patterns. The following three programs are most famous and widely used for powder diffraction indexing; the program ITO[41] which is based on the zone-finding procedure[42]; the program TREOR[43][44] which adopted the trial-and-error indexing; the program DICVOL[45]-[49] in which the cell parameters are exhaustively explored the specified unit cell space. The success rate of these programs to give the correct solution is very high if the precise peak positions are inputted. However it is usually difficult to obtain the precise peak positions from powder diffraction data, especially for the organic crystals, because of the peak overlaps, impurity peaks, and the systematic errors such as zero position error, sample positional error. Thus, recent indexing programs were written to improve the treatment of such peak overlap effect, impurity peaks, and systematic errors. For example, program DICVOL incorporated the technique to estimate the zero positional error, which is called reflection-pair method[50]. The recent notable programs such as the program TOPAS[51] which is based on the trial-and-error technique, McMaille[52] which adopted the genetic algorithm indexing, X-Cell[53] which is based on dichotomy method as well as DICVOL, also consider the existence of the peak position errors and the existence of impurity peaks in order to gain the success rate of indexing calculation.

1.2.3. Rietveld Method (Crystal Structure Refinement)

The most famous and widely used original method in the powder diffraction analysis is Rietveld method. The crystal structure refinement is usually carried out using integrated intensities in a single crystal diffraction analysis. However, it has problem to apply to the powder diffraction data, because of the difficulty to estimate the precise integrated intensity from extremely overlapped powder diffraction pattern. In this context, Rietveld proposed in 1969 the technique to refine the crystal structure using whole profile patterns (which means one profile

point is considered as a one data instead of integrated intensity)[55]. The advantage of this technique is that this technique does not require the extraction of the integrated intensity prior to the refinement.

The powder diffraction pattern of the structural model is calculated using the following information: (1) lattice parameters (peak positions); (2) atomic positions and atomic displacement parameters (peak intensities); (3) 2θ-dependent analytical functions to describe the peak shapes and peak widths; (4) a description of the background intensity. In the least-square refinement process, not only the crystal structure parameters such as atomic positions or atomic displacement parameters, but also the profile shape and the background parameters are refined.

Actually, the first proposal of Rietveld was applied to analyze the neutron powder diffraction data. However, now the technique was applied to not only to neutron but also to X-ray powder diffraction data[56], and many Rietveld method software were developed [57]-[63]. Also, this technique is recently used for organic crystal structure refinement and most of recent *ab initio* powder diffraction analysis carried out the Rietveld refinement as the final procedure of powder diffraction analysis.

Usually, the goodness of the refinement is judged by reliable factors as shown in Table 1-1. The most important R factor is R_{wp} because in the Rietveld refinement the parameters are refined to reduce this value. The lowest R_{wp} is different for the measurement conditions and/or the compounds, because the R_{wp} is not determined only by the crystal structure but also it is affected by the peak shape, backgroud level. Thus, the value of R_{wp} given by Rietveld refinement should be compared with the value which is obtained by pattern decomposition, because the R_{wp} given by pattern decomposition is the theoretically lowest value. If the R_{wp} given by Rietveld refinement is near to the value given by pattern decomposition such as Le Bail method and Pawley method(which is described in the next section), the crystal structure would be correctly analyzed.

$$R_F = \frac{\sum |(I_K(\text{'obs'}))^{1/2} - (I_K(\text{calc})^{1/2})|}{\sum (I_K(\text{'obs'}))^{1/2}} \qquad (\text{'}R\text{-structure factor'})$$

$$R_B = \frac{\sum |I_K(\text{'obs'}) - I_K(\text{calc})|}{\sum I_K(\text{'obs'})} \qquad (\text{'}R\text{-Bragg factor'})$$

$$R_p = \frac{\sum |y_i(\text{obs}) - y_i(\text{calc})|}{\sum y_i(\text{obs})} \qquad (\text{'}R\text{-pattern'})$$

$$R_{wp} = \left\{ \frac{\sum w_i (y_i(\text{obs}) - y_i(\text{calc}))^2}{\sum w_i (y_i(\text{obs}))^2} \right\}^{1/2} \qquad (\text{'}R\text{-weighted pattern'})$$

Here I_K is the intensity assigned to the Kth Bragg reflection at the end of the refinement cycles. In the expressions for R_F and R_B the 'obs' (for observed) is put in quotation marks because the Bragg intensity, I_K, is rarely observed directly; instead the I_K values are obtained from programmatic allocation of the total observed intensity in a 'scramble' of overlapped reflections to the individual reflections, according to the ratios of those reflection intensities in the calculated pattern.

The '*Goodness-of-fit*' indicator, S, is

$$S = [S_y/(N - P)]^{1/2} = R_{wp}/R_e$$

where

$$R_e = \text{'}R\text{-expected'} = [(N - P)/\sum w_i y_{oi}^2]^{1/2}.$$

Table 1-1 : Some often-used reliable factors. (R. A. Young, *The Rietveld Method*, **1993**,Oxford Univ. Press).

1.2.4. Pattern Decomposition

In the structure analysis, the powder diffraction pattern is decomposed into the individual reflection using pattern decomposition technique, in order to estimate the integrated intensities and/or estimate the profile parameters of the powder diffraction pattern. The obtained information, such as integrated intensities, profile parameters and unit cell parameters, is used in the subsequent analysis such as structure solution procedure or in the Rietveld structural refinement.

The most commonly used "pattern decomposition" techniques are based on the use of Rietveld method in which the whole powder diffraction pattern is decomposed in one step. These techniques adopt a least-squares approach to fit a calculated profile and the experimental powder diffraction pattern by refinement of the lattice parameters, the zero-point error, the peak profile parameters, and the background parameters. Two methodologies are proposed for handling the integrated intensities. One is proposed by Pawley that is the integrated intensities are also treated as refinement parameters and the integrated intensities are determined from least-square fitting[(64)(65)]. However, this "Pawley method" is usually unstable in the refinement procedure, because of the higher correlation between the integrated intensities of the overlapped reflections and because the refined parameters become great number according to the number of reflections. Thus, Le Bail proposed another method in which the integrated intensities are not treated as parameters[(66)]. This method called "Le Bail method" is succeeded to stabilize the refinement and is now used in many programs. Usually, these techniques have similar routine with Rietveld method, thus, these techniques are also incorporated in a Rietveld method softwares which showed in the foregoing section[(57)-(63)].

1.2.5. Crystal Structure Determination

If the decomposition of powder diffraction pattern has succeeded, one can apply the Patterson method or direct method to determine the crystal structure. In 1992, Giaccovazzo and his co-worker reported a software of direct method which was optimized to the powder diffraction data by considering the peak over lap effect and by special treatment of weak reflection intensities[(67)]. Further

investigations to determine the crystal structures from powder diffraction data were carried out by same group[68]-[79] and this technique has incorporated into program EXPO package which consists of indexing, intensity extraction, structure determination by direct method and Rietveld refinement[80]-[82]. However, the technique of a direct method itself is not sufficiently effective for the structure determination of organic crystal structure and it was failed in many cases, therefore, the group incorporates the concept of the direct space strategy into the software and is combined with direct method [83]-[88].

The direct space strategy acted a most important role in the recent development of organic crystal structure analysis from powder diffraction data. In the direct-space method for solving crystal structures from powder diffraction data, trial crystal structures are generated in direct space(also it can be called real space). The trial structure is compared directly between the powder diffraction pattern calculated for the trial structure and the experimental powder diffraction pattern and the goodness of the structure is calculated using a reliable factor such as R_{wp}, R_p, R_I. The direct space strategy for structure solution aims to find the trial crystal structure that has the lowest possible R factor, and the approach is equivalent to exploring R factor hypersurface to find the global minimum on the hypersurface (Figure 1-6a). The parameters are traditionally considered as atom coordinates, however, if considering all atoms in the unit cell, the number of parameters extremely increase and it makes difficult to solve the crystal structures. Thus, in a recent direct space strategy, only torsional freedoms are permit to the molecules which exist in the crystal lattice and the other parameters are constrained to the reference values (this means there is no freedom for the bond length and angle). By using of this kind of rigid molecules model, the crystal structure is expressed in following parameters; positional parameters of molecule (x, y, z), orientational parameters of molecule (θ, ϕ, ψ) and torsional parameters of rigid molecule (τ_1, τ_2, τ_3, …), thus, the problem to determine the crystal structure can be converted to the problem to determine these parameters.

The most straightforward way to determine these parameters, which can explain the experimental powder diffraction pattern, is exhaustive search of R factor hypersurface. The method is called grid search method(GS). In GS technique the parameter space is split into grid and all grid points are searched exhaustively. This technique is incorporated into program Organa[89]. Because

GS is the exhaustive search technique, it is most certain way to explore the crystal structure. However, it requires a lot of time to calculate the whole hypersurface, thus, it is not suitable for a crystal structures which have a large number of parameters should be determined.

The alternative technique to determine the parameter set is the global optimization method. In the global optimization method, the parameters which achieve the lower *R* factor is considered as the more optimal parameter set and the parameters are optimized for it. As the optimization method, three following techniques were used in the powder diffraction analysis. Monte-Carlo method(MC): a new trial structure is generated randomly around the present parameter set and if the new model has lower *R* factor, the model is accepted and if the new model has higher *R* factor, parameters are accepted stochastically. The program ESPIOR[(90)] is known to adopt MC strategy. Simulated Annealing method(SA): the main strategy is the similar to that of MC but the stochastic tolerance to accept the new trial structure is decrease in proportion to the number of movement. This strategy can be considered as the similar process of annealing process of metal, thus, this method is called simulated annealing method. The program DASH[(91)], TOPAS[(92)], FOX[(93)] and PSSP[(94)] are known to adopt SA for solving the crystal structure. Genetic Algorithm method(GA): the parameter sets (the number of parameter sets are called population) are optimized by mating(parameter exchange), mutation(random movement), and selection(only suitable parameter sets remains in the next generation) (Figure 1-6b). The direct space GA technique is incorporated in the program EAGER[(95)-(100)]. These techniques (MC, SA, GA) are good match nicely with the problem to determine the crystal structure from powder diffraction data, thus, the programs, as shown above, gave the number of successes in determination of the organic crystal structures.

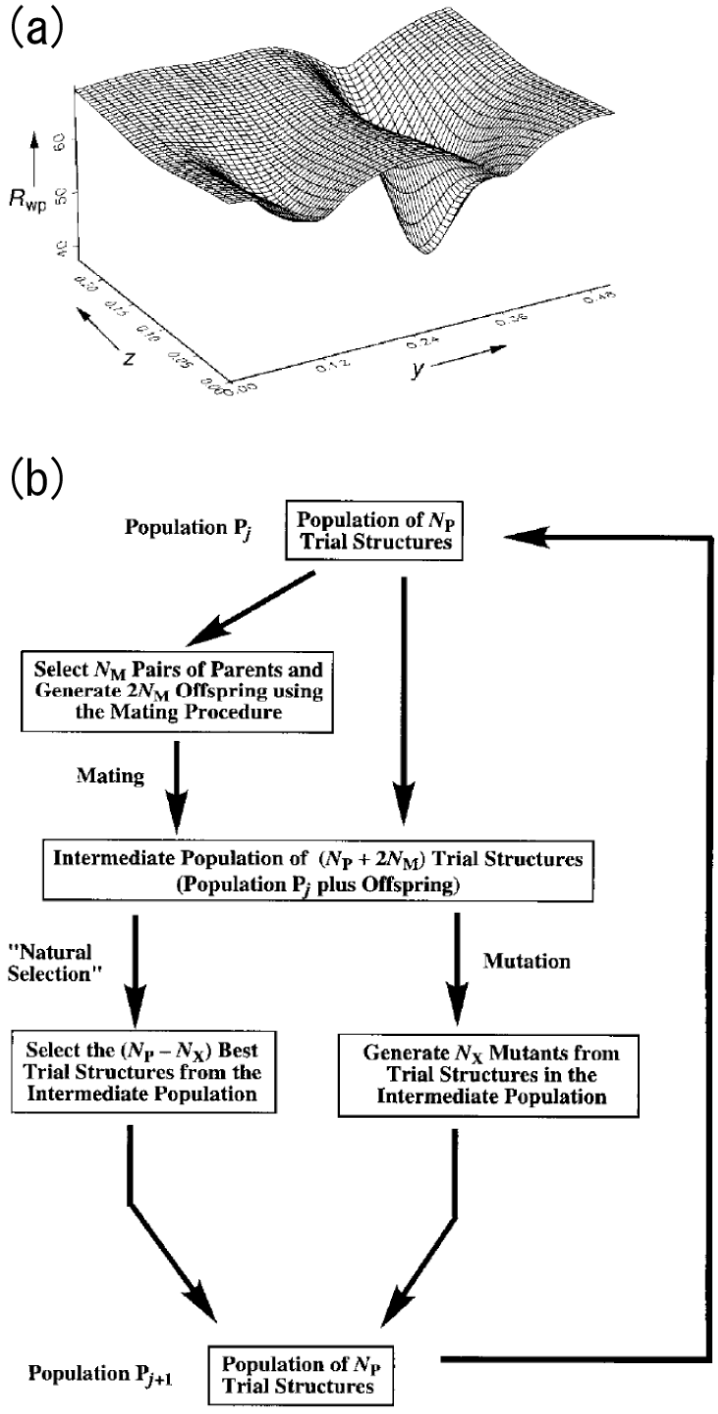

Figure 1-6 (a) A two-dimensional section through the Rwp hypersurface for lithium zirconate (Li6Zr2O7). (b) Flow chart representing the evolution of the population from one generation (population Pj) to the next generation (population Pj+1) in the genetic algorithm for powder structure solution. K. D. M. Harris, *et. al. Angew. Chem. Int. Ed.* 2001, 40, 1626- 1651.

1.2.6. Practical Examples of *ab initio* Powder Crystal Structure Analysis

The direct space crystal structure determination successfully boosted the possibilities to determine and analyze the unknown organic crystal structure from powder diffraction data, which is generally called "*ab initio* crystal structure determination from powder diffraction data". This technique has been applied to several situations such as difficult to obtain single crystals by recrystallization[(101)-(114)], the phase could obtain only by polymorphic transformations[(115)(116)], and the phase obtained by solid-state grinding[(117)(118)]. Figure 1-7 shows some examples. From small simple molecule (such as trithiocyanuric) to complex organic salt (such as melaminium dihydrogenpyrophosphate), the crystal structures have been successfully determined from powder diffraction data.

Also, there are some examples that the crystal structures of the desolvated crystalline phases have been determined from powder diffraction data. Platteau reported the crystal structures of hygroscopic and stable anhydrous forms of α-lactose which were determined from powder X-ray diffraction data. They revealed that the instability of hydroscopic anhydrous form comes from the destruction of hydrogen bonds which exists in the hydrate form[(120)(121)]. Other unstable unsolvated examples were reported by Guo *et al.*. In their studies, the crystal structures of unsolvated trithiocyanuric acid benzene-1,2,3-tricarboxylic acid were determined from powder X-ray diffraction data. All these studies are important because such transformed phases are impossible to solve the crystal structure by conventional single diffraction method and *ab initio* powder crystal structure analysis is necessary for revealing these crystal structures. However, it is regret that all these studies did not discuss the transformation mechanisms.

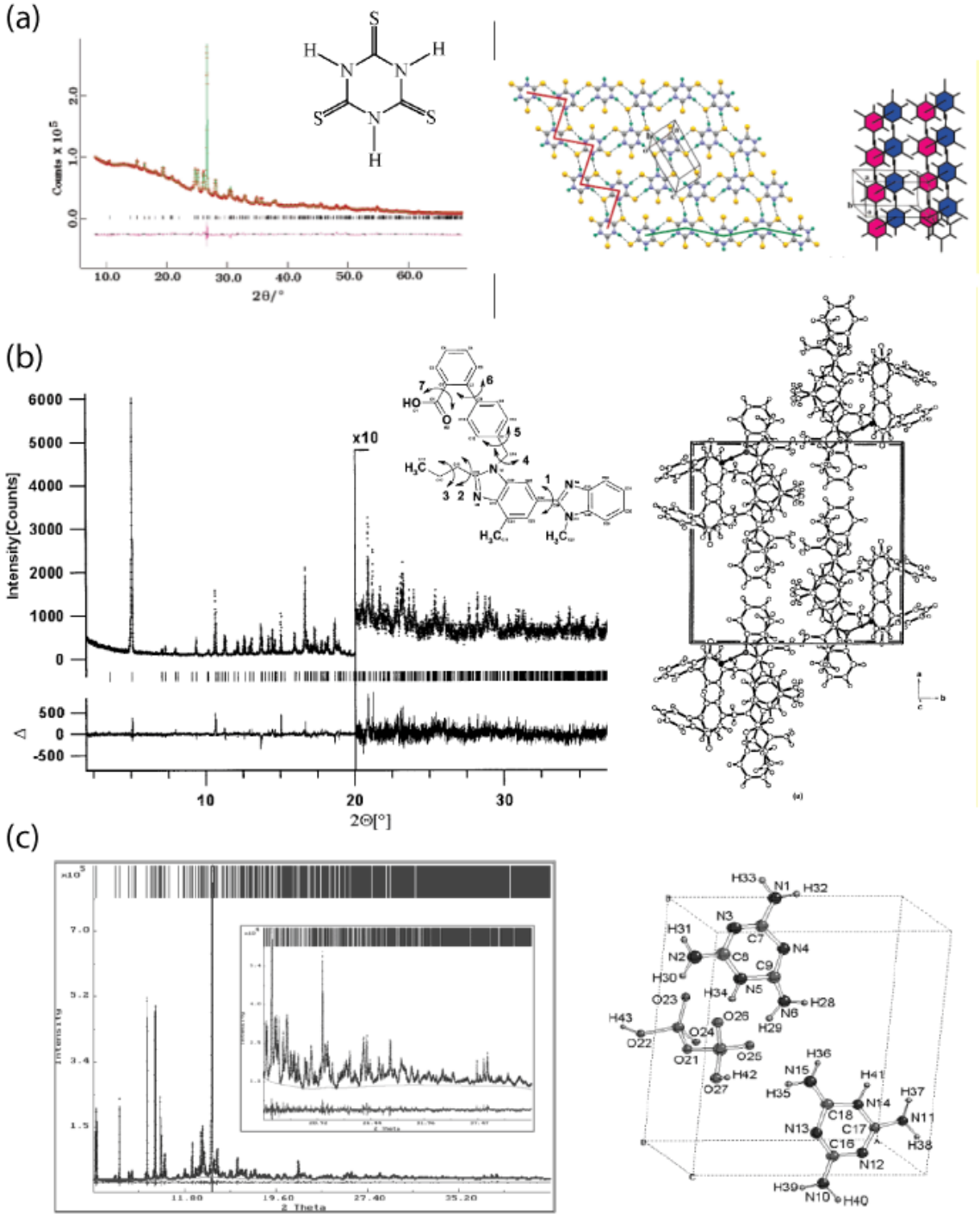

Figure 1-7 : Some examples of *ab initio* crystal structure determination from powder diffraction data. (a) Trithiocyanuric acid unsolvated form.[123] (b) Termisaltan form A.[102] (c) Melaminium dihydrogenpyro- phosphate.[107]

1.3. Purpose of This Dissertation

As described in section 1.1.2, there are lots of interests in the polymorphic and pseudopolymorphic transformations. In order to understand the transformation mechanisms and to reveal the properties of the transformed phases, the crystal structures are most important information. However, in many cases, such transformation gave the polycrystalline materials, although the starting phase can be obtained as a single crystal, so that the single crystal X-ray diffraction analysis cannot apply to the investigation such transformations. Therefore many interesting and/or important transformations mechanism have not been revealed. Especially, the pseudopolymorphic transformations (desolvation and solvation) are not sufficiently studied because it generally accompanied large structural changes which caused by the solvent release and/or sorption (Figure 1-4).

On the other hands the opportunities for carrying out complete structure determination of organic molecular materials from powder X-ray diffraction data (*ab initio* powder crystal structure analysis) have developed considerably in recent years. This technique enables us to analyze the crystal structures which cannot obtain as single crystal form as described in section 1.2 (obviously include polycrystalline phase obtained by the transformations). Therefore, this newly technique, *ab initio* powder crystal structure analysis, would be the key technology to reveal the pseudopolymorphic transformations.

In this context, the purpose of the dissertation is the establishing the pseudopolymorphic transformation mechanisms using *ab initio* powder crystal structure analysis technique. The target phenomenon are the solvent vapor induced pseudopolymorphic transformations of co-crystal of 5-methyl-2-pyridone and trimesic acid, dehydration of pharmaceutical lisinopril dihydrate, and dehydration and polymorphic transformation of pharmaceutical acrinol. These phenomenon are very interesting and important in the scientific and industrial points of view (the details are described in each sections), however, the detail mechanisms of the phenomenon have not been established because of the problem discussed above.

Reference

(1) J. Bernstein, *Polymorphism in Molecular Crystals*, Clarendon Press, Oxford, UK, 2002.

(2) A. Nangia, *Cryst. Growth Des.*, **2006**, 6, 2-4.

(3) J. N. Moorthy and K. Venkatesan, *Bull. Chem. Soc. Jpn.*, **1994**, 67, 1-6.

(4) W. C. Schinzer, M. S. Bergren, D. S. Aldrich, R. S. Chao, M. J. Dunn, A. Jeganathan, L. M. Madden, *J. Pharm. Sci.*, **1997**, 86, 1426-1431.

(5) S. R. Vippagunta, H. G. Brittain, D. J.W. Grant, *Adv. Drug Del. Rev.*, **2001**, 48, 3–26.

(6) S. Byrn, R. Pfeiffer, M. Ganey, C. Hoiberg, G. Poochikian, *Pharm. Res.*, **1995**, 12, 945-954.

(7) K. R. Morris, U. J. Griesser, C. J. Eckhardt, J. G. Stowell, *Adv. Drug Del. Rev.*, **2001**, 48, 91-114.

(8) M. J. Potrzebowski, G. D. Bujacz, A. Bujacz, S. Olejniczak, P. Napora, J. Helin´ ski, W. Ciesielski, J. Gajda, *J. Phys. Chem. B*. **2006**, 110, 761-771.

(9) S. A. Moggach, D. R. Allan, S. J. Clark, M. J. Gutmann, S. Parsons, C. R. Pulhama, L. Sawyerd, *Acta Cryst.*, **2006**. B62, 296–309.

(10) F. H. Herbstein, *Acta Cryst.,* **2006,** B62, 341–383.

(11) D. Chopra, T. N. Guru Row, *Cryst. Growth Des.*, **2008**, 8, 848–853.

(12) R. G. Gonnade, M. M. Bhadbhade, M. S. Shashidhar, *CrystEngComm*, **2008**, 10, 288–296.

(13) M. R. Chierotti, R. Gobetto, L. Pellegrino, L. Milone, P. Venturello, *Cryst. Growth Des.*, **2008**, 8, 1454–1457.

(14) P. Roussel, F. Bentiss, M. Drache, P. Conflant, M. Lagrenee, J. Wignacourt, *J. Mol. Struct.*, **2006**, 798, 134–140.

(15) D. Braga, M. Gandolfi, M. Lusi, M. Polito, K. Rubini, F. Grepioni, *Cryst. Growth Des.*, **2007**, 7, 919-924.

(16) E. Deiters, V. Bulach, M. W. Hosseini, *Chem. Commun.*, **2005**, 3906–3908.

(17) M. Shibakami, M. Tamura, A. Sekiya, *J. Am. Chem. Soc.* **1995**, 117, 4499-4505.

(18) L. R. Nassimbeni, M. L. Kilkenny, *J. Chem. Soc., Dalton Trans.*, **2001**, 1172–1175.

(19) M. R. Caira, L. R. Nassimbeni, F. Toda, D. Vujovic, *J. Chem. Soc., Perkin Trans. 2*, **2001**, 2119–2124.

(20) A. Jacobs, L. R. Nassimbeni, H. Sub, B. Taljaardc, *Org. Biomol. Chem.* , **2005**, 3, 1319–1322.

(21) G. Ramon, A. W. Coleman, L. R. Nassimbeni, B. Taljaard, *Cryst. Growth Des.*, **2005**, 5, 2331-2335.

(22) A. Jacobs, N. Faleni, L. R. Nassimbeni, J. H. Taljaard, *Cryst. Growth Des.*, **2007**, 7, 1003-1006.

(23) B. Sarma, A. Nangia, *CrystEngComm*, **2007**, 9, 628–631.

(24) A. Bashkirava, P. C. Andrews, P. C. Junk, E. G. Robertson, L. Spiccia, N. Vanderhoek, *Chem. Asian J.*, **2007**, 2, 530-538.

(25) S. Yamamura, Y. Sugawara, Hi Terao, M. M. Matsushita, T. Sugawara, *Chem. Phys.*, **2006**, 322, 392–398.

(26) K. Yoshizawa, S. Toyota, F. Toda, *Chem. Commun.*, **2004**, 1844-1845.

(27) J. Th. H. van Eupen, W. W. J. Elffrink, R. Keltjens, P. Bennema, R. de Gelder, J. M. M. Smits, E. R. H. van Eck, A. P. M. Kentgens, M. A. Deij, H. Meekes, E. Vlieg, *Cryst. Growth Des.*, **2008**, 8, 71-79.

(28) S. Dharmayat, R. B. Hammond, X. Lai, C. Ma, E. Purba, K. J. Roberts, Z. Chen, E. Martin, J. Morris, R. Bytheway, *Cryst. Growth Des.*, **2008**, 8, 2205-2216.

(29) J. Han, S. Gupte, R. Suryanarayanan, *Int J. Pharm.*, **1998**, 170, 63-72.

(30) I. Miroshnyk, L. Khriachtchev, S. Mirza, J. Rantanen, J. Heinmki, J. Yliruusi, *Cryst. Growth Des.*, **2006**, 6, 369-374.

(31) C. Cardell, A. Sa´nchez-Navas, F. J. Olmo-Reyes, J. D. Martı´n-Ramos *Anal. Chem.*, **2007**, 79, 4455-4462.

(32) J. Sheng, G. M. Venkatesh, S. P. Duddu, D. J. W. Grant, *J. Pharm. Sci.*, **1999**, 88, 1021-1029.

(33) G. Bettinetti, P. Mura, M. Sorrenti, M. T. FAUCCI, A. Negri, *J. Pharm. Sci.*, **1999**, 88, 1133-1139.

(34) D. Giron, Ch. Goldbronn, M. Mutz, S. Pfeffer, Ph. Piechon, Ph. Schwab, *J. Therm. Anal. Cal.*, **2002**, 68, 453-465.

(35) C. Zhang, J. Wang, Y. Wang, *Ind. Eng. Chem. Res.*, **2005**, 44, 7057-7061.

(36) G. Bettinetti, M. R. Caira, A. Callegari, M. Merli, M. Sorrenti, C. Tadini, *J. Pharm. Sci.*, **2000**, 89, 478-489.

(37) R. L. Te, U. J. Griesser, K. R. Morris, S. R. Byrn, J. G. Stowell, *Cryst. Growth Des.*, **2003**, 3, 997-1004.

(38) Y. Kim, H. C. Paskow, R. W. Rousseau, *Cryst. Growth Des.*, **2005**, 5,

1623-1632.

(39) A. L. Gillon, R. J. Davey, R. Storey, N. Feeder, G. Nichols, G. Dent, D. C. Apperley, *J. Phys. Chem. B*, **2005**, 109, 5341-5347.

(40) K. Kobayashi, H. Fukuhara, T. Hata, Y. Ohashi, *Chem. Pharm. Bull.* **2003**, 51, 1356-1362.

(41) J. W. Visser, *J. Appl. Cryst.*, **1969**, 2, 89-95.

(42) T. ITO, *Nature, Lond.*, **1949**, 164, 755-756.

(43) P. E. Werner, L. Eriksson, M. Westdahl, *J. Appl. Cryst.*, **1985**, 18, 367-370.

(44) A. Altomare, C. Giacovazzo, A. Guagliardi, A. G. G. Moliterni, R. Rizzi, P. E. Werner, *J. Appl. Cryst.*, **2000**, 33, 1180-1186.

(45) P. D. Louer, M. Louer, *J. Appl. Cryst.*, **1972**, 5, 271-275.

(46) P. D. Louer, R. Vargas, *J. Appl. Cryst.*, **1982**, 15, 542-545.

(47) A. Boultif, D. Louer, *J. Appl. Cryst.*, **1991**, 24, 987-993.

(48) A. Boultif, D. Louer, *J. Appl. Cryst.*, **2004**, 37, 724-731.

(49) D. Louer, A. Boultif, *Z. Kristallogr. Suppl.* **2006**, 23, 225-230

(50) C. Dong, F. Wu, H. Chen, *J. Appl. Cryst.*, **1999**, 32, 850-853.

(51) M. A. Neumann, *J. Appl. Cryst.*, **2003**, 36, 356-365.

(52) A. Le Bail, *Powder Diffraction*, **2004**, 19, 249-254.

(53) A. A. Coelho, *J. Appl. Cryst.*, **2000**, 36, 86-95.

(54) B. M. Kariuki, S. A. Belmonte, M. I. McMahon, R. L. Johnston, K. D. M. Harris, R. J. Nelmes, *J. Synchrotron Rad.*, **1999**, 6, 87-92.

(55) H. M. Rietveld, *J. Appl. Cryst.*, **1969**, 2, 65-71.

(56) R. A. Young, , P. E. Mackie, R. B. Von Dreele, **1977**, *J. Appl. Cryst.*, 10, 262-269.

(57) A.C. Larson & R.B. Von Dreele, "General Structure Analysis System (GSAS)", Los Alamos National Laboratory Report LAUR 86-748 (1994).

(58) EXPGUI/GSAS web site : http://www.ncnr.nist.gov/programs/crystallography/software/gsas.html

(59) J. Rodriguez-Carvajal, "FULLPROF: A Program for Rietveld Refinement and Pattern Matching Analysis", Abstracts of the Satellite Meeting on Powder Diffraction of the XV Congress of the IUCr, p. 127, Toulouse, France (1990).,

(60) FULLPROF/WinPLOTR web site : http://www-llb.cea.fr/fullweb/powder.htm

(61) Petricek,V., Dusek,M. & Palatinus,L.(2000). Jana2000. The crystallographic computing system. Institute of Physics, Praha, Czech Republic. , JANA2000 web site : http://www-xray.fzu.cz/jana/Jana2000/jana.html

(62) F. Izumi and T. Ikeda, *Mater. Sci. Forum*, **2000**, 321-324, 198-203.

(63) F. Izumi and K. Momma, *Proc. XX Conf. Appl. Crystallogr., Solid State Phenom.*, **2007**, 130, 15-20.

(64) G. S. Pawley, *J. Appl. Cryst.*, **1981**, 14, 357-361.

(65) H. Toraya, *J. Appl. Cryst.*, **1986**, 19, 440-447.

(66) A. Le Bail, *Mater. Res. Bull.*, **1988**, 23, 447-452.

(67) G. Cascarano, L. Favia, C. Giacovazzo, *J. Appl. Cryst.*, **1992**, 25, 310-317.

(68) A. Altomare, B. Carrozzini, C. Giacovazzo, A. Guagliardi , A. G. G. Moliterni, R. Rizzi, *J. Appl. Cryst.*, **1996**, 29, 667-673.

(69) A. Altomare, J. Foadi, C. Giacovazzo, A. Guagliardi , A. G. G. Moliterni, *J. Appl. Cryst.*, **1996**, 29, 674-681.

(70) B. Carrozzini, C. Giacovazzo, A. Guagliardi , M. C. Burla, G. Polidori, *J. Appl. Cryst.*, **1997**,30, 92-97.

(71) A. Altomare, J. Foadi, C. Giacovazzo, A. G. G. Moliterni, M. C. Burla, G. Polidori, *J. Appl. Cryst.*, **1998**, 31, 74-77

(72) . A. Altomare, J. Foadi, C. Giacovazzo, A. Guagliardi , A. G. G. Moliterni, R. Rizzi, *J. Appl. Cryst.*, **1999**, 32, 963-967.

(73) A. Altomare, C. Giacovazzo, A. G. G. Moliterni, R. Rizzi, *J. Appl. Cryst.*, **2001**, 34, 704-709.

(74) A. Altomare, C. Giacovazzo, M. Ianigro, A. G. G. Moliterni, R. Rizzi, *J. Appl. Cryst.*, **2002**, 35, 21-27.

(75) A. Altomare, R. Caliandro, C. Cuocci, C. Giacovazzo, A. G. G. Moliterni, R. Rizzi, *J. Appl. Cryst.*, **2003**, 36, 906-913.

(76) A. Altomare, R. Caliandro, C. Cuocci, I. Silva, C. Giacovazzo, A. G. G. Moliterni, R. Rizzi, *J. Appl. Cryst.*, **2004**, 37, 204-209.

(77) A. Altomare, R. Caliandro, M. Camalli, C. Cuocci, I. Silva, C. Giacovazzo, A. G. G. Moliterni, R. Spagna, *J. Appl. Cryst.*, **2004**, 37, 57-966.

(78) A. Altomare, R. Caliandro, M. Camalli, C. Cuocci, I. Silva, C. Giacovazzo, A. G.

G. Moliterni, R. Rizzi, *J. Appl. Cryst.*, **2005**, 38, 760-766.

(79) A. Altomare, M. Camalli, C. Giacovazzo, A. G. G. Moliterni, R. Rizzi, , *J. Appl. Cryst.*, **2007** 40, 344-348.

(80) A. Altomare, M. C. Burla, M. Camalli, B. Carrozzini, G. Cascarano, C. Giacovazzo, A. Guagliardi , A. G. G. Moliterni, G. Polidori, R. Rizzi, *J. Appl. Cryst.*, **1999**,32, 339-340.

(81) A. Altomare, R. Caliandro, M. Camalli, C. Cuocci, C. Giacovazzo, A. G. G. Moliterni, R. Rizzi, *J. Appl. Cryst.*, **2004**, 37, 1025-1028.

(82) A. Altomare, C. Cuocci, C. Giacovazzo, A. G. G. Moliterni, R. Rizzi, *J. Appl. Cryst.*, **2006**, 39, 558-562.

(83) A. Altomare, C. Giacovazzo, A. Guagliardi , A. G. G. Moliterni, R. Rizzi, *J. Appl. Cryst.*, **2000**, 33, 1305-1310.

(84) A. Altomare, C. Cuocci, C. Giacovazzo, A. Guagliardi , A. G. G. Moliterni, R. Rizzi, *J. Appl. Cryst.*, **2002**, 35, 182-184.

(85) C. Giacovazzo, A. Altomare, C. Cuocci, A. Guagliardi , A. G. G. Moliterni, R. Rizzi, *J. Appl. Cryst.*, **2002**, 35, 422-429.

(86) A. Altomare, R. Caliandro, C. Giacovazzo, A. Guagliardi , A. G. G. Moliterni, R. Rizzi, *J. Appl. Cryst.*, **2003**, 36, 230-238.

(87) A. Altomare, C. Cuocci, C. Giacovazzo, A. G. G. Moliterni, R. Rizzi, *J. Appl. Cryst.*, **2006**, 39, 145-150.

(88) A. Altomare, R. Caliandro, C. Cuocci, C. Giacovazzo, A. Guagliardi , A. G. G. Moliterni, R. Rizzi, C. Platteau, *J. Appl. Cryst.*, **2008**, 41, 56-61.

(89) V. Brodski, R. Peschar, H. Shenk, *J. Appl. Cryst.*, **2005**, 38, 688-693.

(90) A. Le Bail, *Materials Science Forum*, **2001**, 378-381, 65-70.

(91) W. I. F. David, K. Shankland, J. Cole, S. Maginn, W. D. S. Motherwell, R. Taylor, (2001). DASH user manual. Cambridge Crystallographic Data Centre, Cambridge, UK.

(92) A. A. Coelho, *J. Appl. Cryst.*, **2003**, 36, 86-95.

(93) V. Favre-Nicolin, R. Cerny, *J. Appl. Cryst.*, **2002**, 35, 734-743.

(94) S. Pagola, P. W. Stephens, D. S. Bohle, A. D. Kosar, S. K. Madsen, *Nature (London)*, **2000**, 404, 307-310.

(95) S. Habershon, G. W. B. M. Turner, Kariuki, E. Y. Cheung, A. J. Hanson, E. Tedesco, D. Albesa-Jove´, M. H. Chao, O. J. Lanning, R. L. Johnston, K. D. M. Harris, EAGER A Computer Program for Direct-Space Structure Solution from

Powder X-ray Diffraction Data; Cardiff University and University of Birmingham.

(96) B. M. Kariuki, H. Serrano-González, R. L. Johnston, K. D. M. Harris, *Chem. Phys. Lett.*,**1997**, 280, 189-195.

(97) K. D. M. Harris, R. L. Johnston, B. M. Kariuki, *Acta Cryst. A*, **1998**, 54, 632-645.

(98) G. W. Turner, E. Tedesco, K. D. M. Harris, R. L. Johnston, B. M. Kariuki, *Chem. Phys. Lett.*, **2000**, 321, 183-190.

(99) S. Habershon, K. D. M. Harris, R. L. Johnston, *J. Comp. Chem.*, **2003**, 24, 1766-1774.

(100) E. Y. Cheung, E. E. McCabe, K. D. M. Harris, R. L. Johnston, E. Tedesco, K. M. P. Raja, P. Balaram, *Angew. Chem. Int. Ed.*, **2002**, 41, 494-496.

(101) K. D. M. Harris, M. Tremayne, P. Lightfoot, P. G. Bruce, *J. Am. Chem. Soc.* **1994**, 116, 3543-3547.

(102) R. E. Dinnebier, P. Sieger, H. Nar, K. Shankland, W. I. F. David, *J. Pharm. Sci.*, **2000**, 89, 1465-1479.

(103) Y.-H. Kiang, A. Huq, P. W. Stephens, W. Xu, *J. Pharm. Sci.*, **2003**, 92, 1844-1853.

(104) Z. Pan, E. Y. Cheung, K. D. M. Harris, E. C. Constable, C. E. Housecroft, *Cryst. Growth Des.*, **2004**, 4, 451-455.

(105) M. Tremayne, L. Grice, J. C. Pyatt, C. C. Seaton, B. M. Kariuki, H. H. Y. Tsui, S. L. Price, J. C. Cherryman, *J. Am. Chem. Soc.* **2004**, 126, 7071-7081.

(106) M. Rukiah, J. Lefebvre, O. Hernandez, W. van Beekc, M. Serpelloni, *J. Appl. Cryst.*, **2004**, 37, 766-722.

(107) V. Brodski, R. Peschar, H. Schenk, A. Brinkmann, E. R. H. van Eck, A. P. M. Kentgens, B. Coussens, A. Braam, *J. Phys. Chem. B*, **2004**, 108, 15069-15076.

(108) J. Lefebvre, J.-F. Willart, V. Caron, R. Lefort, F. Affouard, F. Dane`de, *Acta Cryst. B*, **2005**, 61, 455-463.

(109) Z. Pan, Eugene Y. Cheung, K. D. M. Harris, E. C. Constable, C. E. Housecroft, *Cryst. Growth Des.*, **2005**, 5, 2084-2090.

(110) J. K. Harper, D. M. Grant, Y. Zhang, P. L. Lee, R. Von Dreele, *J. Am. Chem. Soc.* **2006**, 128, 1547-1552.

(111) E. Y. Cheung, K. D.M. Harris, T. Kang, J. R. Scheffer, J. Trotter, *J. Am. Chem. Soc.* **2006**, 128, 15554-15555.

(112) Z. Pan, M. Xu, E. Y. Cheung, K. D. M. Harris, E. C. Constable, C. E. Housecroft,

J. Phys. Chem. B, **2006**, 110, 11620-11623.

(113) I. Barsky, J. Bernstein, P. W. Stephens, K. H. Stone, E. Cheung, M. B. Hickey, J.-O. Henck, *Cryst. Growth Des.*, **2008**, 8, 67-70.

(114) E. E. Avila, A. J. Mora, G. E. Delgado, R. R. Contreras, A. N. Fitchc and M. Brunellic, *Acta Cryst. B*, **2005**, 64, 217-222.

(115) D. Fujimoto, R. Tamura, Z. Lepp, H. Takahashi, T. Ushio, *Cryst. Growth Des.*, **2003**, 3, 973-979.

(116) W. I. F. David, K. Shankland, C. R. Pulham, N. Blagden, R. J. Davey, M. Song, *Angew. Chem. Int. Ed.*, **2005**, 44, 7032-7035.

(117) E. Y. Cheung, S. J. Kitchin, K. D. M. Harris, Y. Imai, N. Tajima, R. Kuroda, *J. Am. Chem. Soc.* **2003**, 125, 14658-14659

(118) A. V. Trask, J. van de Streek, W. D. S. Motherwell, W. Jones, *Growth Des.*, **2005**, 5, 2233-2241.

(119) V. V. Chernyshev, D. Machon, A. N. Fitch, S. A. Zaitsev, A. V. Yatsenko, A. N. Shmakovd, H.-P. Weber, *Acta Cryst. B*, **2003**, 59, 787-793.

(120) C. Platteau, J. Lefebvre, F. Affouard, P. Derollez, *Acta Cryst. B*, **2004**, 60, 453-460.

(121) C. Platteau, J. Lefebvre, F. Affouard, J.-F. Willart, P. Derolleza, F. Mallet, *Acta Cryst. B*, **2005**, 61, 185-191.

(122) F. Guo, K. D. M. Harris, *J. Am. Chem. Soc.* **2005**, 127, 7314-7315.

(123) F. Guo, E. Y. Cheung, K. D. M. Harris, V. R. Pedireddi, *Cryst. Growth Des.*, **2006**, 6, 846-848.

Chapter 2

Vapor Induced Crystalline Transformation

2.1. Abstract

A new co-crystal (phase **H**) of 5-methyl-2-pyridone (**5MP**) and trimesic acid (**TMA**) has been prepared by grinding a methanol solvate co-crystal (phase **M**) of **5MP** and **TMA** under ambient conditions. Powder X-ray diffraction indicates that the new co-crystal phase **H** is structurally different from the methanol solvate co-crystal (phase **M**) and an unsolvated co-crystal (phase **U**) of **5MP** and **TMA** reported previously. In the present work, the crystal structure of the new phase **H** has been determined directly from powder X-ray diffraction data, allowing insights to be gained regarding the mechanism of the transformation from **M** to **H**. The structural analysis reveals that phase **H** is a hydrate of **5MP** and **TMA**, and thus the transformation from **M** to **H** is a solvent exchange process. The rate of this process is shown to be accelerated significantly by grinding. Further vapor induced transformations have been investigated for phases **M**, **H** and **U**, and insights regarding transformation mechanisms have been established from consideration of the crystal structures. Interestingly, while the phase **M** and **H** are not photoreactive phase of 5MP, the unsolvated phase **U** is photoreactive and it produced a pure [4+4] *cis-syn* dimer of **5MP**. From crystal structure comparison, it was revealed that the difference of photoreactivities can be clearly explained from the reaction cavities but not only from the distance or arrangement of reaction centers.

2.2. Introduction

The effect of solvent vapors on the properties of solids is widely studied in many fields. In pharmaceutical sciences, the effect of water vapor has been investigated extensively in relation to hydration and dehydration phenomena, because such transformations can often affect the physical properties or bioavailability of drugs[(1)(2)]. In materials sciences, solvent adsorption and exchange phenomena are widely studied for metal-organic framework structures[(3)(6)] and inclusion compounds[(5)-(9)], because of their potential applications, for example in storage, separation and sensor technologies. Furthermore, solvent vapor has also been exploited to accelerate reactions the solid state.[(10)] An important aspect of exposure of a solid material to solvent vapors is to understand whether any changes of crystal structure occur, as structure clearly has an important bearing on the physical, chemical and biological properties of the material. However, in many cases, single crystals of the starting phase are found to disintegrate to produce a polycrystalline material upon transformations induced by solvent vapor, thus limiting the opportunities to obtain information on the structural changes associated with such processes by single crystal X-ray diffraction analysis. In some cases, it might be possible to obtain a single crystal of the transformed phase (as confirmed by comparison of powder X-ray diffraction data) by another crystallization method, but in many cases, single crystals of the transformed phase cannot be obtained by any other method. Techniques for carrying out structure determination directly from powder X-ray diffraction data are clearly essential for structural characterization of the polycrystalline product materials obtained directly in such transformations.

The opportunities for carrying out complete structure determination of organic molecular materials from powder X-ray diffraction data have developed considerably in recent years[(11)-(24)], particularly through the development of the direct-space strategy for structure solution[(25)]. Because these techniques have the potential to provide structural understanding of polycrystalline products obtained from solid state transformations (e.g. originating from single crystal materials of the type discussed above), these techniques have a key role to play in understanding structural properties of materials produced from solid state grinding processes, solid state reactions, desolvation processes, and polymorphic

transformations[26]-[32].

Previously, the solvent-vapor induced transformation of a co-crystal of 5-methyl-2-pyridone (**5MP**; Figure 2-1) and trimesic acid (**TMA**; Figure 2-1) was studied as part of an investigation of the photoreactivity of 2-pyridone derivatives in co-crystals[33]. Although a methanol solvate co-crystal (denoted **M**; **5MP**:**TMA**:MeOH = 1:1:1) obtained from methanol solution was not photoreactive, this co-crystal transforms to a photoreactive co-crystal on exposure to acetonitrile vapor, or on heating. Structure determination from powder X-ray diffraction data revealed that the transformed material is an unsolvated co-crystal (denoted **U**; **5MP**:**TMA** = 1:1). Thus, it is clear that the transformation induced by acetonitrile vapor is a desolvation process.

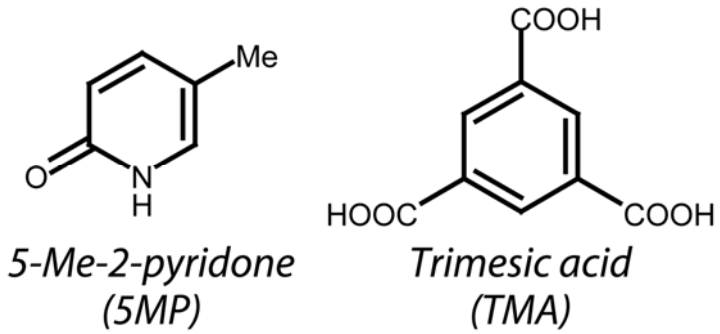

Figure 2-1 : Molecular structures of 5MP and TMA.

The present paper reports experiments in which we have shown that grinding **M** under ambient conditions gives rise to a transformation to produce a polycrystalline sample of a new co-crystal, denoted **H**. Structural properties of this new phase have been established by structure determination from powder X-ray diffraction data, and further investigations of transformations induced by solvent vapors for phases **M**, **H** and **U** have been investigated, yielding further insights regarding the transformation mechanisms. Finally, the difference of the photoreactivities in each crystals is discussed from the analyzed crystal structures.

2.3. Experimental

The new co-crystal material **H** was obtained by grinding a polycrystalline sample of **M** for about 10 mins using a mortar and pestle under ambient conditions. As shown in Figure 2-2, the powder X-ray diffraction pattern of **H** is different from those of **M** and **U**, and thus the crystal structure of **H** is different from **M** and **U**. TGA studies suggest that **H** contains one water molecule for each molecule of **5MP** and **TMA**. The crystal structure of **H** has been determined directly from powder X-ray diffraction data as discussed below. Upon heating, we have found that **H** transforms to **U** (we recall that **M** also transforms to **U** upon heating[33]).

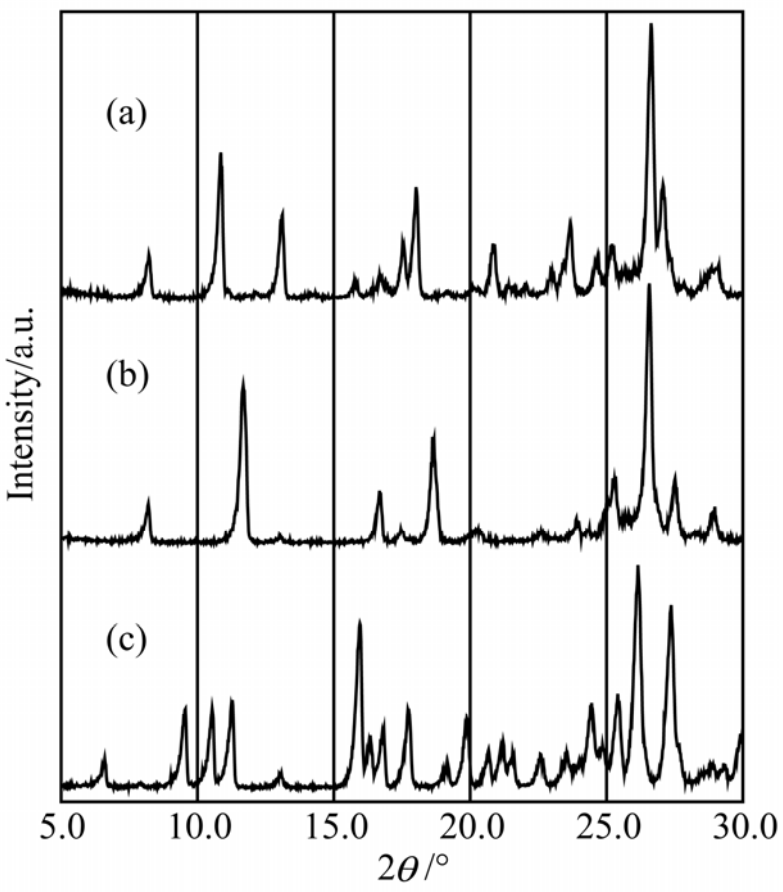

Figure 2-2. Powder X-ray diffraction patterns (CuKα, λ = 1.5418 Å) for (a) phase **M**, (b) phase **H**, and (c) phase **U**.

2.3.1. Synchrotron X-ray Powder Diffraction Measurement

Synchrotron X-ray powder diffraction data were recorded for **H** at 300 K on beamline BL19B2 at SPring-8 (Debye-Scherer camera equipped with a curved Imaging Plate detector) with wavelength 1.23689(2) Å (0.3 mm diameter borosilicate glass capillary, with sample spinning during measurement; data collection time 15 mins).

2.3.2. Structure Determination of Phase H from Powder X-ray Diffraction Data

The powder X-ray diffraction pattern of **H** was indexed using the program ITO,[34] giving the following unit cell (M20 = 21.9[35]) with triclinic metric symmetry: a = 10.526 Å, b = 10.973 Å, c = 7.094 Å, α = 107.939°, β = 97.628°, γ = 88.137°, V = 772.57 Å^3. Given the volume of this unit cell, and consideration of density, the number of formula units in the unit cell is assigned as Z = 2. Structure determination focused first on space group $P\bar{1}$ (with the intention to consider space group P1 if structure determination in $P\bar{1}$ proved unsuccessful). Profile fitting using the Le Bail method[36] gave a good quality fit with R_{wp} = 3.81% and R_p = 2.51%. The unit cell parameters and profile parameters obtained from the Le Bail fitting procedure were used in the subsequent structure solution calculation. Structure solution was carried out using the direct-space genetic algorithm (GA) technique incorporated in the program EAGER[37)-(41)]. The structural fragment comprised one **5MP** molecule, one **TMA** molecule and one water molecule, representing a total of 18 structural variables (three translational variables for each of the 5MP, TMA and water molecules, three orientational variables for each of the 5MP and TMA molecules, and three torsional variables for the carboxylic acid groups of the TMA molecule). The GA calculation involved the evolution of 20 generations for a population of 100 structures, with 50 mating operations and 25 mutation operations carried out per generation. Following structure solution, Rietveld refinement[42] was carried out using the GSAS program[43]. Standard restraints were applied to bond lengths and bond angles, planar restraints were applied to aromatic rings, and a global isotropic displacement parameter was used. As the **5MP** molecule has pseudo-symmetry (see Figure 2-3), the orientation of the **5MP** molecule in the structure was given

careful scrutiny. In the best structure solution obtained from the GA calculation, **5MP** forms a dimer with a carboxylic acid group of **TMA** through the formation of N–H···O and O–H···O hydrogen bonds, and there are no unreasonable short contacts. On the other hand, in the structures obtained by flipping the **5MP** molecule according to the pseudo-symmetry (Figure 3), some unreasonable structural features are observed for hydrogen bonding and intermolecular distances, suggesting that the structure obtained from the GA calculation is correct. Similarly, the C–OH and C=O bonds of the carboxylic acid groups of **TMA** were assigned from the formation of reasonable hydrogen bonding interactions. The final Rietveld refinement gave following parameters: a = 10.5423(2) Å, b = 10.9487(3) Å, c = 7.0994(1) Å, α = 107.910(2)°, β = 97.747(1)°, γ = 88.088(1)°, V = 772.58(3) Å^3, R_{wp} = 5.17%, R_p = 3.53%, R_F^2 = 8.03% (2θ range, 5.0 – 69.99°; 6500 profile points; 126 refined variables). The final Rietveld plot is shown in Figure 2-4 and crystal structures is shown in Figure 2-5 and Figure 2-6.

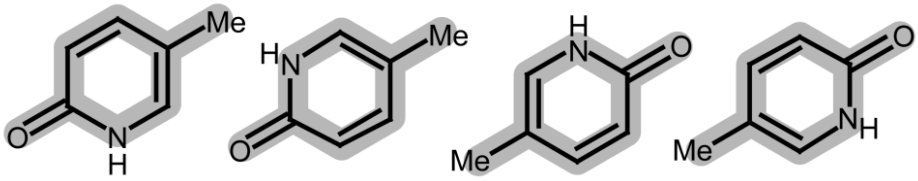

Figure 2-3 : Pseudo-symmetry of 5MP.

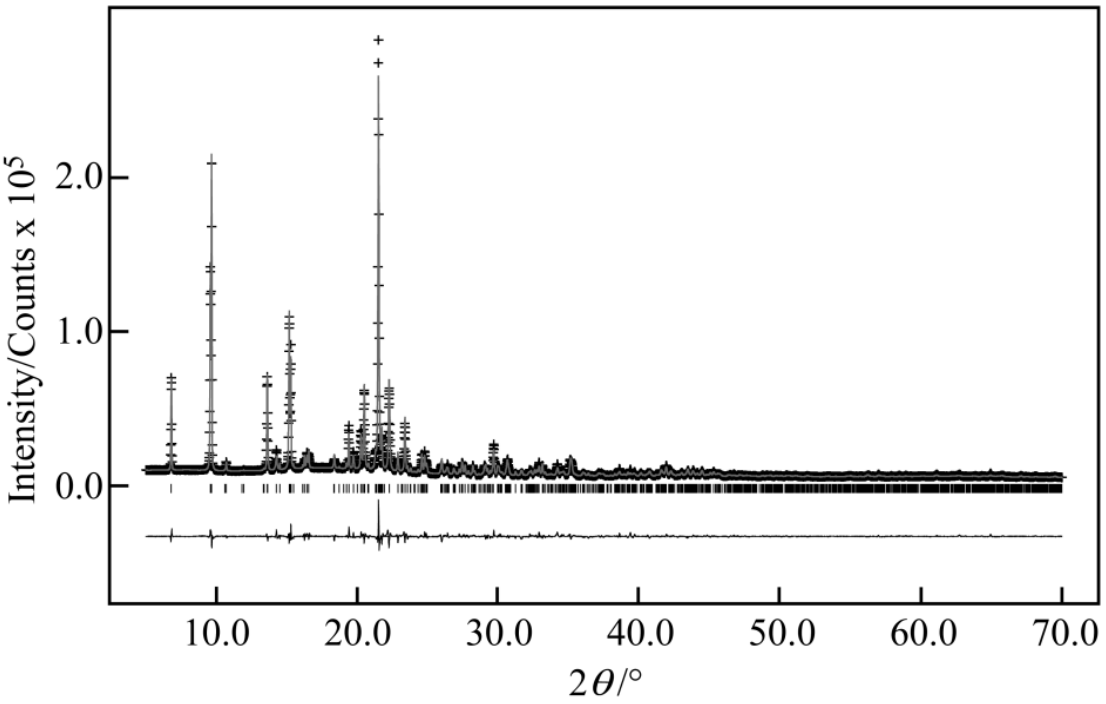

Figure 2-4 : Final Rietveld refinement for phase **H**, showing the experimental powder X-ray diffraction pattern (+ marks), calculated powder X-ray diffraction pattern (solid line) and difference profile (lower line). Tick marks indicate peak positions.

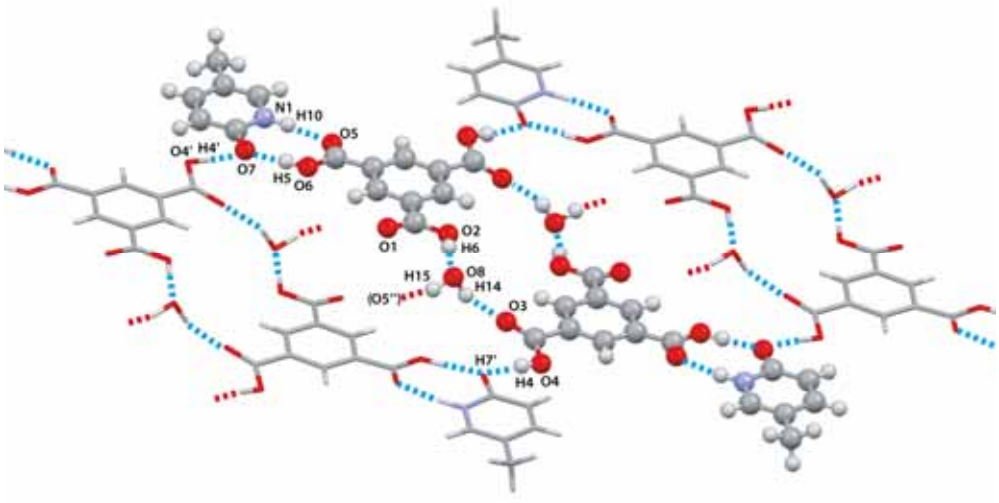

Figure 2-5 : Crystal structure of phase **H**, with hydrogen bonds indicated by dashed lines. The hydrogen bond donor O8–H15 interacts with O5 in the upper layer, which is labeled O5". The part of the structure shown as a ball-and-stick model represents the "hydrogen bonding unit".

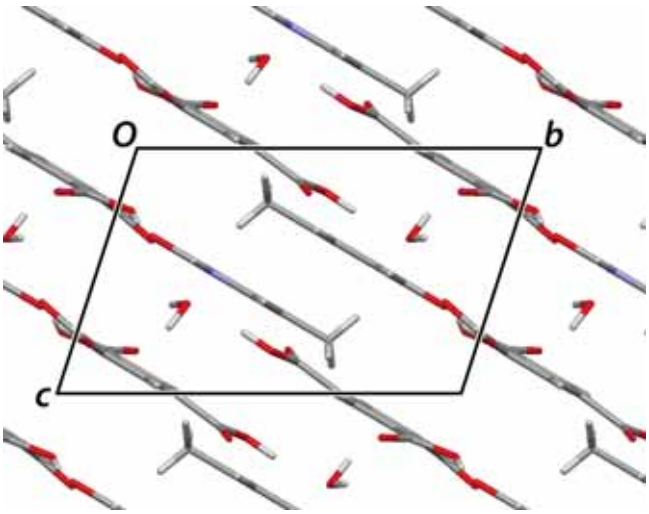

Figure 2-6 : Crystal structure of phase **H** viewed along the *a*-axis (parallel to the plane of the hydrogen bonding unit), showing the sheet-like nature of the structure.

2.3.3. Transformations on Exposure to Solvent Vapor

The apparatus used to expose solid materials to solvent vapor is shown in Figure 2-7a, and comprises a closed plastic container that was half filled by solvent. The solvent vapors considered in this work were water, methanol, acetonitrile, ethanol, acetone, hexane and diethyl ether. A powder sample of the material of interest was packed into a sample holder for powder X-ray diffraction measurements, and placed on an upturned beaker to expose the sample to the solvent vapor. All experiments were carried out at ambient temperature, and the plastic container was not evacuated prior to the start of the experiments. After removal of the solid material, powder X-ray diffraction data were recorded on a Rigaku RINT-2400 powder X-ray diffractometer to monitor (*ex situ*) any structural changes that had occurred due to exposure to solvent vapor (Figure 2-2). If no changes were observed in the powder X-ray diffraction pattern after 4 days, it was concluded that no transformation occurs for the given material on exposure to the solvent vapor. If, on the other hand, changes were observed in the powder X-ray diffraction pattern within 4 days, the exposure to solvent vapor was continued for as long as necessary until the powder X-ray diffraction pattern showed that the transformation had reached completion.

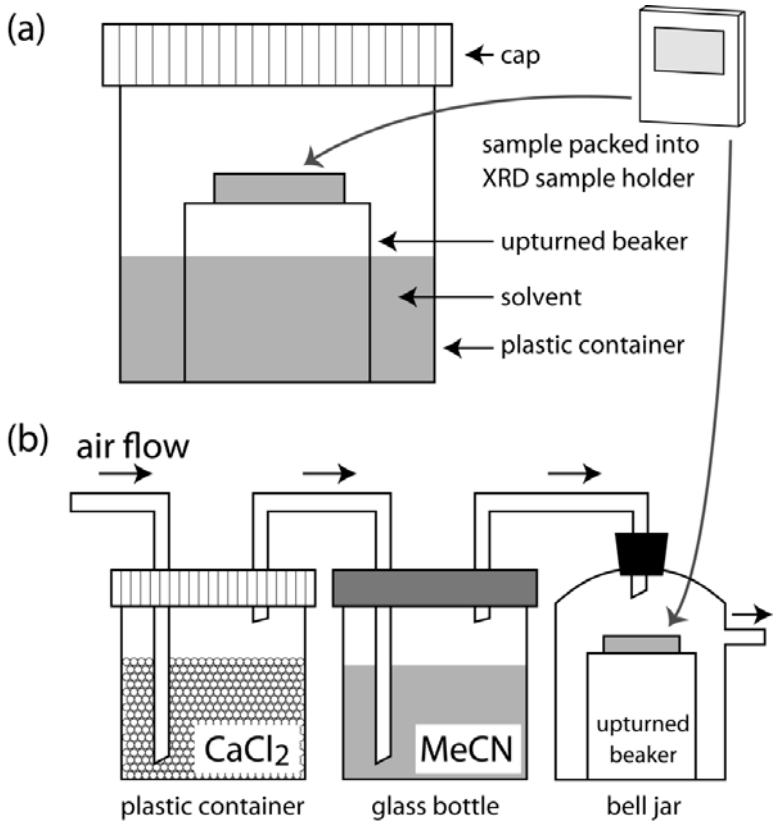

Figure 2-7 : Schematic illustration of the experimental set-up for exposing solid materials to solvent vapor under (a) static conditions and (b) flow conditions.

In another type of experiment, phase **H** was exposed to acetonitrile vapor under flow conditions at ambient temperature, using the apparatus shown in Figure 2-7b. In this experiment, flowing air was passed initially through $CaCl_2$ (to dry the air), then bubbled through liquid acetonitrile, and finally flowed over the polycrystalline sample of **H**. Changes in the solid sample were monitored (*ex situ*) by powder X-ray diffraction, as discussed above. Also, in order to explore the role of acetonitrile vapor in this experiment, a control experiment was carried out in which dry air containing no acetonitrile vapor (i.e. without bubbling the dry air through acetonitrile) was flowed over a sample of **H**.

In addition, for phases **M** and **H**, further experiments were performed involving drying the solid material and exposure of the solid material to vacuum. Drying was carried out using a desiccator with silica gel as desiccant, and exposure to vacuum was carried out using a rotary pump (6.7×10^{-2} Pa) connect to a desiccator.

2.4. Results and Discussion

2.4.1. Structural Properties of Phase H

As shown in Figure 2-5, the crystal structure of the new phase **H** comprises sheets of **5MP**, **TMA** and water molecules. The **5MP** and **TMA** molecules form a ring with N1–H10···O5 (N···O, 2.75 Å) and O6–H5···O7 (O···O, 2.53 Å) hydrogen bonds, and **TMA** and water molecules form a ring (with inversion symmetry) constructed from O2–H6···O8 (O···O, 2.67Å) and O8–H14···O3 (O···O, 2.74Å) hydrogen bonds. These hydrogen bonding motifs give rise to the "hydrogen bonding unit" defined in Figure 2-5. A similar hydrogen bonding unit is also observed in the structure of **M** (Figure 2-8a, CCDC deposition number 263741), but the structures of **M** and **H** differ in the arrangement of these hydrogen bonding units. Although a given hydrogen bonding unit is connected to neighbouring hydrogen bonding units by O–H···O hydrogen bonds in both structures, the structures differ in the details of how these units are connected to each other. In **M**, the hydrogen bonding units are connected not only to adjacent units in the same plane (light blue dashed lines in Figure 2-8a) but also to units above and below (red dashed lines). In **H**, on the other hand, the hydrogen bonding units are connected only to adjacent units in the same plane (light blue lines in Figure 2-5). As a result, the structure of **H** is sheet-like (Figure 2-6), whereas the structure of **M** is not sheet-like (Figure 2-8b). The difference in the arrangement of hydrogen bonding units is manifested in the difference of space groups for **M** ($P2_1/n$) and **H** ($P\bar{1}$). Further comparison between these structures is discussed later.

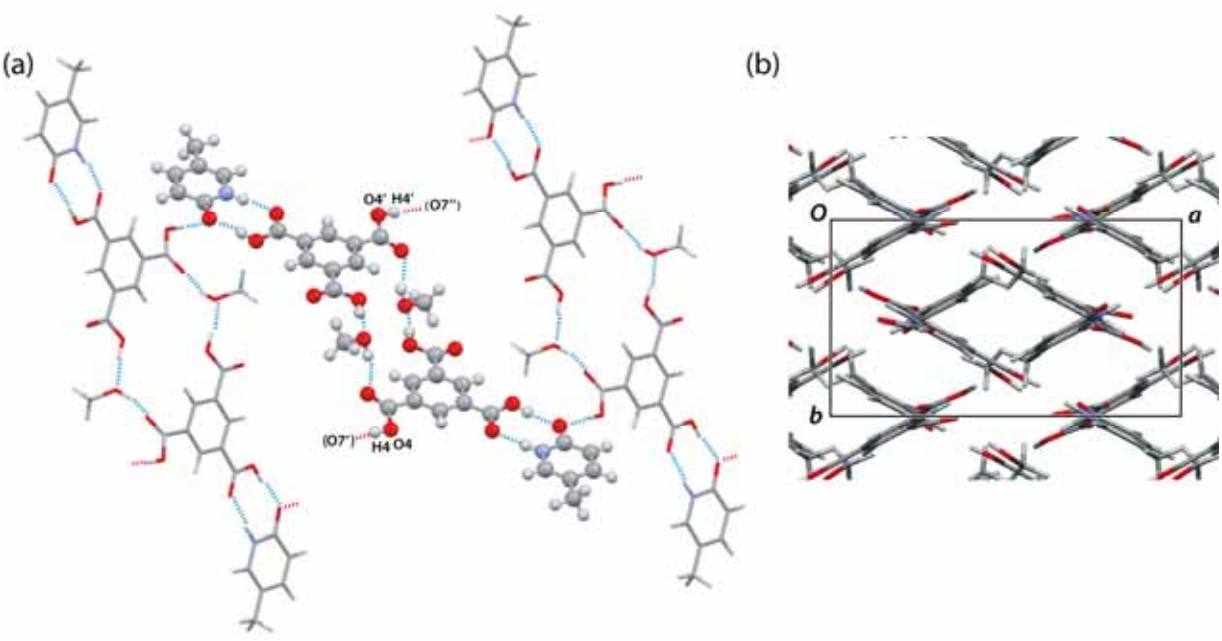

Figure 2-8 : (a) Crystal structure of phase **M**, with hydrogen bonds indicated by dashed lines. The part of the structure shown as the ball-and-stick model represents the hydrogen bonding unit. (b) Crystal structure of phase **M** viewed along the *c*-axis (parallel to the plane of the hydrogen bonding unit), showing that the structure is not sheet-like.

2.4.2. Transformation Induced by Grinding

Clearly, the transformation induced by grinding crystals of **M** is a solvent exchange process, as the methanol present in **M** is replaced by the water present in **H**. In order to investigate whether grinding is critical for this transformation, a single crystal of **M** was left under ambient conditions, without grinding. Over a period of time, the crystal of **M** was observed to transform to **H**, with the original single crystal disintegrating to form a polycrystalline material (but maintaining the overall shape of the original crystal). The time required for this transformation (about one month) was significantly longer than with grinding. This observation indicates that exposing crystals of **M** to an ambient atmosphere (without grinding) is sufficient to bring about the transformation from **M** to **H**, but it is clear that grinding serves to accelerate the transformation. Following this observation, we now assess in more detail the effect of solvent vapor in relation to transformations between phases **M**, **H** and **U**.

2.4.3. Transformations Induced by Solvent Vapor

The results from the experiments involving exposure of materials **M**, **H** and **U** to a range of different solvent vapors are summarized in Scheme 2-1. As expected, **H** and **U** are observed to transform to **M** on exposure to methanol vapor, and **M** and **U** are observed to transform to **H** on exposure to water vapor. Furthermore, exposure of **M** and **H** to acetonitrile, acetone or ethanol vapors gives rise to desolvation transformations to produce **U**. Although the transformation from **M** to **U** on exposure to acetonitrile vapor was already reported in previous literature[33], the transformations that occur on exposure to acetone and ethanol vapors were newly discovered in the present study. It is relevant to note that crystals of **M**, **H** and **U** are insoluble in acetonitrile, acetone and ethanol, so it is unlikely that partial dissolution of these materials can explain the results of the experiments involving exposure to the solvent vapors.

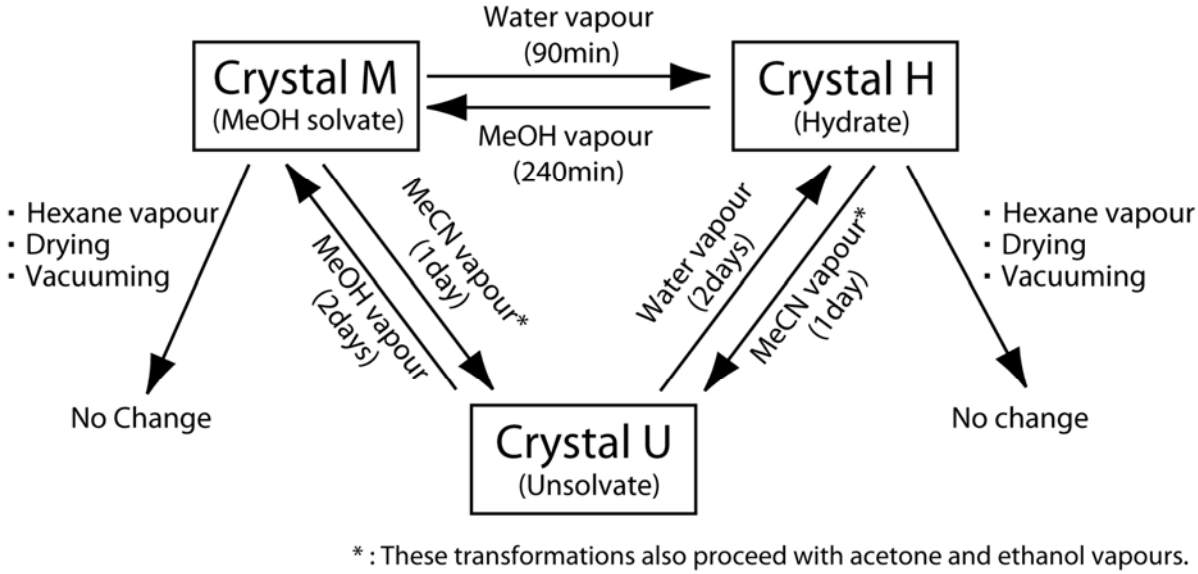

Scheme 2-1: Summary of results of experiments involving exposure of materials to solvent vapor, drying, and exposure to vacuum.

In addition to the experiments to investigate exposure of phase **H** to solvent vapors under "static" conditions (using the apparatus shown in Figure 2-7a), we have also investigated the exposure of **H** to acetonitrile vapor in a flow experiment, in which dry air, bubbled through liquid acetonitrile, was flowed

over a sample of **H**. Under these conditions, we also observe that **H** undergoes a desolvation process to produce **U**, reaching completion within 4 days. On the other hand, no structural change was observed in a control experiment carried out under the same conditions but with only dry air (not containing acetonitrile vapor) flowed over the sample of **H**. Thus, these experiments confirm that the solvent vapor plays a direct role in mediating the transformation from **H** to **U** (and rules out the possibility that the transformation observed in the "static" experiments might arise only from the role of the liquid phase present within the sealed vessel (see Figure 2-7a)).

In contrast to the desolvation processes observed on exposure of **M** and **H** to acetonitrile, acetone and ethanol vapors, these phases do not to undergo any transformations in the experiments involving drying, exposure to vacuum, exposure to hexane vapor, or exposure to diethyl ether vapor. These observations suggest that, in the desolvation processes induced by solvent vapor, a specific affinity between the solvent present in the vapor phase and the solvent present in the crystal structure may be necessary.

An interesting aspect of these experiments is the time required for the transformations to occur on exposure to solvent vapors. The solvent exchange transformation from **M** to **H** is complete in a few hours. However, the transformations of **U** to form the solvate structures **M** or **H** on exposure to methanol and water vapors respectively require about two days. In order to investigate the transformation times in greater detail, dynamic vapor sorption (DVS) experiments were carried out for samples of **M** and **U**. Figure 2-9 shows the mass changes observed for **M** and **U** under conditions of 97% relative humidity and 25°C. The decrease in mass observed for **M** corresponds to the exchange of methanol by water, whereas the increase in mass observed for **U** corresponds to hydration (theoretical mass changes for complete transformations: –3.99% for **M**, 5.64% for **U**). The transformation from **M** to **H** reaches completion in about 180 minutes with a mass change of –3.25% (Figure 2-9a). The observed mass loss is close to the theoretical value, and the discrepancy may be attributed to the difficulty in maintaining a pure sample of **M** at the start of the DVS measurement (the DVS experiment requires time to stabilize the balance and humidity before measurement, and it is likely that some amount of **H** is formed before the actual start of the measurement, leading to the measured mass loss being lower than the theoretical value). In contrast, the

transformation from **U** to **H** does not reach completion after 10000 mins (mass change +1.85%). In this case, the increase of mass is very gradual, and the measurement was stopped before the transformation was complete. These results indicate that the solvent exchange transformation between **M** and **H** proceeds readily, but that hydration of **U** is a much less facile process. The results of the DVS experiments are consistent with the results of the experiments involving exposure of the materials to solvent vapors, and confirmed by powder X-ray diffraction analysis, although the transformation time is quite different in each case because of the different experimental conditions.

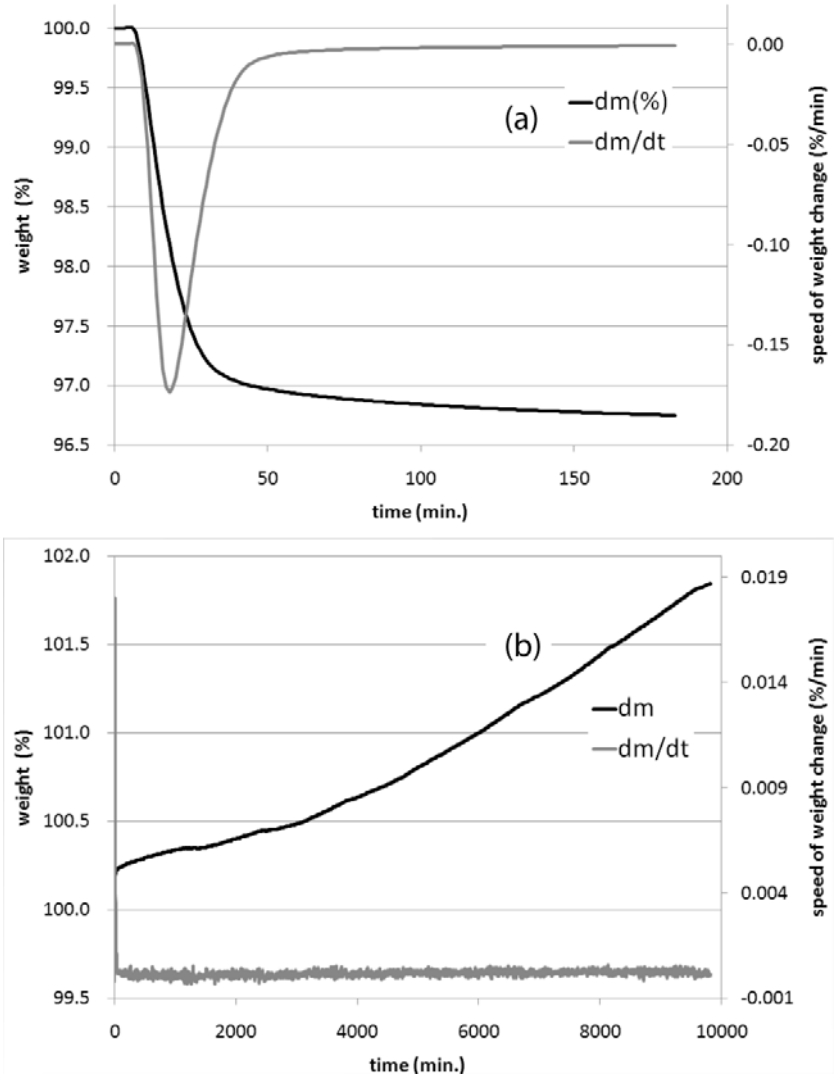

Figure 2-9 : DVS plots, measured at 25°C and 97% relative humidity, for (a) phase **M**, and (b) phase **H**. The transformation did not reach completion in the case of phase **H**, with the measurement stopped at 10000 mins.

From the experiments discussed above, it is clear that solvent exchange between **M** and **H** proceeds readily, but the transformations from **U** to either **M** or **H** proceed much more slowly. We now assess the extent to which the relative ease of these transformations can be rationalized on the basis of the structural properties of **M**, **H** and **U**.

2.4.4. Mechanistic Aspects of Solvent Exchange Transformations of M and H

As discussed above, the structures of **M** and **H** have similar hydrogen bonding units, and the relative arrangements of these hydrogen bonding units are shown in Figure 2-10(a) and 10(b) respectively. Although the stacking of hydrogen bonding units is different in these structures, both structures have clearly defined solvent channels (indicated by light blue dashed lines). In Figure 2-10(c) and 10(d), the structures are viewed along the direction of the solvent channel (*b*-axis for **M**; *c*-axis for **H**), showing a straight solvent channel in both cases. The existence of solvent channels often affects the ease of occurrence of solvation or desolvation processes. However, the experiments involving drying and exposure to vacuum of **M** and **H** did not induce desolvation and dehydration, and the stability to loss of methanol and water under these conditions may reflect the fact that the methanol and water molecules are held in these structures through robust hydrogen bonding. The stabilities of **M** and **H** under these conditions, in which solvent vapor is absent, suggest that interaction between solvent vapor and the crystalline solid plays a direct and important role in mediating the solvent exchange transformations in these materials.

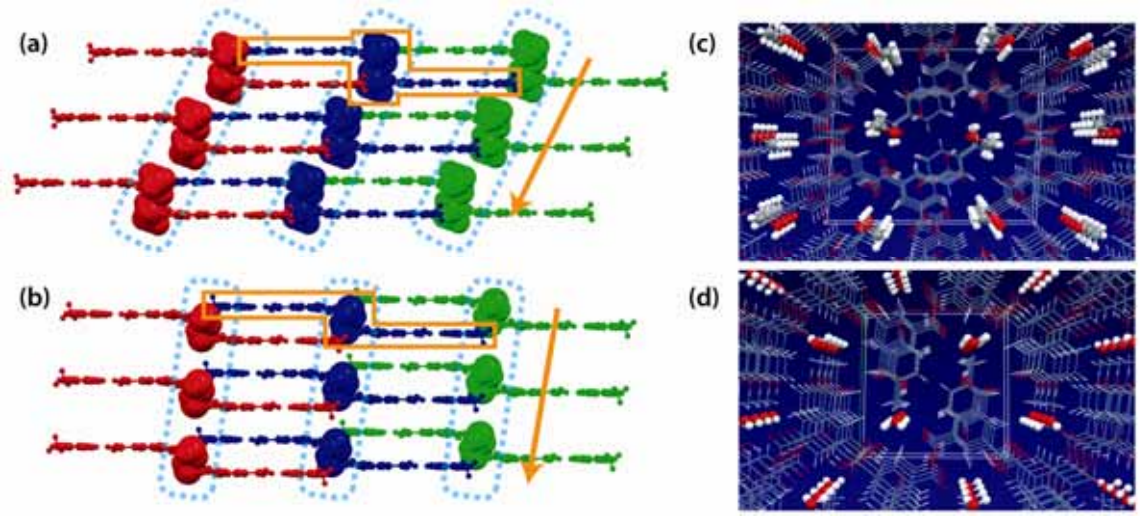

Figure 2-10 : Stacking of hydrogen bonding units in the crystal structures of (a) phase **M** and (b) phase **H**. The orange solid line shows a hydrogen bonding unit and the light blue dashed lines show the solvent channels. The figures on the right side show the crystal structures of (c) phase **M** viewed along the *b*-axis and (d) phase **H** viewed along the *c*-axis. The solvent molecules are shown as a ball-and-stick model.

From the structural similarities between **M** and **H** and the stabilities of the solvate structures (with respect to desolvation), it is expected that solvent exchange might occur through the solvent channel, with preservation of the hydrogen bonding unit, thus promoting the facile occurrence of the transformations between **M** and **H**. Furthermore, the fact that a significantly longer time is required for **U** to transform to the solvate phases **M** and **H** suggests that the solvent exchange transformations between **M** and **H** do not proceed via the unsolvated phase **U**.

2.4.5. Transformations from U to M or H

The structure of **U** (Figure 2-11, CCDC deposition number 602110) differs significantly from the structures of **M** and **H**, and comprises layers of **5MP** and **TMA** molecules (Figure 2-11(a)) with a hydrogen bonding scheme (Figure 2-11(b)) that is quite different from those in **M** and **H**. Given the differences in the hydrogen bonding schemes, and the absence of solvent channels, it is anticipated that the transformation from **U** to either **M** or **H** would involve

significant structural reorganization, which is reflected in the much longer transformation times observed. Although the powder sample of **U** does not appear to dissolve upon exposure to solvent vapors, the possibility that the transformations from **U** to **M** or **H** may proceed through the occurrence of local recrystallization cannot be ruled out.

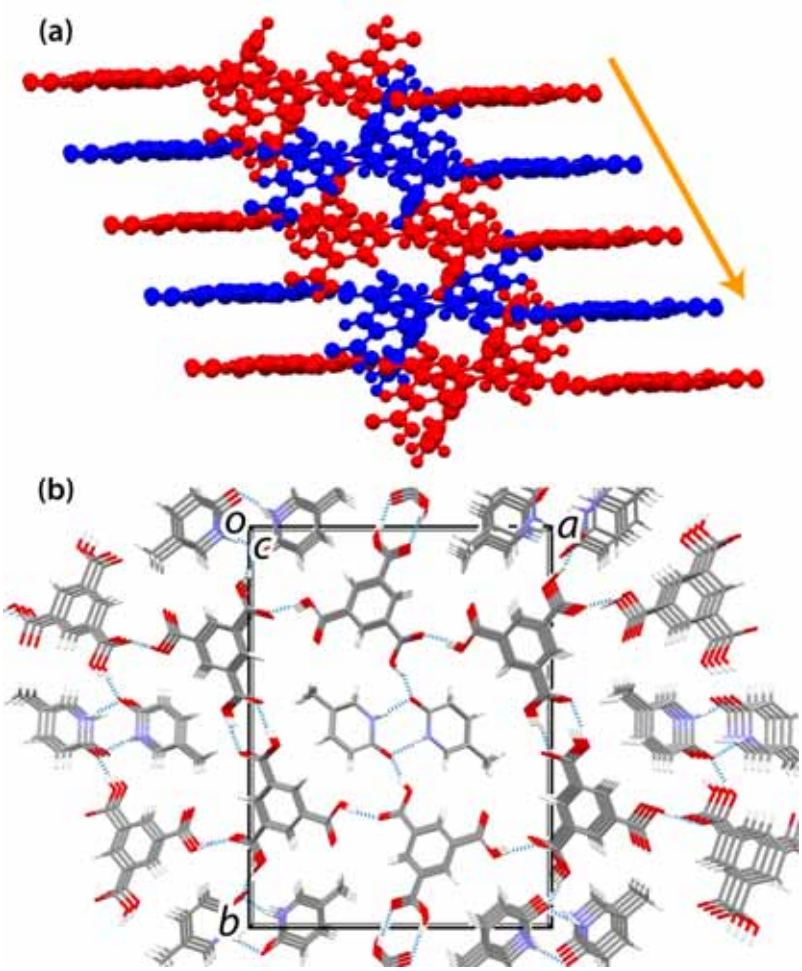

Figure 2-11 : Crystal structure of phase **U**: (a) showing the stacking of the layered structure, and (b) viewed along the *c*-axis [corresponding to the view along the arrow shown in (a)].

2.4.6. Photoreactivities

Finally, the difference of the photoreactivities is discussed. Although the methanol solvated **M** and hydrate **H** are not photoreactive for the **5MP** molecules by UV irradiation, the unsolvated crystal **U** is photoreactive and which produced [4+4] *cis-syn* dimer. In order to reveal the mechanism of such different photoreactivities, the nearest **5MP** pairs, which can be considered as the most reactable molecules in the crystal, in each crystal are investigated. As shown in Figure 2-12, the nearest **5MP** pairs have parallel olefin arrangement (the pairs are all related by symmetry operations, such as inversion center or translation operations) in there crystals. In such cases, it was said that the most important factor is the distance between the reaction center and the π-overlap of reacted olefin[43]. Generally, the distance between the reaction centers is less than 4.2Å for the reactive phase, however, the distances look sufficiently satisfy this condition in all cases (as shown in Figure 2-12 , **M** for 3.55Å,**H** for 4.08 Å,**U** for 3.84 Å). On the other hands, the degree of the π-overlaps, which can be evaluated by the displacement of double bonds upon projection, clearly suggest that the crystal **H** does not have suitable condition for the photo-dimerization reaction because the usual reactive double bond have less than 1.6Å[43]. However, if only the distances of reactive double bonds and the degree of the π-overlaps are compared between crystal **M** and **U**, crystal **M** has better conditions than crystal **U**. Thus these values cannot be considered as the sufficient criteria for understanding the photoreactivities of **5MP**. Thus another concept which is called “reaction cavity” was introduced into these crystals, in order to establish the precise criteria for understanding the photoreactivity of **5MP**. The reaction cavity defined by Y. Ohashi[45] was used here. The drawn reaction cavities of crystal **M**, **H** and **U**, and the calculated volume of the reaction cavities are also shown in Figure 2-12. Clearly the reaction cavities are different for these crystals and it was revealed that the reactive crystal **U** has the largest volume. In addition to the volume, the shape of reaction cavity of crystal **U** looks to have suitable space for approaching the 5MP pair than those of crystal **M** and **H**. Therefore, in the **5MP** case, the precise criteria of photoreactivity might be determined by their reaction cavity volumes and/or the cavity shape.

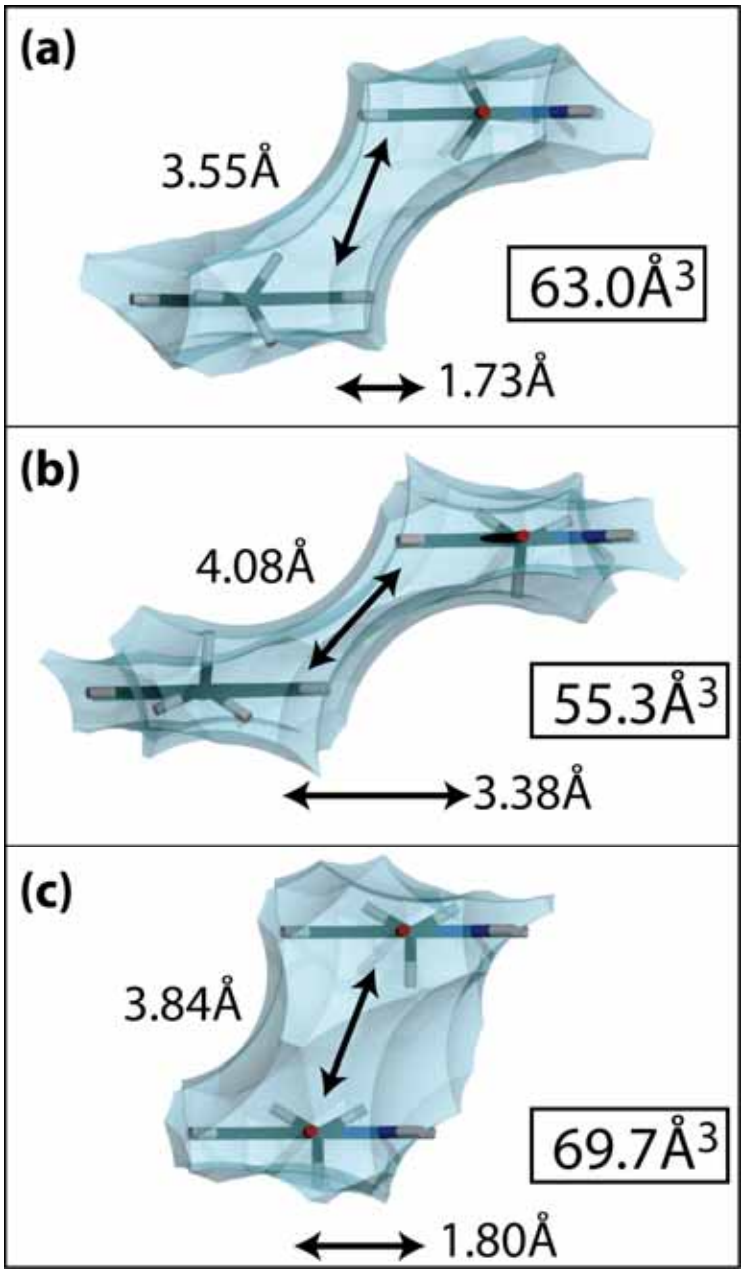

Figure 2-12 The nearest 5MP pair in the crystal (a) **M**, (b) **H**, and (c) **U**. The values show the distances of reactive double bonds, the displacement of double bonds upon projection, and the reaction cavity volume.

2.5. Concluding Remarks

As discussed above, a new hydrate co-crystal (**H**) of **5MP** and **TMA** has been obtained on grinding the methanol solvate co-crystal (**M**) of **5MP** and **TMA** under ambient conditions, and the structure has been determined directly from powder X-ray diffraction data. The transformation is a solvent exchange process induced by water vapor in the ambient atmosphere, and the role of grinding is primarily to accelerate the transformation. In order to obtain further insights regarding solvation and desolvation processes within this series of co-crystals, experiments involving exposure of the methanol solvate (**M**), hydrate (**H**) and unsolvated (**U**) co-crystals to different solvent vapors were carried out. The various transformations induced among these co-crystals by exposure to solvent vapors are summarized in Scheme 2-1.

For solvent exchange processes, aspects of the transformation mechanism may be understood by considering changes in the crystal structure and the rate of the transformation. The similarity of crystal structures (in terms of hydrogen bonding units) of **M** and **H**, and the fact that the rate of transformation from **M** to **H** is higher than the rate of transformation of **U** to form **M** or **H**, are consistent with the solvent exchange process occurring through the solvent channel, with the intermediate state preserving this channel and the basic hydrogen bonding unit. On the other hand, transformation of **U** to form solvate structures, upon exposure to solvent vapors, involves major structural changes, and consequently may require considerably longer time to complete the structural transformation.

In addition, we have found that desolvation processes of **M** and **H** may be induced by exposure of these materials to different solvent vapors (acetonitrile, ethanol and acetone), but not by exposure to other vapors (hexane or diethyl ether) or by drying or exposure to vacuum. These observations suggest that a certain degree of affinity between the solvent molecules included in the solid solvate structure and the solvent molecules in the vapor phase is necessary to induce such desolvation processes. One interesting point is that, in the cases reported here, exposure to solvent vapor is able to effect desolvation, whereas the physical forces of drying or exposure to vacuum are unable to effect desolvation. As shown in this paper, exposure of solid materials to solvent vapor can produce interesting and specific effects to modify solid state structures and

properties.

Reference

(1) Khankari, K. R.; Grant, D. J. W. *Thermochimica Acta* **1995**, 248, 61-79.

(2) Byrn, S.; Pfeiffer, R.; Ganey, M.; Hoiberg C.; Poochilian, G. *Pharm. Res.* **1995**, 12, 945-954.

(3) Kitagawa, S.; Uemura, K. Chem. Soc. Rev. **2005**, 34, 109-119.

(4) Kawano, M.; Fujita, M. *Coord. Chem. Rev.* 2007, 251, 2592-2605.

(5) Jacobs, A.; Faleni, N.; Nassimbeni, L. R.; Taljaard, J. H. *Cryst. Growth Des.* **2007**, 7, 1003-1006.

(6) Ramon, G.; Coleman, A. W.; Nassimbeni, L. R.; Taljaard, B. *Cryst. Growth Des.* **2005**, 5, 2331-2335.

(7) Jacobs, A.; Nassimbeni, L. R.; Su, H.; Taljaard, B. *Org. Biomol. Chem.* **2005**, 3, 1319-1322.

(8) Caira, M. R.; Nassimbeni, L. R.; Toda, F.; Vujovic, D. *J. Chem. Soc., Perkin Trans.* **2001**, 2, 2119-2124.

(9) Nassimbeni, L. R.; Kilkenny, M. L. *J. Chem. Soc. Dalton Trans.* **2001**, 1172–1175.

(10) Nakamatsu, S.; Toyota, S.; Jones, W.; Toda, F. *Chem. Commun.* **2005**, 3808-3810.

(11) Harris, K. D. M.; Tremayne, M. *Chem. Mater.* **1996**, 8, 554.

(12) Harris, K. D. M.; Tremayne, M.; Kariuki, B. M. *Angew. Chem. Int. Ed.* **2001**, 40, 1626.

(13) Chernyshev, V.V. *Russian Chem. Bull.* **2001**, 50, 2273.

(14) David, W. I. F.; Shankland, K.; McCusker, L. B.; Baerlocher, C., Ed.; *Structure Determination from Powder Diffraction Data*, OUP/IUCr, **2002**.

(15) Huq, A.; Stephens, P. W. *J. Pharm. Sci.* **2003**, 92, 244.

(16) Harris, K. D. M.; Cheung, E. Y. *Chem. Soc. Rev.* 2004, 33, 526.

(17) Tremayne, M. *Phil. Trans. R. Soc.* **2004**, 362, 2691.

(18) Favre-Nicolin, V.; Cerny, R. *Z. Kristallogr.* **2004**, 219, 847.

(19) Shankland, K.; Markvardsen, A. J.; David, W. I. F. *Z. Kristallogr.* **2004**, 219, 857.

(20) Brodski, V.; Peschar, R.; Schenk, H. *J. Appl. Crystallogr.* **2005**, 38, 688.

(21) Cerny, R. Croat. Chem. Acta **2006**, 79, 319.

(22) Karki, S.; Fabian, L.; Friscic, T.; Jones, W. *Org. Lett.* **2007**, 9, 3133.

(23) Tsue, H.; Horiguchi, M.; Tamura, R.; Fujii, K.; Uekusa, H. *J. Synth. Org. Chem. Japan* **2007**, 65, 1203.

(24) David, W.I.F.; Shankland, K. *Acta Crystallogr. Sect. A* **2008**, 64, 52.

(25) Harris, K. D. M.; Tremayne, M.; Lightfoot, P.; Bruce, P. G. *J. Am. Chem. Soc.* **1994**, 116, 3543.

(26) Cheung, E.Y.; Kitchin, S.J.; Harris, K.D.M.; Imai, Y.; Tajima, N.; Kuroda, R. *J. Am. Chem. Soc.* **2003**, 125, 14658–14659.

(27) Guo, F.; Harris, K. D. M. *J. Am. Chem. Soc.* **2005**, 127, 7314-7315.

(28) Mora, A. J.; Avila, E. E.; Delgado, G. E.; Fitch, A. N.; Brunelli, M. *Acta Cryst. B* **2005**, 61, 96-102.

(29) Platteau, C.; Lefebvre, J.; Affouard, F.; Willart, J. F.; Derollez, P.; Mallet, F. *Acta Cryst. B* **2005**, 61, 185-191.

(30) Guguta, C.; Meekes, H.; Gelder, R. *Cryst. Growth Des.* **2006**, 6, 2686-2692.

(31) Guo, F.; Cheung, E. Y.; Harris, K. D. M.; Pedireddi, V. R. *Cryst. Growth Des.* **2006**, 6, 846-848.

(32) Albesa-Jové, D.; Pan, Z.; Harris, K.D.M.; Uekusa, H. *Cryst. Growth Des.* **2008**, 8, 3641-3645.

(33) Hirano, A.; Toyota, S.; Toda, F.; Fujii, K.; Uekusa, H. *Angew. Chem. Int. Ed.* **2005**, 45 ,6013-6016.

(34) Visser, J. W. *J. Appl. Cryst.* **1969**, 2, 89-95.

(35) Wolff, P. M. *J. Appl. Cryst.* **1972**, 5, 243.

(36) Le Bail, A.; Duroy, H.; Fourquet, J.L. *Mater. Res. Bull.*, **1988**, 23, 447.

(37) Kariuki, B. M.; Serrano-González, H.; Johnston, R. L.; Harris, K. D. M. *Chem. Phys. Lett.* **1997**, 280, 189.

(38) Harris, K. D. M.; Johnston, R. L.; Kariuki, B. M. *Acta Crystallogr., Sect. A*: Found Crystallogr. **1998**, 54, 632.

(39) Turner, G. W.; Tedesco, E.; Harris, K. D. M.; Johnston, R. L.; Kariuki, B. M. *Chem. Phys. Lett.* **2000**, 321, 183.

(40) Habershon, S.; Harris, K. D. M.; Johnston, R. L. *J. Comp. Chem.* **2003**, 24, 1766.

(41) Cheung, E. Y.; McCabe, E. E.; Harris, K. D. M.; Johnston, R. L.; Tedesco, E.; Raja, K. M. P.; Balaram, P. *Angew. Chem. Int. Ed.* **2002**, 41, 494.

(42) Rietveld, H. M. 1969, *J. Appl. Cryst.* **1969**, 2, 65-71.

(43) Larson, A. C.; Von Dreele, R. B. *GSAS*; Los Alamos Laboratory Report No. LA-UR-86-748; Los Alamos National Laboratory: Los Alamos, NM, **1987**.

(44) V. Ramamurthy, K. Venkatesan, *Chem. Rev.* **87**, 433, (1987).

(45) Y. Ohashi, K. Yanagi, T. Kurihara, Y. Sasada, Y. Ohgo, *J. Am. Chem. Soc.* **103**, 5805 (1981).

Chapter 3

Dehydration and Hydration of Lisinopril

3.1. Abstract

A widely used anti-hypertension drug, lisinopril is known to be obtained as dihydrate form by recrystallization and the dihydrate form was known to undergo two step dehydration via monohydrate form. Such a dehydration is very important in the pharmaceutical area because such solid state transformations usually affect to the pharmaceutical properties such as solubility, dissolution rate, bioavailability and so on. However, although crystal structures of these hydrates or anhydrous form are necessary for understanding the transformation mechanisms and the properties of resulted forms, there is no report on their crystal structures because of difficulty to obtain a single crystal for these forms. Thus, in the present work, crystal structures of lisinopril dihydrate, monohydrate and anhydrous forms are determined from powder X-ray diffraction data and the mechanistic aspects of two step dehydration process has been established from the crystal structural changes. Furthermore, the hydration mechanisms of monohydrate and anhydrous forms were clearly understood from these crystal structures and it was revealed that the hydration process is not a simple reverse pathway of the dehydration process. Finally, DVS measurements were carried out and the results clearly support these dehydration and hydration mechanisms.

3.2. Introduction

Many organic crystalline solids can exist as polymorphs, hydrates or solvates, or the combination of these. The existence of these alternative crystalline phases is critical problem, especially for the pharmaceutical compounds, because these alternative phases usually have different physical or chemical properties which are important for the drug use, such as solubility, dissolution rate, stability and bioavailability[(1)(2)]. Thus, well investigation about the existence of alternative phases and well understanding about their properties are very important for pharmaceutical compounds. Also, understanding the transformation mechanism among these alternative phases is very important, because such transformations are frequently occurred during the drug manufacturing process or upon storage of the drug substance or dosage form[(3)].

Grant *et. al.* reported the nature of pharmaceutical hydrates and he showed many analytical techniques for understanding the properties of pharmaceutical hydrates and the mechanistic aspects of the hydration or dehydration processes[(4)]. Among these analytical techniques, crystal structure analysis is one of the powerful techniques to understand the mechanistic aspects of the hydration or dehydration process. According to such background, there are several literatures which focused on the mechanistic aspects of hydration or dehydration process using single crystal structure analysis technique[(5)(6)]. However, in many cases, single crystals of the starting phase are found to disintegrate to produce a polycrystalline material upon dehydration or hydration process, thus limiting the opportunities to obtain information on the structural changes associated with such processes by single crystal X-ray diffraction analysis. In some cases, it might be possible to obtain a single crystal of the transformed phase (as confirmed by comparison of powder X-ray diffraction data) by another crystallization method, but in many cases, single crystals of the dehydrated or hydrated phase cannot be obtained by any other method. Techniques for carrying out structure determination directly from powder X-ray diffraction data are clearly essential for structural characterization of the polycrystalline product materials obtained directly in such dehydration or hydration.

The opportunities for carrying out complete structure determination of organic molecular materials from powder X-ray diffraction data have developed considerably in recent years[(7)-(19)], particularly through the development of the

direct-space strategy for structure solution[20]. Because these techniques have the potential to provide structural understanding of polycrystalline products obtained from solid state transformations (e.g. originating from single crystal materials of the type discussed above), these techniques have a key role to play in understanding structural properties of materials produced from solid state grinding processes, solid state reactions, desolvation processes, and polymorphic transformations[21]-[28].

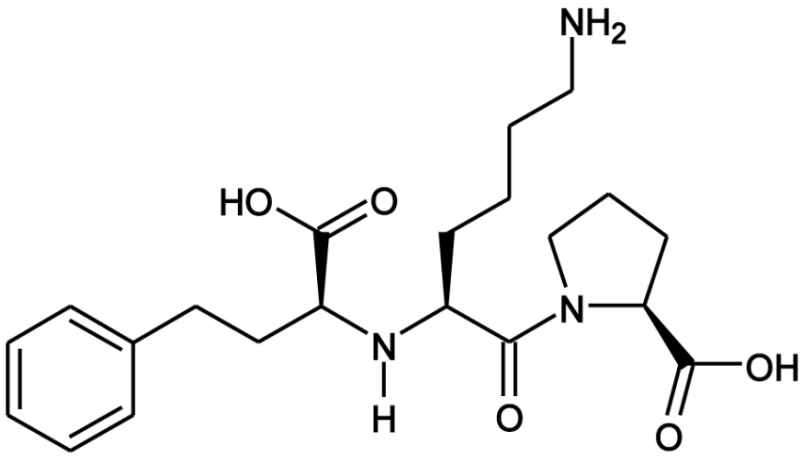

Figure 3-1 : Molecular structure of Lisinopril.

In the present work, lisinopril was focused for the target compound for the systematic understanding about the pharmaceutical dehydration or hydration process. Lisinopril (N2-[(S)-1-carboxy-3-phenylpropil]-L-lysyl)-L-proline,) is widely used anti-hypertension drug, based on the ability to inhibit the activity of angiotensin-converting enzyme (ACE)[30]-[32]. The inhibiting activity of lisinopril is considered to be related to the ability to interact with ACE, thus, there were several studies to investigate the interaction between lisinopril and ACE[33][34] or metal ion[35][36] (because ACE is known as zinc metalloenzyme) from crystal structure analysis. Dihydrate form is known as the most stable crystalline form which is used as ethical medicine and is known to dehydrate via monohydrate form to anhydrous form by temperature elevating[37][38]. However, because of difficulty to obtain a single crystal which is suitable size for diffraction measurement, there is no structural report for these lisinopril crystalline phases, including stable dihydrate form. Thus, the structural information of hydrates and

the mechanism of dehydration or hydration process are unknown. In the present study, in order to reveal the structural properties and mechanistic aspects of dehydration or hydration, crystal structures of lisinopril hydrates, including anhydrous form, were determined from powder diffraction data.

3.3. Experiment

3.3.1. Preparation

Lisinopril dihydrate was purchased from Wako Pure Chemical Industries, Ltd. Recrystallization of lisinopril from water solution gave pure powdered dihydrate form and was used for synchrotron X-ray diffraction measurement, thermal analysis(TG/DTA, DSC, XRD-DSC) and dynamic vapor sorption experiments. The preparation of monohydrate and anhydrous forms for synchrotron X-ray powder measurement is described in the synchrotron measurement section.

3.3.2. Thermal analysis

TG/DTA was measured on a Rigaku Thermo Plus 2. 6.026 mg of lisinopril dihydrate form was heated in a rate of 0.5 K/min. The TG curve was recorded from 27°C up to 180°C under a dry nitrogen atmosphere with a flux of 100 ml/min. The simultaneous DSC and X-ray diffraction measurement (XRD-DSC) was performed on a Rigaku D/MAX 2400 diffractometer and a Rigaku Thermo Plus 2 differential scanning calorimeter at a heating rate of 3°C/min.

3.3.3. Dynamic Vapor Sorption

Dynamic vapor sorption was measured on Dynamic vapor sorption – advantage (SMS Ltd, UK). 3.96 mg of powdered dihydrate form was mouted on a valence and the dehydration process was monitored by mass change at 38.7°C with relative humidity 0% condition. After complete dehydration, relative humidity was set to 10 % and hydration process was measured for anhydrous form. The measurement was continued until no mass change was observed.

3.3.4. Synchrotron X-ray powder diffraction measurement

Synchrotron X-ray powder diffraction data were recorded for lisinopril dihydrate form at ambient condition on beamline 4B2 (Multiple Detector System) at Photon Factory, Tsukuba, Japan with wavelength 1.20853 (2) Å. The sample was mounted on flat sample holder and diffraction measurement was performed using reflection mode with rotation of sample holder. Data collection

time was ca. 12 hours.

For monohydrate and anhydrous forms, synchrotron X-ray powder diffraction data were recorded on beamline BL19B2 at SPring-8 (Debye-Scherer camera equipped with a curved Imaging Plate detector). Because monohydrate form easily returns to dihydrate form at ambient condition and the transformation temperature of dihydrate to monohydrate form and monohydrate to anhydrous form is not sufficiently separate, monohydrate form is difficult to prepare purely. However, pure monohydrate form was successfully prepared by slow temperature elevating of dihydrate form, which was introduced into 0.3 mm diameter borosilicate glass capillary without sealed, on the goniometer. Thus, synchrotron powder X-ray diffraction measurement was carried out *in situ* condition at 84°C with sample spinning and wavelength 1.20033 (1) Å. The data collection time was 20 minutes. Also, lisinopril anhydrous form easily returns to dihydrate form as well as monohydrate form at ambient condition, however, hydration of anhydrous form can be prevented in a dried condition, so that the synchrotron measurement was performed at ambient condition using sealed 0.3 mm diameter borosilicate glass capillary. The measurement was performed with wavelength 1.19770(1) Å and the data collection time was 60 minutes.

3.4. Results and Discussion

3.4.1. Thermal Analysis

As already reported, two step dehydration can be seen by two DTA endothermic peaks (Figure 3-2). The mass decrease of 4.1% for first dehydration and 8.5% for second dehydration suggests the existence of monohydrate form. In order to characterize these forms, XRD-DSC measurement (simultaneous XRD and DSC measument) was carried out for dihydrate form. The XRD pattern changes were observed by first and second dehydration process (Figure 3-3). As shown in close-up XRD pattern (Figure 3-4), dihydrate form and monohydrate form have quite similar XRD pattern, although anhydrous form has different XRD pattern from those of dihydrate and monohydrate forms. These results indicate that the first dehydration takes small structural change and the second dehydration takes lager structural change than that of first dehydration process. In order to reveal the structural changes in detail, crystal structure analyses were carried out for dihydrate, monohydrate and anhydrous form. Unfortunately, suitable single crystal for X-ray diffraction was not obtained for dihydrate form by recrystallization from solution, thus, all crystal structures were determined from powder X-ray diffraction data.

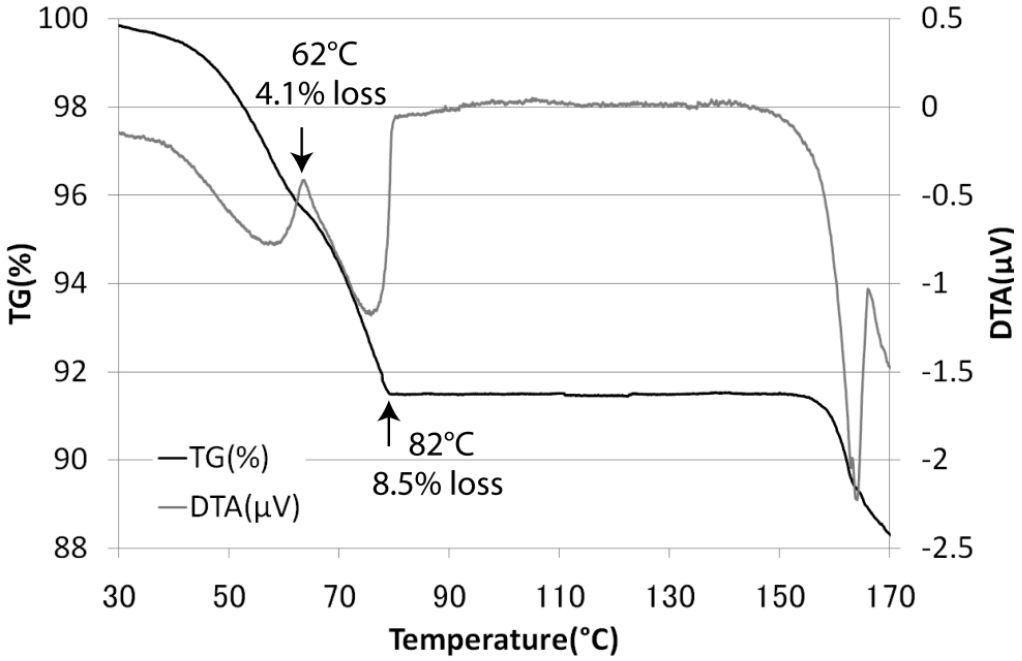

Figure 3-2 : TG/DTA plot of lisinopril dihydrate form.

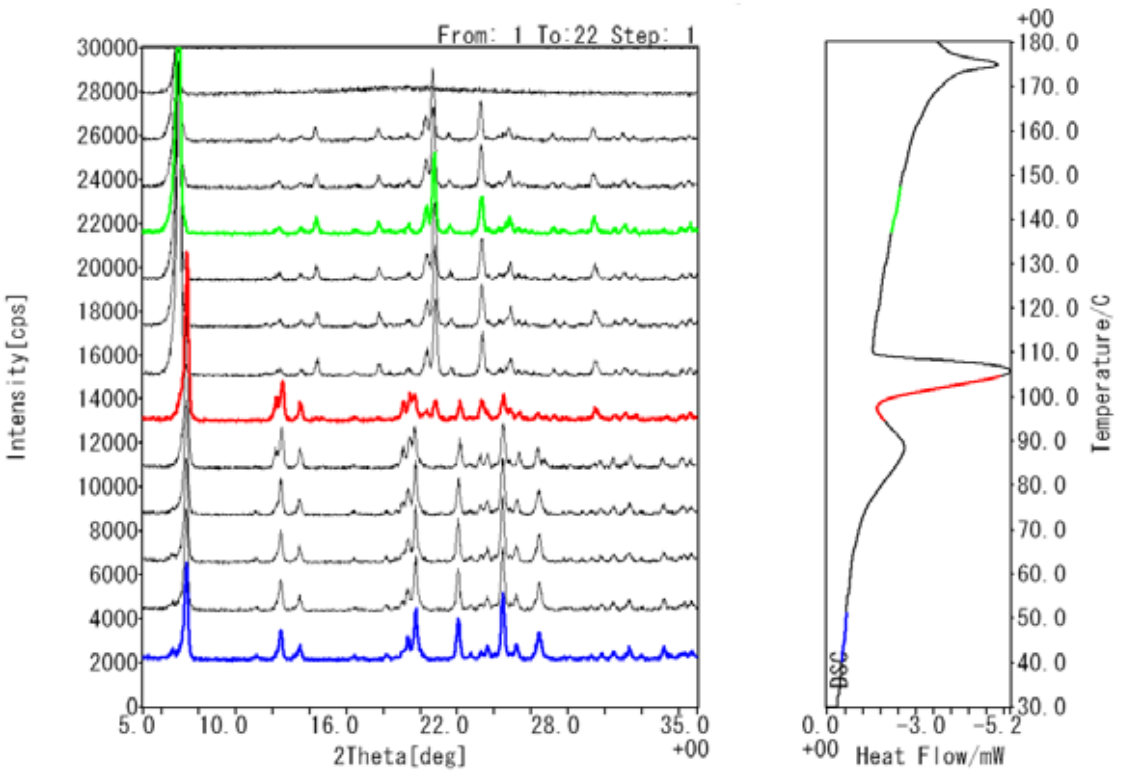

Figure 3-3 : XRD-DSC plot of lisinopril dihydrate form

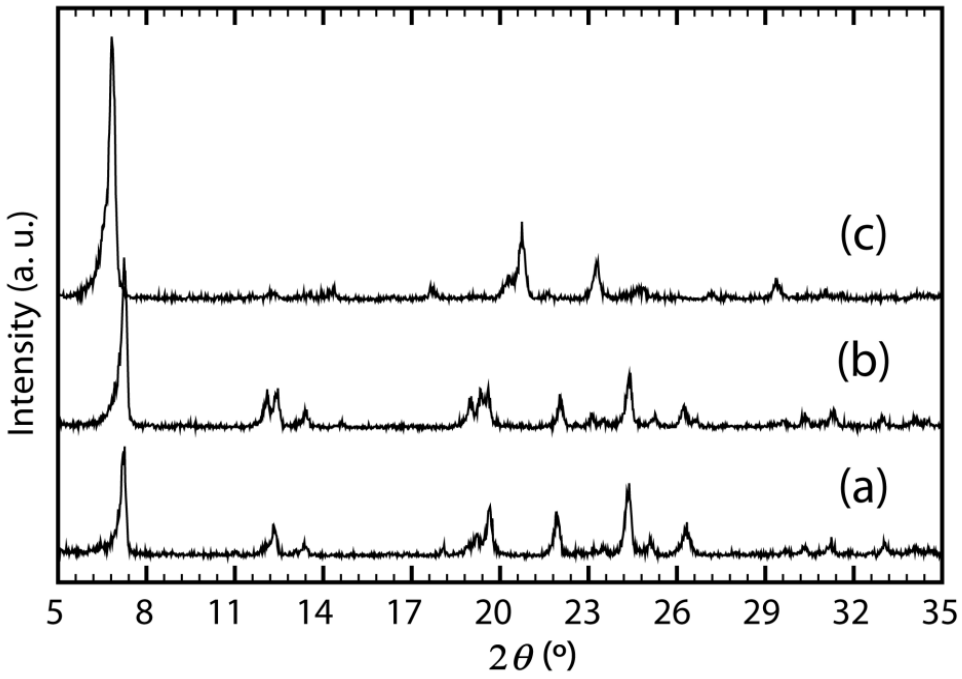

Figure 3-4 : XRD patterns of Lisinopril (a) dihydrate, (b) monohydrate and (c) anhydrous form, measured on XRD-DSC instrument.

3.4.2. Structure Determination from Powder X-ray Diffraction Data

The powder X-ray diffraction pattern of dihydrate form was indexed using the program DICVOL04[39] giving the following unit cell (M20 = 39.7[40], F20 = 139.7[41]) with monoclinic metric symmetry: a = 14.6516 Å, b = 5.9015 Å, c = 14.2884 Å, β = 113.162°, V = 1135.89 Å^3. Given the volume of this unit cell, and consideration of density, the number of formula units in the unit cell is assigned as Z = 2. From the estimated Z value and systematic absences, the space group was determined as $P2_1$. Profile fitting using the Pawley method[42] gave a good quality fit with R_{wp} = 9.55% and χ^2 = 17.240(these values were calculated on background subtracted intensity). Structure solution was carried out using the simulated annealing method incorporated in the program DASH[43]. The structural fragment comprised one lisinopril molecule and two waters, representing a total of 24 structural variables. Twenty runs with 10^7 simulated annealing moves per run were performed for structure solution. The best solution had *profile* χ^2 73.70 and *intensity* χ^2 66.25. Following structure solution, Rietveld refinement[44] was carried out using the GSAS program[45]. Standard restraints were applied to bond lengths and bond angles, planar restraints were applied to aromatic rings, and a global isotropic displacement parameter was used. The final Rietveld refinement gave following parameters: a = 14.6607(1) Å, b = 5.91012(6) Å, c = 14.3052(1) Å, β = 113.1447(6)°, V = 1139.73(2) Å^3, R_{wp} = 5.83%, R_p = 4.40%, R_F^2 = 6.30% (corresponding Le Bail profile fitting gave R_{wp} = 4.08%, R_p = 2.95%). The final Rietveld plot is shown in Figure 3-5a.

The powder X-ray diffraction pattern of monohydrate form was analyzed with the same manner with dihydrate form. The indexed unit cell was a = 14.6610 Å, b = 5.9094 Å, c = 14.2186 Å, β = 112.859°, V = 1135.13 Å^3 (DICVOL04, M20 = 83.6, F20 = 278.1, monoclinic) and which is similar with the unit cell of dihydrate form, thus, the space group was determined as $P2_1$ which is same with dihydrate form. Profile fitting using the Pawley method gave a good quality fit with R_{wp} = 10.35% and χ^2 = 3.171. The structure was determined by the program DASH (structural fragment comprised one lisinopril molecule and one water, representing a total of 21 structural variables) and twenty runs with 10^7 simulated annealing moves per run gave the best solution with *profile* χ^2 8.33 and *intensity* χ^2 40.24. The final Rietveld refinement (GSAS) gave following

parameters: a = 14.6677(3) Å, b = 5.9124(1) Å, c = 14.2254(3) Å, β = 112.880(1)°, V = 1136.58(5) Å^3, R_{wp} = 4.90%, R_p = 3.44%, R_F^2 = 11.14% (corresponding Le Bail profile fitting gave R_{wp} = 3.23%, R_p = 2.41%). The final Rietveld plot is shown in Figure 3-5b.

Also, the powder X-ray diffraction pattern of anhydrous form was analyzed with the same manner with dihydrate form and monohydrate form. The indexed unit cell was a = 14.6193 Å, b = 5.9409 Å, c = 14.2894 Å, β = 116.527°, V = 1110.41 Å^3 (DICVOL04, M20 = 57.3, F20 = 196.0, monoclinic) and which is similar with the unit cell of dihydrate form, thus, the space group was determined as $P2_1$ which is same with dihydrate form. Profile fitting using the Pawley method gave a good quality fit with R_{wp} = 19.80% and χ^2 = 25.574. The structure was determined by the program DASH (structural fragment comprised one lisinopril molecule, representing a total of 18 structural variables) and twenty runs with 10^7 simulated annealing moves per run gave the best solution with *profile* χ^2 89.58 and *intensity* χ^2 42.51. Because the measured sample contained some dihydrate form, multi phase Rietveld refinement was performed for anhydrous form with dihydrate form as Le Bail refinement mode. The final Rietveld refinement gave following parameters: a = 15.1769 (3) Å, b = 5.94511(8) Å, c = 14.2291 (3) Å, β = 120.6209(9)°, V = 1104.84 (4) Å^3, R_{wp} = 6.56%, R_p = 4.35%, R_F^2 = 4.69% (corresponding Le Bail profile fitting gave R_{wp} = 3.89%, R_p = 2.50%). The final Rietveld plot is shown in Figure 3-5c.

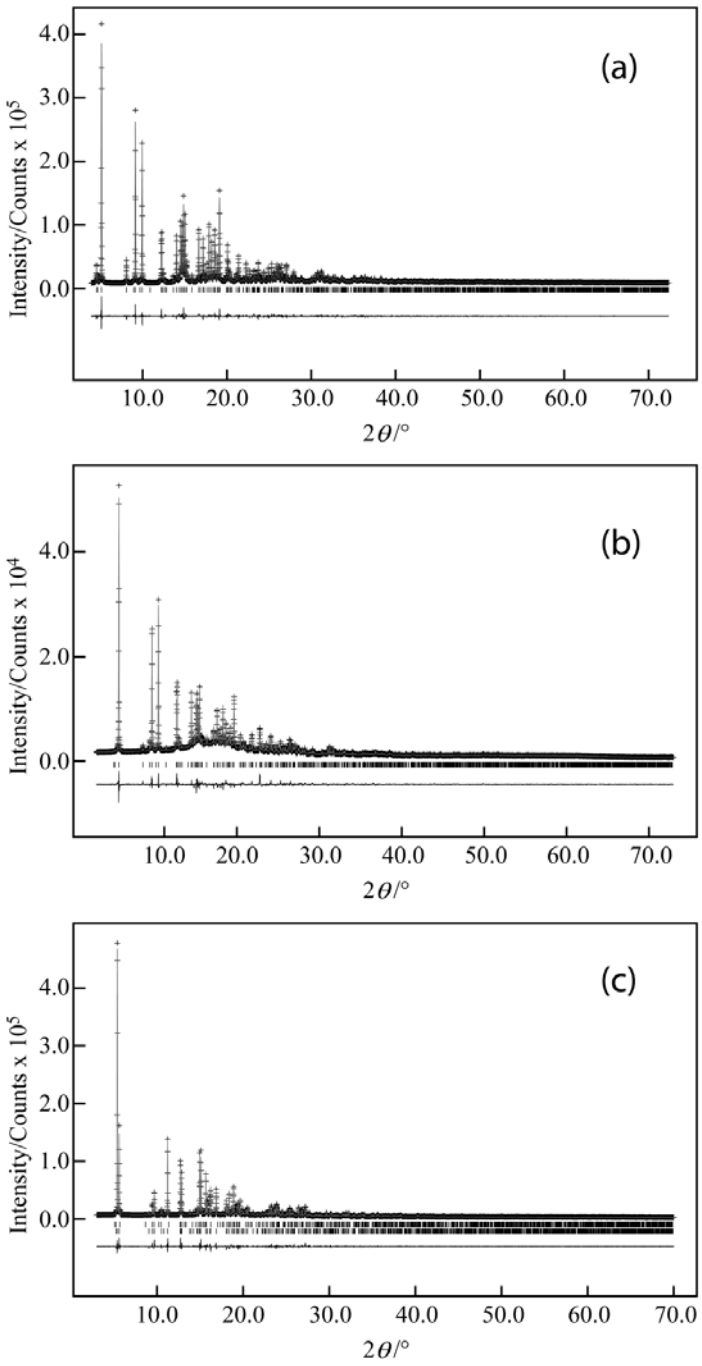

Figure 3-5 : Final Rietveld refinement for Lisinopril (a) dihydrate form, (b) monohydrate form and (c) anhydrous form, showing the experimental powder X-ray diffraction pattern (+ marks), calculated powder X-ray diffraction pattern (solid line) and difference profile (lower line). Tick marks indicate peak positions. For anhydrous form (c), upper and lower tick mark indicate peak positions of anhydrous form and impurity dihydrate form, respectively.

3.4.3. Crystal Structure of Dihydrate Form

As shown in Figure 3-6(a), lisinopril dihydrate form has a stacking of lisinopril molecule along the *b* axis (2_1 screw axis) and it makes two types of water channels. One channel is labeled as central channel, which exists at the center of unit cell, and the other channel is labeled as side channel, which exists at the side of unit cell (Figure 3-6(a)). In these two channels each water molecules are hydrogen bonded to adjacent water and lisinopril molecules. Figure 3-7 shows hydrogen bonds of these two waters in dihydrate form. In the side channel water (H62-O61-H63), there are three types of hydrogen bonds for one water molecule, O61-H62…N13' (O…N, 2.80Å), O61-H63…O11'' (O…O, 2.84Å), O11-H40…O61 (O…O, 2.65Å). The central channel water is, also, connected by three hydrogen bonds, however, two of them are equivalent O65-H65…O64 (O…O, 3.10Å) hydrogen bond and the other is O64-H66…O12 (O…O, 2.86Å) hydrogen bond. Comparing these hydrogen bonds of the side and central channel waters, it is obvious that the side channel water has shorter hydrogen bonds than those of the central channel water. The difference of hydrogen bond distances indicates that the side channel water is the stronger hydrogen bonded than the central channel water. From these considerations, it is natural to expect that the weaker hydrogen bonded central channel water will be released in the first dehydration, and subsequently the side channel water will be released in the second dehydration process.

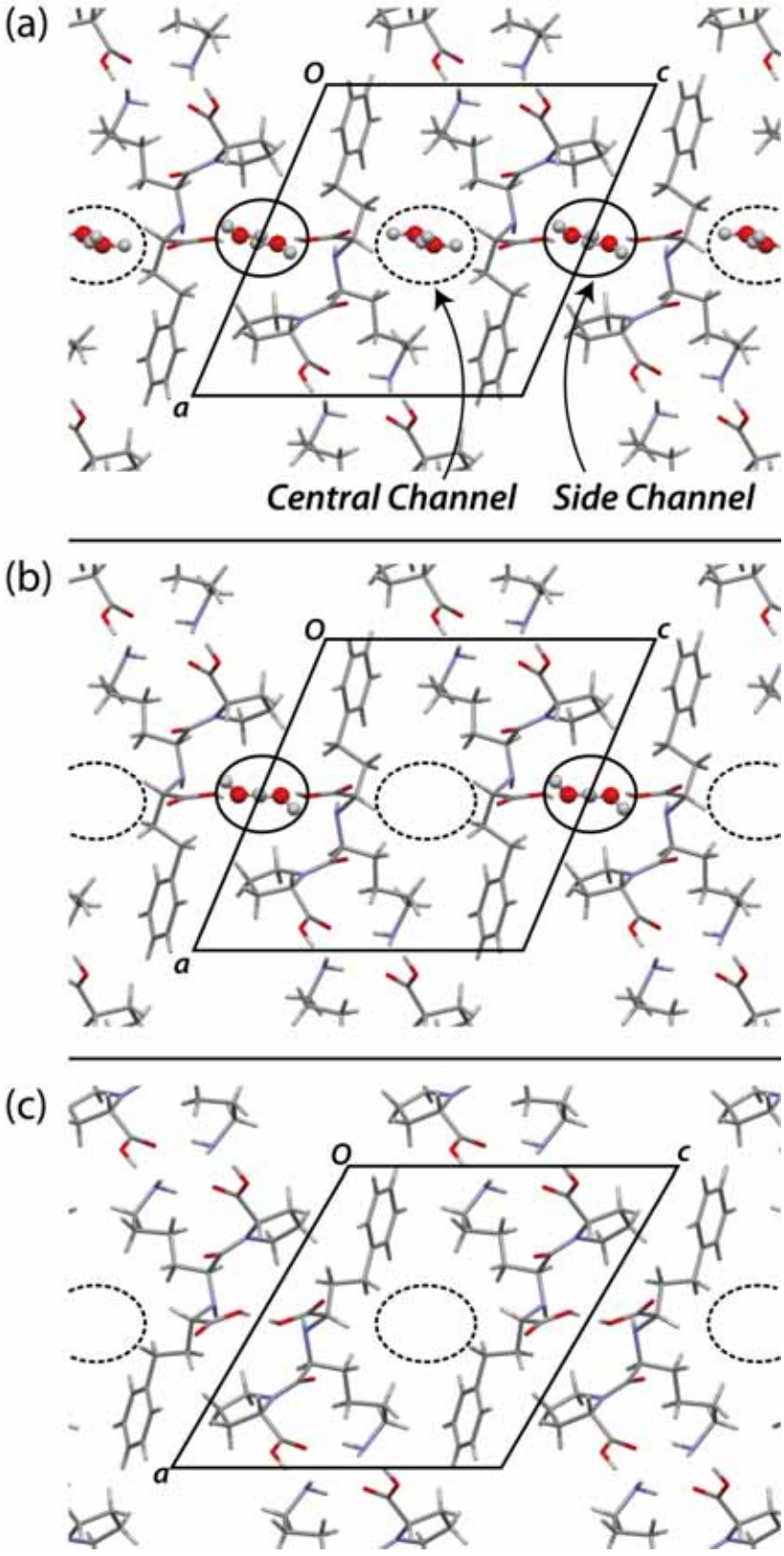

Figure 3-6 : Crystal structures of Lisinopril (a) dihydrate, (b) monohydrate and (c) anhydrous form, view along the *b* axis.

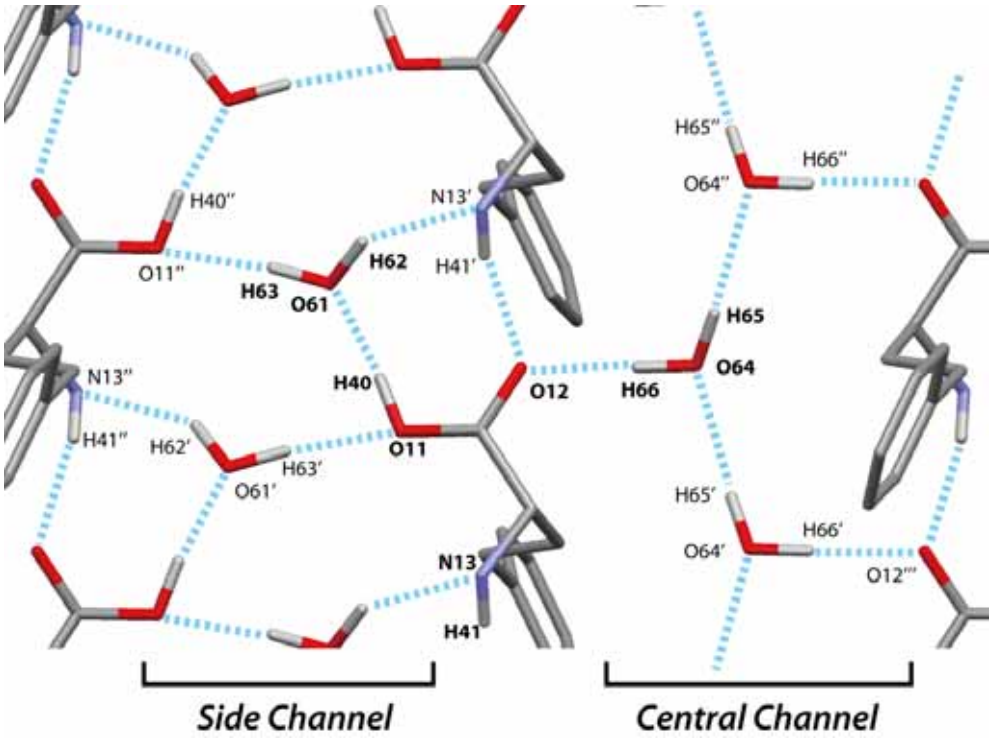

Figure 3-7 : Side view of water channels in lisinopril dihydrate form. Sky blue dash lines show the hydrogen bonds.

3.4.4. Crystal Structure of Monohydrate Form and Mechanism of First Dehydration

Figure 3-6(b) shows the crystal structure of monohydrate form view along the *b* axis. The crystal structure of monohydrate form has similar packing that of dihydrate structure with same space group $P2_1$ and molecular stacking exists along the *b* axis according to the 2_1 screw axis. As expected from the structure of dihydrate form, the central channel water was removed in this structure. However, interestingly, after removal of central channel water, the channel was not closed and a vacant channel remains in its structure.

Generally, such a large empty channel is considered as unstable structure and, in such dehydration processes, the conformational changes or modifications of molecular arrangement are required (for example see ref. (5),(6)). The vacant channel volume is calculated to be 67.9 $Å^3$ per unit cell[46] and the central channel volume of dihydrate form is calculated to be 75.0 $Å^3$ per unit cell. Even allowing a consideration about the difference in temperature conditions for

synchrotron measurement (357K for monohydrate form and at ambient temperature (ca. 300K) for dihydrate form.), the central channel volume is significantly decreased after first dehydration. The reason of such volume decrease can be explained by the force to close the vacant central channel. The decrease of the central channel volume is considered to affect the hydrogen bonds in the side channel and the hydrogen bond lengths in the side channel are somewhat increased averagely compare to those of dihydrate structure, O61-H62…N13' (O…N, 2.73Å), O61-H63…O11'' (O…O, 2.93Å), O11-H40…O61 (O…O, 2.80Å).

Although it is difficult to establish the reason of why the vacant central channel is not closed, one of the reasons can be considered from the structure in the central channel. As shown in the Figure 3-7, it is obvious that the central channel does not have well defined hydrogen bond donor or acceptor, such as carboxylic acid or amine which can be seen in the side channel. The absence of strong hydrogen donor or acceptor means that the large stabilization by conformational change in the central channel is not expected and the conformational change might not be necessary in this vacant channel.

On the other hands, there is not significant structural change in the side channel except the extension of hydrogen bonds as discussed above. Thus, the structural change in first dehydration process is only loss of water of the central channel. The small structural change is consistent with the similarity of XRD pattern (Figure 3-4). There is no significant change for unit cell constants and molecular packing and conformation, the diffraction positions and intensities are to be quite similar. However, the existence of the vacant central channel (67.9 $Å^3$ per unit cell) is considered as the reason of instability for a vapor and the vacant central channel will take in water (volume of a water is ca. 32$Å^3$) readily, thus the monohydrate form easily returns to dihydrate form.

3.4.5. Crystal Structure of Anhydrous Form and Mechanism of Second Dehydration

Crystal structure of anhydrous form is shown in Figure 3-6(c). Anhydrous form has also similar packing with those of dihydrate and monohydrate form. However, the large difference can be seen in the closed side channel. In the second dehydration process, water of the side channel was removed and the

side channel was closed. The interesting point is a twist motion of ethylphenyl substitute of lisinopril molecule which is accompanied of closing of the side channel. Because of steric repulsion, lisinopril molecules cannot approach each other to close the side channel with retaining its conformation. Thus, the twist of ethylphenyl substitute about 160° make the suitable conformation to approach each other and it enables to close the side channel.

The hydrogen bonds in the closed side channel are shown in Figure 3-8. Instead of water mediated hydrogen bonds which exists in dihydrate and monohydrate structure, there are O11-H40...N13' (O…N, 3.05Å) and N13''-H41''...O12 (N...O, 3.13Å) hydrogen bonds. In addition, a weak O11-H40…O11' (O…O, 3.48Å) hydrogen bond is observed. These hydrogen bonds are relatively long (standard O…O is 2.8Å and O…N is 2.7Å) and are far from ideal hydrogen bond conditions. However, under the restrictions of molecular shape or crystal packing effect, so that it can be considered that it is difficult to construct ideal hydrogen bonds. The non-ideal hydrogen bonding conditions can be considered as one of the reasons of instability of anhydrous form and why dihydrate form usually appears by recrystallization.

The primary reason of easy hydration of anhydrous form is the existence of the vacant central channel which is also observed in monohydrate form. The vacant central channel volume of anhydrous structure is 96.0Å^3 per unit cell. This volume is significantly larger than that of monohydrate central channel (67.9 Å^3 per unit cell). This volume is also significant size to take in a water as well as monohydrate structure and this can be considered as the primary reason of easy hydration.

The reason of increasing of the vacant central channel can be explained from the channel closing motion of the side channel. By closing of the side channel, lisinopril molecules translated to the opposite direction from the central channel, in order to construct hydrogen bonds in the side channel as explained above, thus, as a result, the volume of the vacant central channel is increased in anhydrous strcture. In another view point, the reason of why the side channel was closed and the vacant central channel was increased can be explained by the difference of the existence of hydrogen bond donor and acceptor in these two channels. Although the central channel does not have definitive hydrogen bond donor or acceptor, the side channel has relatively strong hydrogen bond donor and acceptor (carboxylic acid and secondary amine). The existence of

relatively strong hydrogen bond donor and acceptor in the side channel might cause the interaction between each other to construct the more stable conditions, thus, the closing motion of the side channel might occur. On the other hands, large stabilization by closing of the central channel cannot be expected because of the nonexistence of well defined hydrogen bond donor or acceptor. From this reason, the central channel does not close and it retains the vacant channel.

The difference of XRD pattern of anhydrous form from those of dihydrate and monohydrate form can be explained from the change of crystal structure in the second dehydration process. The change of diffraction intensities comes from closing of the side channel and the change of diffraction peak positions comes from the change of unit cell parameters which is due to the closing of the side channel.

3.4.6. Hydration Mechanism

The dehydration mechanism is clearly revealed from the structural change in two step dehydration process. Now, we focus on the mechanistic aspects of hydration process. As mentioned above, the reason of why monohydrate and anhydrous forms easily return to dihydrate form can be explained from the existence of the vacant central channel which is formed in the first dehydration process. If this expectation is correct, it can be said that the hydration process is not a simple reverse of dehydration process, because the dehydration of dihydrate form was start from the central channel. In order to confirm the difference of the dehydration and hydration process, DVS measurement were carried out for dihydrate form and anhydrous form. The mass changes of the dehydration and hydration process were shown in Figure 3-9. The observed mass decrease in dehydration process was 8.37% and mass increase in hydration process was 8.22%. These mass change is corresponding to two water molecules (ideal mass % for one water is 4.08%). In the dehydration process, two step mass changes were observed which can be seen as the rate change of mass change, however, there is no rate change in the hydration process and it proceeded in one step. These results clearly suggest the difference of hydration and dehydration pathway and also it can be concluded that the hydration process is not a simple reverse process of dehydration process. Unfortunately, the hydration completed in 15 mins while only in the condition of 10% relative

humidity, so that it is difficult to observe the XRD change in hydration process. However, from the DVS observation, it is obvious that the hydration is not a simple reverse of the dehydration process and anhydrous form might be directly converted to dihydrate form. The fact of that the anhydrous form for the synchrotron measurement contained some dihydrate form also suggests the direct conversion from anhydrous form to dihydrate form. In the diffraction pattern of anhydrous form, any monohydrate peaks or another unknown form was not observed.

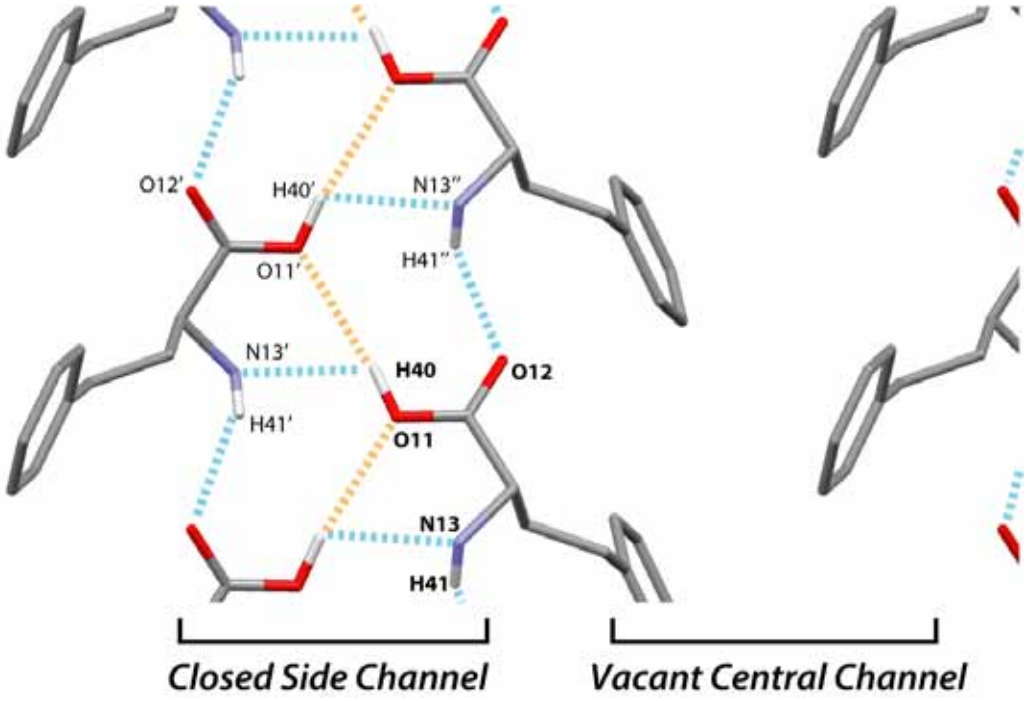

Figure 3-8 : Side view of closed side channel and vacant central channel in lisinopril anhydrous form. Sky blue dash lines show the hydrogen bonds. Pale orange dash lines show the weak hydrogen bonds.

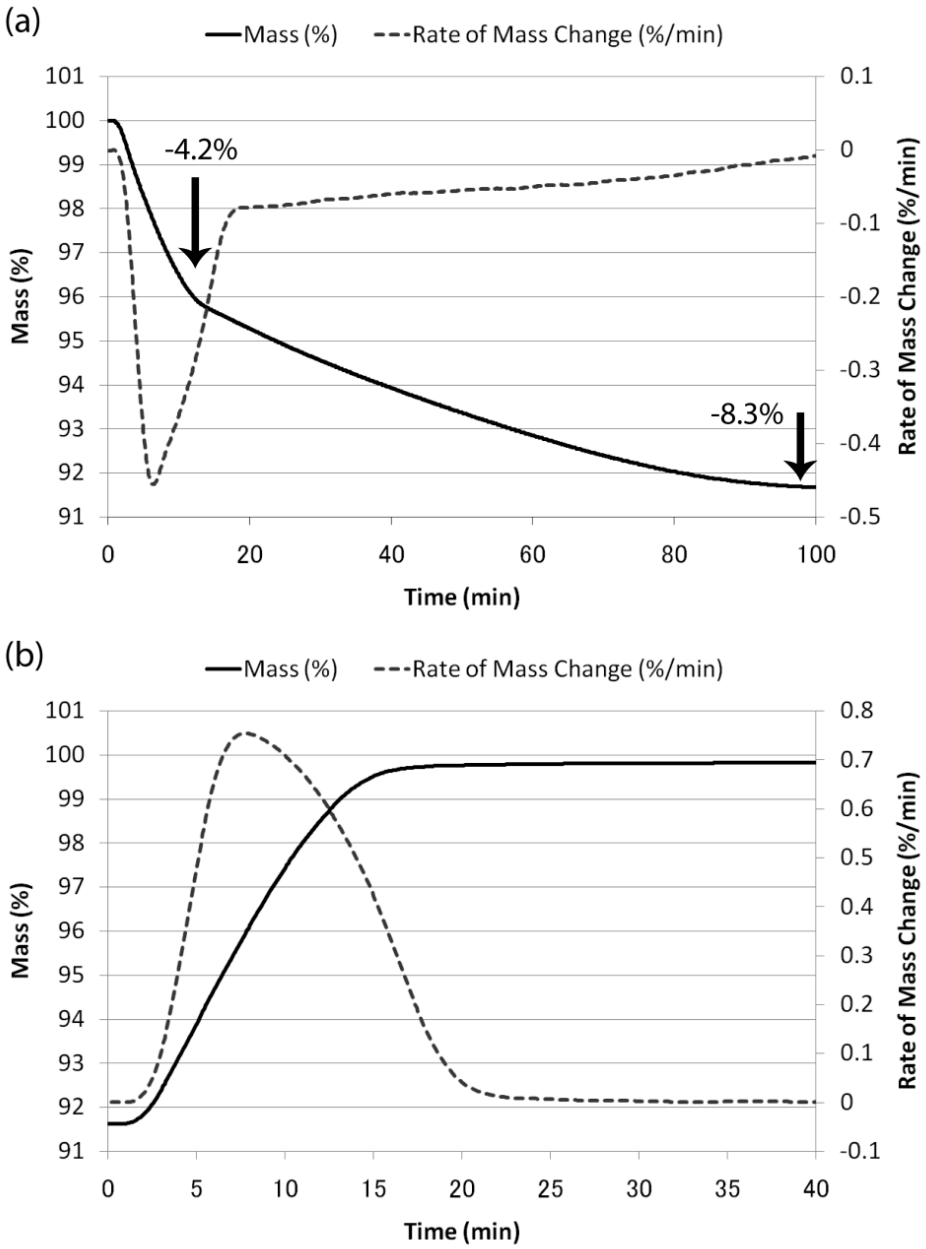

Figure 3-9 : DVS plot of (a) dehydration process of dihydrate form and (b) hydration process of anhydrous form. Solid line shows the mass changes and dash line shows the rate of mass changes.

3.5. Concluding Remarks

Crystal structures of lisinopril dihydrate, monohydrate and anhydrous forms were successfully determined from powder X-ray diffraction data, and the mechanism of two step dehydration of lisinopril dihydrate form was clearly revealed from these structures. The order of dehydration was determined from the hydrogen bond conditions of water channels. In the first dehydration, relatively weak hydrogen bonded water (the central channel) was released and, in the second dehydration, stronger hydrogen bonded water (the side channel water) was released. Interestingly, although the side channel was closed by dehydration process, the central channel was not closed in the dehydration process. Because the remaining vacant central channel in monohydrate and anhydrous form has significant volumes for taking in water, it can be considered as the reason of easily hydration of these forms. From this consideration, the mechanism of hydration process is expected as not a simple reverse of dehydration process. The expectation can be confirmed from the DVS measurement of the dehydration process and hydration process. Although two step dehydration can be seen in the result of DVS measurement, the hydration proceeded in one step and which clearly suggests that the hydration process is not a simple reverse pathway of dehydration process.

As shown in this study, investigation of pharmaceutical dehydration process using ab initio powder X-ray diffraction analysis is powerful technique to understand the dehydration or hydration process. Further investigations about the pharmaceutical dehydration or hydration mechanism are expected for systematic understand.

Reference

(1) J. K. Haleblian, *J. Pharm. Sci.* **1975**, 64, 1269–1288.

(2) S. Data, D. J. W. Grant, *Nature Rev.* **2004**, 3, 42-57.

(3) K. R. Morrisa, U. J. Griesserb, C. J. Eckhardtc, J. G. Stowella, *Adv. Drug Deliv. Rev.* **2001**, 48, 91-114.

(4) R. K. Khankari, D. J. W. Grant, *Thermochim.Acta*, **1995**, 61-79.

(5) R. L. Te, U. J. Griesser, K. R. Morris, S. R. Byrn, J. G. Stowell, *Cryst. Growth & Des.*, **2003**, 3, 997-1004.

(6) K. Kobayashi, H. Fukuhara, T. Hata, Y. Ohashi, *Chem. Pharm. Bull.* **2003**, 51, 1356-1362.

(7) K. D. M. Harris, M. Tremayne, *Chem. Mater.* **1996**, 8, 2554-2570.

(8) K. D. M. Harris, M. Tremayne, B. M. Kariuki, *Angew. Chem. Int. Ed.* **2001**, 40, 1626-1651.

(9) V.V. Chernyshev, *Russian Chem. Bull.* **2001**, 50, 2273.

(10) W. I. F. David, K. Shankland, L. B. McCusker, C. Baerlocher, Ed.; Structure Determination from Powder Diffraction Data, OUP/IUCr, **2002**.

(11) A. Huq, P. W. Stephens, *J. Pharm. Sci.* **2003**, 92, 244-249.

(12) K. D. M. Harris, E. Y. Cheung, *Chem. Soc. Rev.* **2004**, 33, 526-538.

(13) M. Tremayne, *Phil. Trans. R. Soc.* **2004**, 362, 2691-2707.

(14) V. Favre-Nicolin, R. Cerny, *Z. Kristallogr.* **2004**, 219, 847-856.

(15) K. Shankland, A. J. Markvardsen, W. I. F. David, *Z. Kristallogr.* **2004**, 219, 857-865.

(16) V. Brodski, R. Peschar, H. Schenk, *J. Appl. Crystallogr.* **2005**, 38, 688-693.

(17) S. Karki, L. Fabian, T. Friscic, W. Jones, *Org. Lett.* **2007**, 9, 3133-3136.

(18) H. Tsue, M. Horiguchi, R. Tamura, K. Fujii, H. Uekusa, *J. Synth. Org. Chem. Japan* **2007**, 65, 1203-1212.

(19) W.I.F. David, K. Shankland, *Acta Crystallogr. Sect. A* **2008**, 64, 52-64.

(20) K. D. M. Harris, M. Tremayne, P. Lightfoot, P. G. Bruce, *J. Am. Chem. Soc.* **1994**, 116, 3543-3547.

(21) F. Guo, K. D. M. Harris, *J. Am. Chem. Soc.* **2005**, 127, 7314-7315.

(22) A. J. Mora, E. E. Avila, G. E. Delgado, A. N. Fitch, M. Brunelli, *Acta Cryst. B*,

2005,61 , 96-102.

(23) C. Platteau, J. Lefebvre, F. Affouard, J. F. Willart, P. Derollez, F. Mallet, *Acta Cryst. B*, **2005**, 61, 185-191..

(24) A. Hirano, S. Toyota, F. Toda, K.Fujii, H. Uekusa, *Angew. Chem. Int. Ed.* **2005**, 45 ,6013-6016.

(25) C. Guguta, H. Meekes, R. Gelder, *Cryst. Growth & Des.* **2006**, 6, 2686-2692.

(26) F. Guo, E. Y. Cheung, K. D. M. Harris, V. R. Pedireddi, *Cryst. Growth & Des.* **2006**, 6, 846-848.

(27) D. Albesa-Jové, Z. Pan, K. D. M. Harris, H. Uekusa, *Cryst. Growth & Des.***2008**, 8, 3641-3645.

(28) K.Fujii, Y. Ashida, H. Uekusa, A. Hirano, S. Toyota, F. Toda, Z. Pan, K. D. M. Harris, *Cryst. Growth & Des. in press.*

(29) C. P. Price, G. D. Glick, A. J. Matzger, *Angew. Chem. Int. Ed.* **2006**, 45, 2062-2066.

(30) F. Angeli, P. Verdecchia, G. P. Reboldi, R. Gattobigio, M. Benticoglio, J. A. Staessen, C. Porcellati, *Am. J. Cardiology*, **2004**, 93, 240-243.

(31) G. Cremonesi, L. Cavalieri, S. Bacchelli, D. D. Esposti, I. Cikes, J. Dobovisek, J. Zeman, C. Borghi, E. Ambrosioni, *Curr. Ther. Res.* **2003**, 64, 290-300.

(32) B. Soffer, Z. Zhang, K. Miller, B. A. Vogt, S. Shahinfar, *Am. J. Hyp.* **2003**, 16, 795-800.

(33) R. Natesh, S. L. U. Schwanger, E. D. Sturrock, K. Ravi Acharya, *Nature*, **2003**, 421, 551-554.

(34) H. R. Corradi, S. L. U. Schwager, A. T. Nchinda, E. D. Sturrock, K. Ravi Acharya, *J. Mol. Biol.* **2006**, 357, 964-974.

(35) R. S. Pandurangi, K. V. Katti, L. Stillwell, C. L. Barnes, *J. Am. Chem. Soc.* **1998**, 120, 11364-11373.

(36) E. B. Gonzalez, E. Farkas, A. A. Soudi, T. Tan, A. I. Yanovsky, K. B. Nolan, *J. Chem. Soc., Dalton Trans.* **1997**, 2377-2379.

(37) S. Wang, S. Lin, T. Chen, *Chem. Pharm. Bull.* **2000**, 48, 1890-1893.

(38) J. Hinojosa-Trres, J. M. Aceves-Hernandez, J. Hinojosa-Torres, M. Paz, V. M. Castano, E. Agacino-Valdes, *J. Mol. Struct.* **2008**, 886, 51-58.

(39) A. Boultif, D. Louer, *J. Appl. Cryst.* **2004**, 37, 724-731.

(40) P. M. Wolff, *J. Appl. Cryst.* **1972**, 5, 243.

(41) G. S. Smith, R. L. Snyder, *J. Appl. Cryst.* **1979**, 12, 60-65.

(42) G. S. Pawley, *J. Appl. Cryst.* **1981**, 14, 357-361.

(43) W. I. F. David, K. Shankland, J. Cole, S. Maginn, W. D. H. Motherwell, R. Taylor, DASH User Manual. Cambridge Crystallographic Data Centre, Cambridge, UK. (2001).

(44) Rietveld, H. M. 1969, J. Appl. Cryst. 1969, 2, 65-71.

(45) Larson, A. C.; Von Dreele, R. B. GSAS; Los Alamos Laboratory Report No. LA-UR-86-748; Los Alamos National Laboratory: Los Alamos, NM, 1987.

(46) A. L. Speck *J. Appl. Cryst.* **2003**. 36, 7-13.

Chapter 4

Dehydration and Phase Transformation of Acrinol

4.1. Abstract

An extensive used antibacterial agent, acrinol is known to be obtained as monohydrate form by recrystallization. From thermal and powder X-ray diffraction experiments, the crystal to crystal dehydration and polymorphic transformation were found for acrinol monohydrate form by heating. Interestingly, a large difference was observed for the relative humidity on the hydration of anhydrous **A** (after dehydration; hydrated at RH10%) and **B** (after polymorphic transformation; hydrated at RH80%). The crystal structures of these anhydrous forms are necessary for understanding the transformation mechanisms and their hydration properties, however, because of a disintegration of single crystal while transformations, it is impossible to determine these crystal structures by single crystal diffraction analysis. Therefore, the technique of crystal structure determination from powder X-ray diffraction data were applied to these unknown forms and successfully the crystal structures of acrinol anhydrous **A** and **B** were determined. The mechanistic aspects of the dehydration and polymorphic transformation were established from the crystal structural changes and the difference in the hydration humidity of anhydrous **A** and **B** was clearly understood from the crystal structures similarity and difference. In addition to the understanding the transformation mechanisms, a large differences of the initial dissolution rate were found among acrinol hydrate, anhydrous **A** and **B**. The fastest dissolution rate was achieved for anhydrous **B**

and which has five times faster than well used hydrate form. These results clearly suggest the effectiveness of an investigation of alternative forms such as hydrates and polymorphs.

4.2. Introduction

Many organic crystalline solids can exist as polymorphs, hydrates or solvates, or the combination of these. The existence of these alternative crystalline phases is critical problem, especially for the pharmaceutical compounds, because these alternative phases usually have different physical or chemical properties which are important for the drug use, such as solubility, dissolution rate, stability and bioavailability[(1)(2)]. Thus, well investigation about the existence of alternative phases and well understanding about their properties are very important for pharmaceutical compounds. Also, understanding the transformation mechanism among these alternative phases is very important, because such transformations are frequently occurred during the drug manufacturing process or upon storage of the drug substance or dosage form[(3)].

Grant *et. al.* reported the nature of pharmaceutical hydrates and he showed many analytical techniques for understanding the properties of pharmaceutical hydrates and the mechanistic aspects of the hydration or dehydration processes[(4)]. Among these analytical techniques, crystal structure analysis is one of the powerful techniques to understand the mechanistic aspects of the hydration or dehydration process. According to such background, there are several literatures which focused on the mechanistic aspects of hydration or dehydration process using single crystal structure analysis technique[(5)(6)]. However, in many cases, single crystals of the starting phase are found to disintegrate to produce a polycrystalline material upon dehydration or hydration process, thus limiting the opportunities to obtain information on the structural changes associated with such processes by single crystal X-ray diffraction analysis. In some cases, it might be possible to obtain a single crystal of the transformed phase (as confirmed by comparison of powder X-ray diffraction data) by another crystallization method, but in many cases, single crystals of the dehydrated or hydrated phase cannot be obtained by any other method. Techniques for carrying out structure determination directly from powder X-ray diffraction data are clearly essential for structural characterization of the polycrystalline product materials obtained directly in such dehydration, hydration or polymorphic transformations.

The opportunities for carrying out complete structure determination of organic molecular materials from powder X-ray diffraction data have developed

considerably in recent years[7]-[19], particularly through the development of the direct-space strategy for structure solution[20]. Because these techniques have the potential to provide structural understanding of polycrystalline products obtained from solid state transformations (e.g. originating from single crystal materials of the type discussed above), these techniques have a key role to play in understanding structural properties of materials produced from solid state grinding processes, solid state reactions, desolvation processes, and polymorphic transformations[21]-[28].

In the present work, acrinol (Figure 4-1) was focused for the target compound for the systematic understanding for the pharmaceutical dehydration or hydration process. Acrinol, which consist of ethacridine (3,9-diamino-7-ethoxyacridine) and latcid acid, is extensive use as an antibacterial agent. It is known that the monohydrate form is usually appeared by recrystallization and the crystal structure of monohydrate form was already reported[29]. However, there is no report regarding the thermal behavior or crystal structural changes in the dehydration process of acrinol. Thus, the structural information of anhydrous form and the mechanism of dehydration process were not revealed. In the present study, in order to reveal the structural properties thermal analyses were carried for acrinol hydrate and the crystal structures of newly found two anhydrous forms were determined from powder X-ray diffraction data.

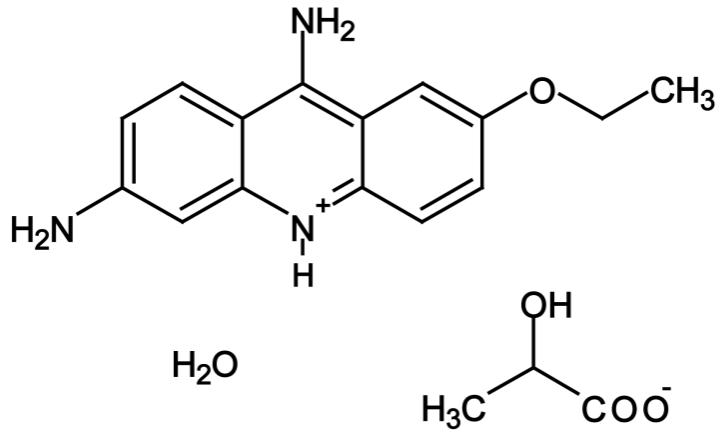

Figure 4-1 : Molecular structure of acrinol.

4.3. Experiment

4.3.1. Preparation

Acrinol was purchased from Tokyo Chemical Industry co., Ltd.. The sample was confirmed as pure hydrate phase from powder X-ray pattern and the sample was used for other experiment without further purification. Anhydrous forms (**A** or **B**) were prepared by heating of this hydrate sample.

4.3.2. Thermal Analysis

TG/DTA was measured on a Rigaku Thermo Plus 2. 16.136 mg of acrinol hydrate was heated in a rate of 0.5 °C/min. The TG curve was recorded from 50 °C up to 350 °C under a dry nitrogen atmosphere with a flux of 100 ml/min. The simultaneous DSC and X-ray diffraction measurement (XRD-DSC) was performed on a Rigaku D/MAX 2400 diffractometer and a Rigaku Thermo Plus 2 differential scanning calorimeter at a heating rate of 3 °C/min.

4.3.3. Dynamic Vapor Sorption

Dynamic vapor sorption was measured on Dynamic vapor sorption – advantage (SMS Ltd, UK) at 40°C. Anhydrous form A or B was mounted on a valance and the relative humidity was increase from 0% to 100% with monitoring the weight by valance.

4.3.4. Synchrotron X-ray powder Diffraction Measurement

Synchrotron X-ray powder diffraction data were recorded for acrinol anhydrous phase A on beamline BL19B2 at SPring-8 (Debye-Scherer camera equipped with a curved Imaging Plate detector). Because anhydrous phase A easily returns to hydrate form at ambient condition, the prepared sample, which was obtained by heating of acrinol hydrate, was sealed into 0.3 mm diameter borosilicate glass capillary quickly in order to prevent a hydration. The measurement was carried out with wavelength 1.197120(4) Å and the data collection time was 30 minutes.

The powder X-ray diffraction data of acrinol anhydrous phase B was recorded

at ambient temperature on a Bruker D8 diffractometer using CuKα1 radiation with linear position-sensitive detector VANTEC which covering 12°in 2θ. The measurement was carried out by transmission mode with the foiled sample which was totated during measurement [2θ range 5°- 70°; step size 0.0167°; data collection time 13 h].

4.3.5. Initial Dissolution Rate

The initial dissolution rates were measured using rotating disk method. The disk was of 10 mm diameter and the each samples were compacted at the force of $1.96x10^4$ N/cm^2. The disk was rotated at 50 rpm at 37°C. The solvent was 900 ml of distilled water. The drug release was determined spectrophotometrically.

4.4. Result and discussion

4.4.1. Characterization of Acrinol Polymorphs

TG and DTA curves of acrinol hydrate were shown in Figure 4-2. On the DTA curve, a decomposition was observed at 242°C as endothermic peak and exothermic polymorphic transformation was found at 187.7°C after dehydration at 100.4°C, which can be confirmed from the mass degrease 5.55% (ideal one water is 4.98%). In order to characterize these phases, simultaneous powder X-ray diffraction and DSC measurement (XRD-DCS) was carried out for acrinol hydrate. As shown in Figure 4-3, it was found that the crystalline acrinol hydrate was transformed to crystalline anhydrous form and this new phase was also transformed to another crystalline form by polymorphic transformation. Thus, it can be said that the dehydration and the polymorphic transformation of acrinol are crystal to crystal transformations. The resulted newly discovered crystalline anhydrous forms are named anhydrous **A** for before polymorphic transformation and anhydrous **B** for after polymorphic transformation.

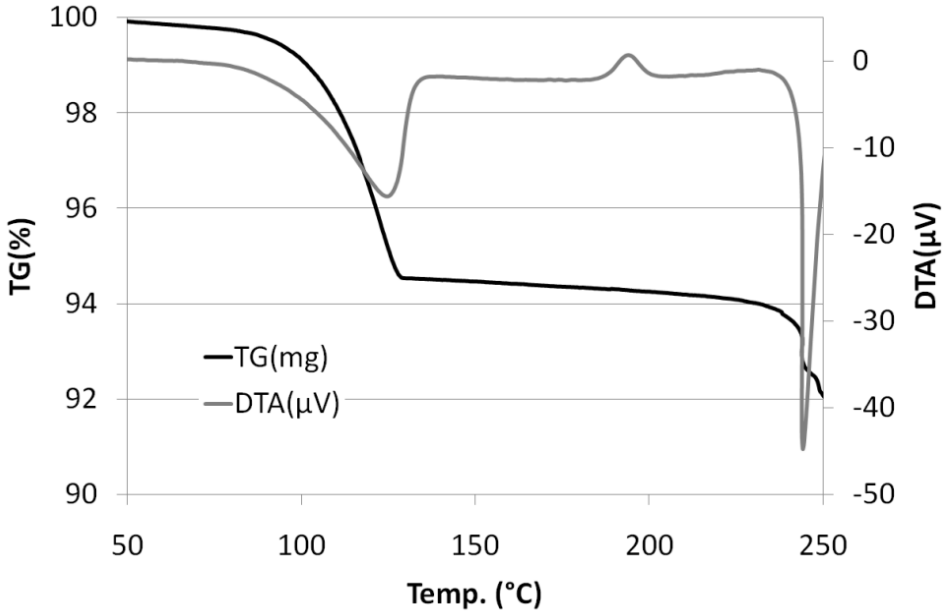

Figure 4-2 : TG/DTA plot of acrinol hydrate.

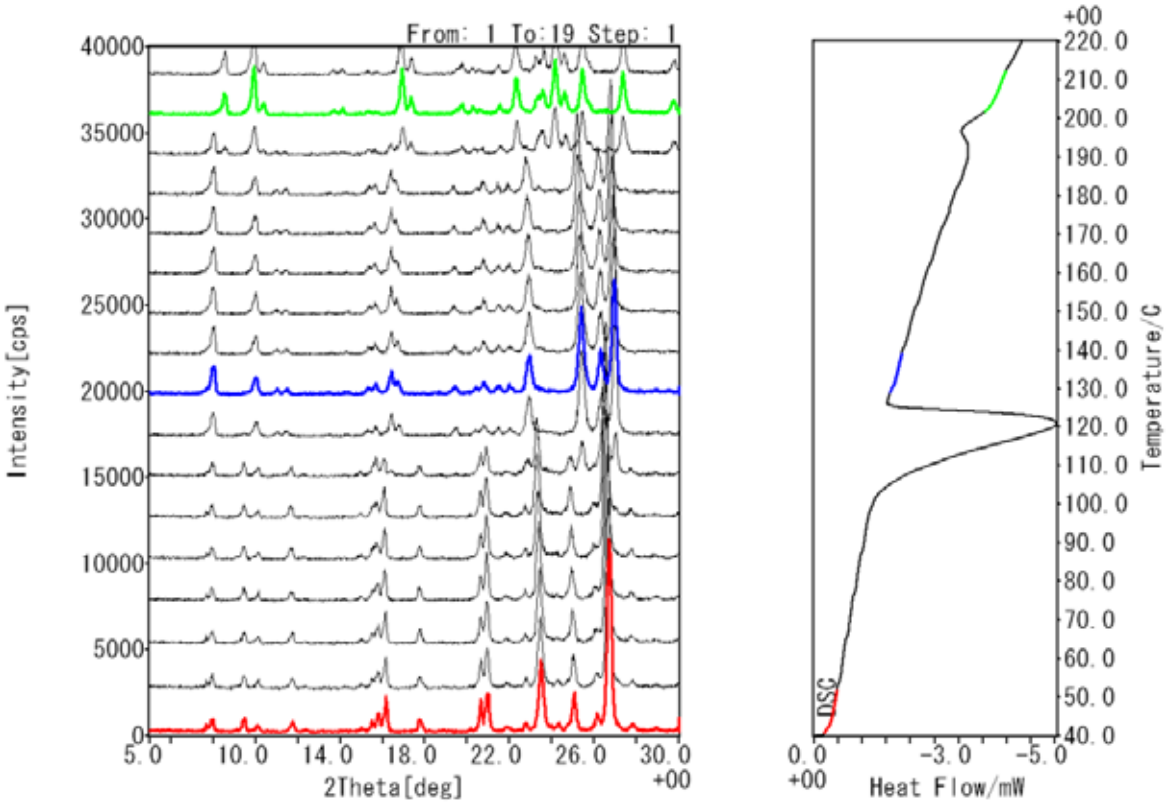

Figure 4-3 : XRD-DSC measurement of acrinol hydrate.

The hydration properties of acrinol anhydrous **A** and **B** were investigated by DVS measurement. Figure 4-4 shows the DVS plots of anhydrous (a) **A** and (b) **B**. Although hydration of anhydrous **A** was occurred at RH10% condition, anhydrous **B** did not hydrate until RH80% condition. Interestingly, the hydration RH conditions are quite different between anhydrous **A** and **B**, and anhydrous **B** is significantly stable for the hydration compare to anhydrous **A**. The large difference in the hydration humidity of anhydrous **A** and **B** is expected to relate to their crystal structures, thus the information on their crystal structures are necessary for understanding their properties. However, a disintegration of single crystal was observed for acrinol hydrate in the dehydration process and ,in addition, the attempt to obtain single crystal of anhydrous phases by recrystallization was failed. Thus the crystal structures of acrinol anhydrous **A** and **B** were determined powder X-ray diffraction data.

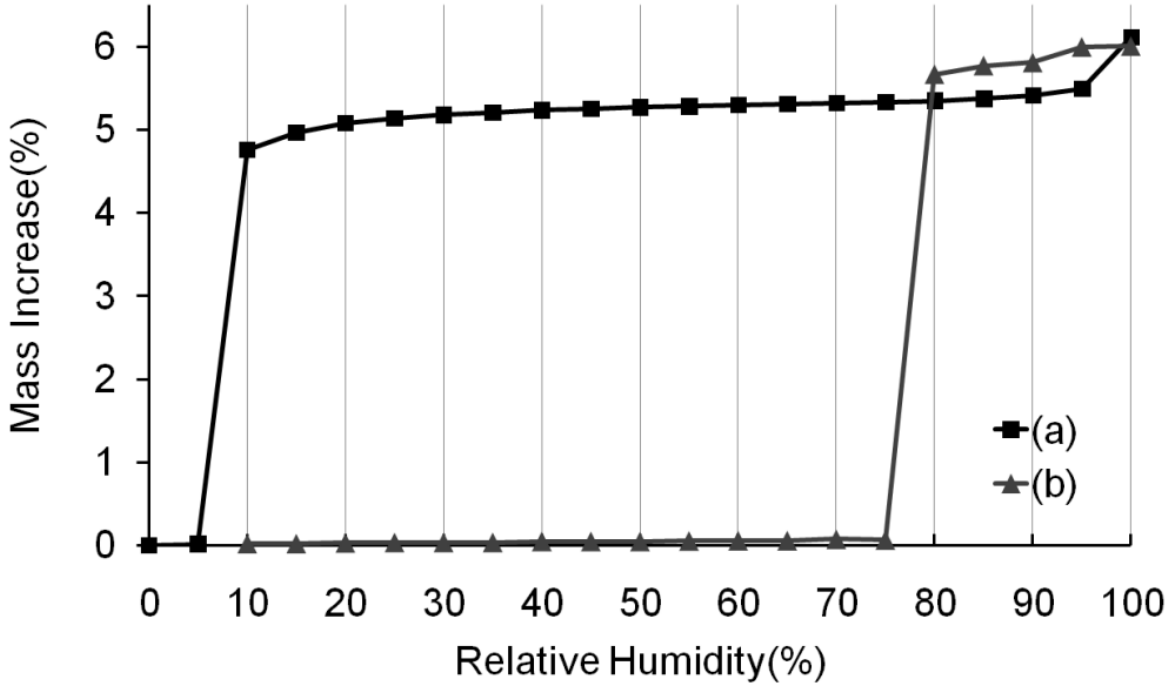

Figure 4-4 : DVS measurement of acrinol (a) anhydrous **A** and (b) anhydrous **B**.

4.4.2. Structure Determination from Powder X-ray Diffraction Data

The powder X-ray diffraction pattern of anhydrous **A** was indexed using the program DICVOL04[39], giving the following unit cell (M20=38.4[31], F20=95.4[41]) with triclinic metric symmetry; a = 8.051 Å, b = 9.355 Å, c = 11.912 Å, α = 102.45°, β = 103.23°, γ = 98.64°, V = 834.76 Å^3. The unit cell parameters are similar to those of acrinol hydrate (a = 7.719 Å, b = 10.043 Å, c = 12.246 Å, α = 108.14°, β = 102.98°, γ = 94.67°, V = 867.3 Å^3, -100°C, $P\bar{1}$), thus, the space group of anhydrous **A** was estimated as $P\bar{1}$. Profile fitting using the Le Bail method[36] gave a good quality fit with R_{wp} = 4.02% and R_p = 2.71%. The unit cell parameters and profile parameters obtained from the Le Bail fitting procedure were used in the subsequent structure solution calculation. Structure solution was carried out using the direct-space genetic algorithm (GA) technique incorporated in the program EAGER[34]-[38]. The structural fragment comprised one ethacridine molecule and one lactic acid molecule, representing a total 14 variables (three translational variables for each of the ethacridine and lactic acid molecules, three orientational variables for each of the ethacridine and lactic

acid, and two torsional variables for the ethoxy group of the ethacridine molecule). The GA calculation involved the evolution of 60 generations for a population of 100 structures, with 50 mating operations and 25 mutation operations carried out per generation. Following structure solution, Rietveld refinement[44] was carried out using the GSAS program[45]. Standard restraints were applied to bond lengths and bond angles, planar restraints were applied to aromatic rings, and a global isotropic displacement parameter was used. The final Rietveld refinement gave following parameters: a = 8.0467(2) Å, b = 9.3558(2) Å, c = 11.9151(2) Å, α = 102.436(2)°, β = 103.177(3)°, γ = 98.648(2)°, V =833.92(3) Å^3. R_{wp} = 5.80%, R_p = 4.31%, R_F^2 = 8.42% (2θ range, 4.01 – 77.13°; 7313profile points; 85 refined variables). The final Rietveld plot is shown in Figure 4-5a.

The powder X-ray diffraction pattern of anhydrous **B** was indexed using the program DICVOL04, giving the following unit cell (M20 = 16.0, F20 = 34.1) with triclinic metric symmetry; a = 14.0307 Å, b = 11.7879 Å, c = 20.9120 Å, β = 100.937°, V = 3395.88 Å^3. Given the volume of this unit cell, and consideration of density, the number of formula units in the unit cell is assigned as Z = 8. From the estimated Z value and systematic absences, the space group was determined as $C2/c$. Profile fitting using the Le Bail method gave a good quality fit with R_{wp} = 2.99% and R_p = 2.08%. The unit cell parameters and profile parameters obtained from the Le Bail fitting procedure were used in the subsequent structure solution calculation. Structure solution and subsequent Rietveld refinement were carried out with the same strategy of anhydrous **A**, except a treatment of one hydrogen (H46) because, considering the hydrogen position from hydrogen bonds and the existence of inversion center at the middle position of two O25 oxygens, H46 hydrogen looks to be disordered and it should split into H46A and H46B to avoid the unreasonable hydrogen contacts. In this structure, one H46 hydrogen bonds to O25 and the other H46 will directs to N19. The final Rietveld refinement gave following parameters: a = 14.0496(5) Å, b = 11.8040(2) Å, c = 20.9323(8) Å, β = 100.936(3)°, V = 3468.4(2) Å^3. R_{wp} = 4.53%, R_p = 3.28%, R_F^2 = 8.54% (2θ range, 5.017 – 69.9299°; 3888profile points; 83 refined variables). The final Rietveld plot is shown in Figure 4-5b.

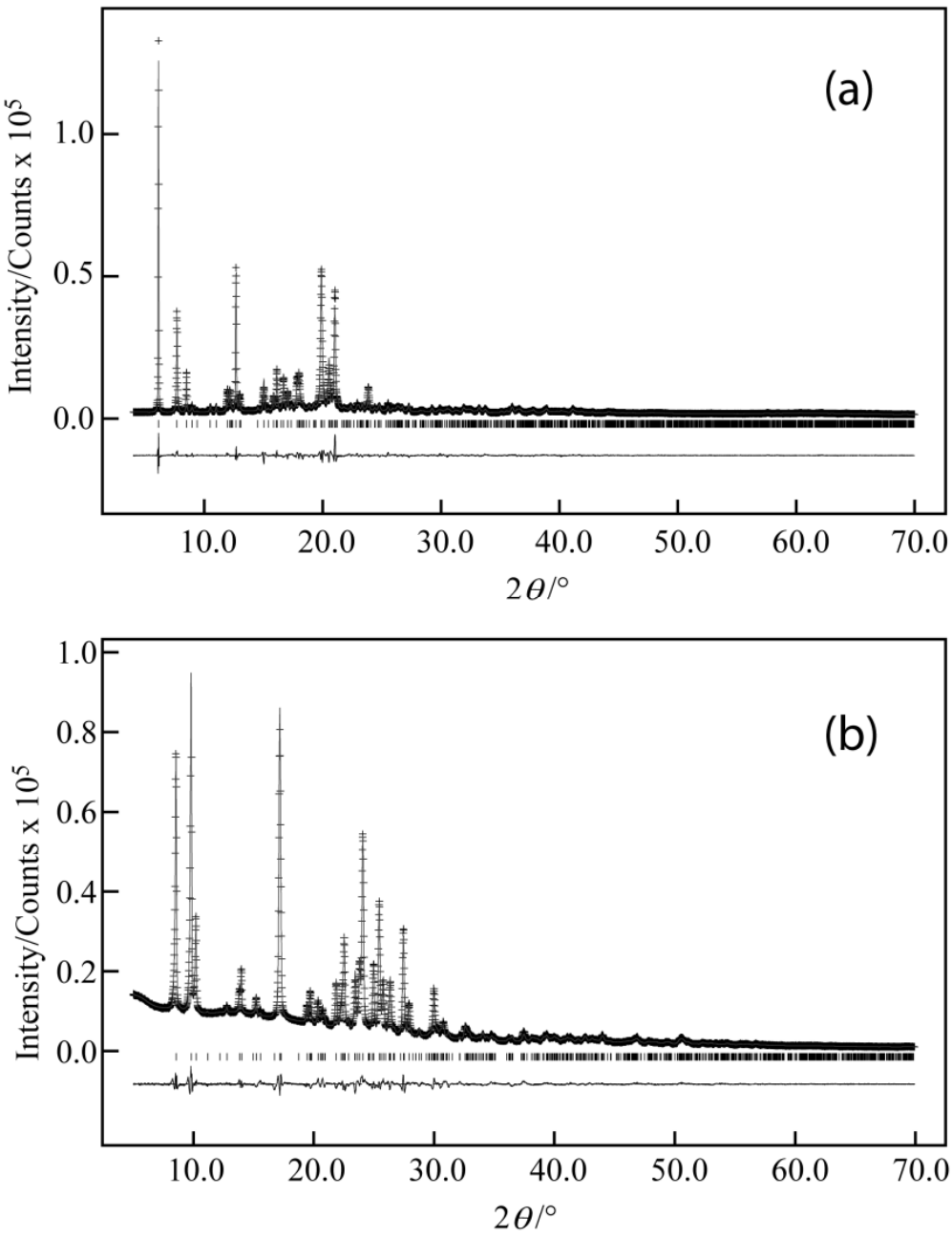

Figure 4-5 : Final Rietveld refinement for acrinol (a) anhydrous **A** (b) anhydrous **B**, showing the experimental powder X-ray diffraction pattern (+ marks), calculated powder X-ray diffraction pattern (solid line) and difference profile (lower line). Tick marks indicate peak positions.

4.4.3. Crystal Structure of Anhydrous A and the Mechanistic Aspects of Dehydration Process

The crystal structure of acrinol hydrate[36] is shown in Figure 4-6 (a) and (b), and the crystal structure of acrinol anhydrous **A** is shown in Figure 4-6 (c) and (d). As it can be also seen in the crystal structure of hydrate, the crystal structure of anhydrous **A** has similar packing arrangements of ehtacridine molecule and lactic acid molecule. The differences among crystal structures of hydrate and anhydrous **A** can be seen in the position of ethacridine molecule and the orientation of lactic acid molecule. In the dehydration process, a translation of ethacridine molecule, which might be caused to close the vacant place made by loss of water, and a rotation of lactic acid, which might be occurred to make reasonable hydrogen bonds, are observed. The hydrogen bonds of hydrate and anhydrous **A** are shown in Figure 4-7b and the distances of donor and acceptor are listed in Table 4-1. Although both structures have hydrogen bonding bridge by lactic acid, they have different bridge conditions. In anhydrous **A**, as shown in Figure 4-7b, O15, which is hydrogen bond acceptor, and N19-H39, which is considered as hydrogen bond donor, do not make hydrogen bond with any hydrogen bond donor and acceptor, while the hydrogen bond donor and acceptor are fully hydrogen bonded in hydrate form . Thus, anhydrous **A** is expected less stable than hydrate form from hydrogen bond conditions points of view, and this can be considered as the reason of why hydrate form is usually appeared by recrystallization and why anhydrous **A** easily returns to hydrate form. Also, the difference of the calculated density supports this assumption. Hydrate (1.35 g/cm^3 at 27°C) has lower density than that of anhydrous **A** (1.37 g/cm^3 at 27°C), thus, hydrate is also expected stable than anyhdrous **A** from the density point of view.

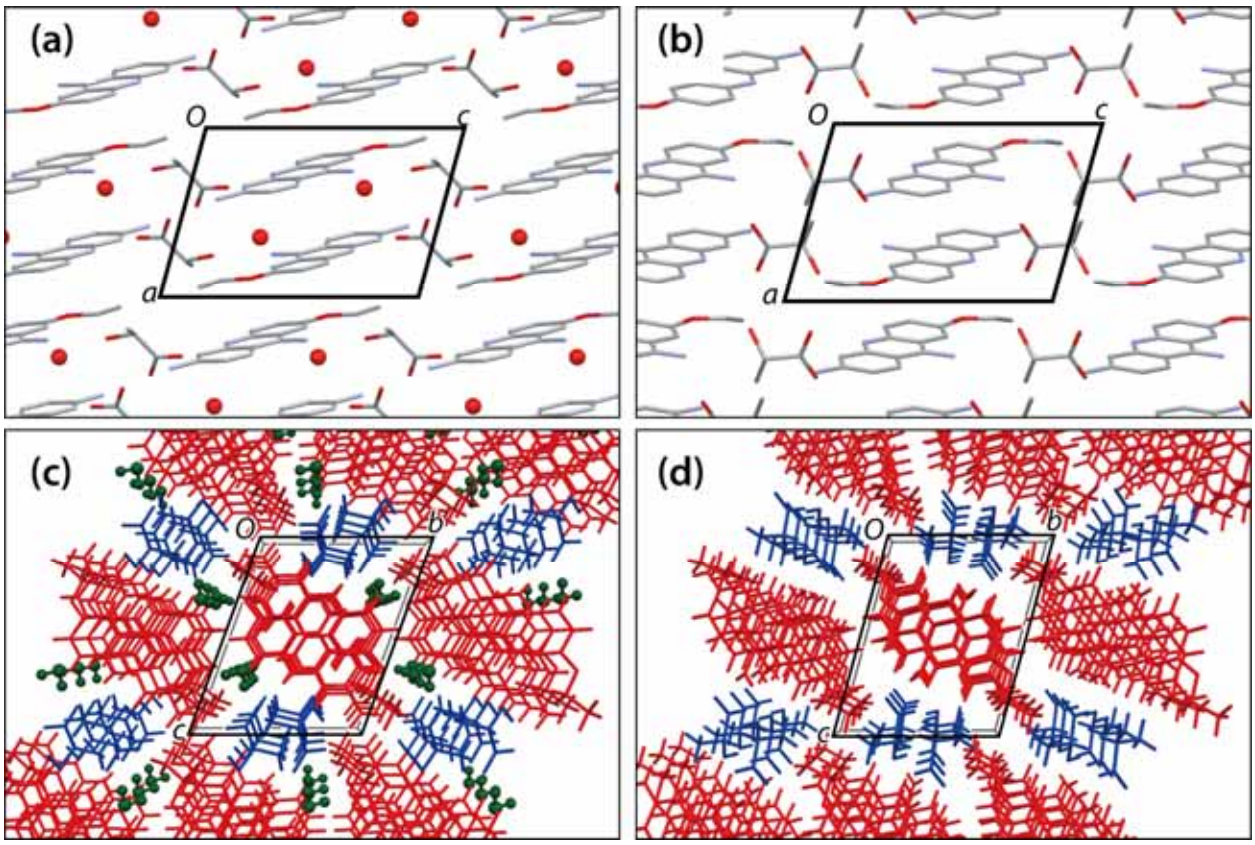

Figure 4-6 : Crystal structures of acrinol (a) hydrate view along *b* axis, (b) anhydrous **A** view along *b* axis, (c) hydrate view along *a* axis, (d) anhydrous **B** view along *a* axis.

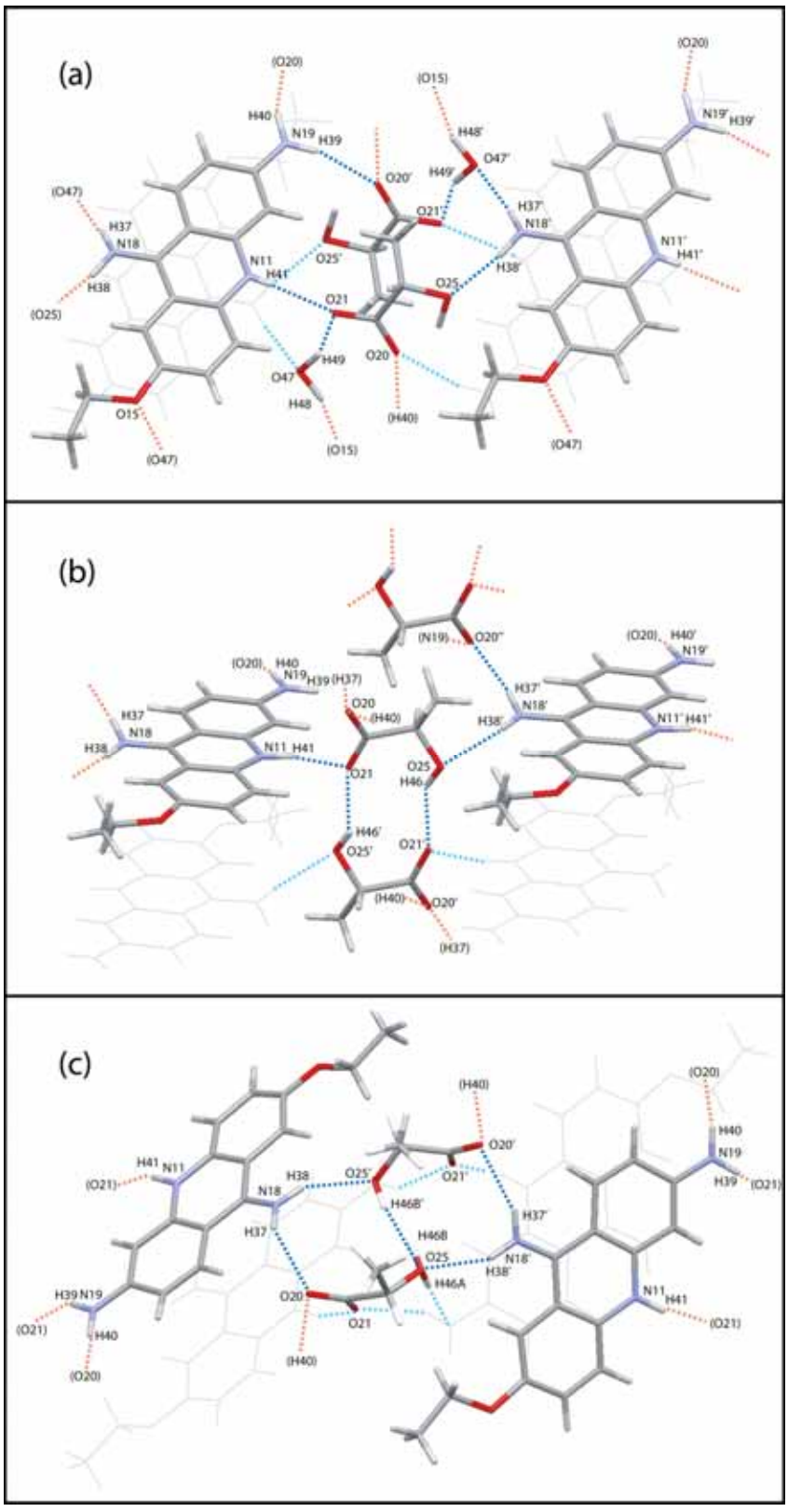

Figure 4-7 : Drawing of hydrogen bonds in crystal structure of acrinol (a) hydrate, (b) anhydrous **A**, (c) anhydrous **B**.

Hydrate		Anhydrous A		Anhydrous B	
N11-H41···O21	2.80 Å	N11-H41···O21	2.65 Å	N11-H41···O21	2.56 Å
N18-H37···O47	2.91 Å	N18-H37···O20	3.02 Å	N18-H37···O20	3.10 Å
N18-H38···O25	2.98 Å	N18-H38···O25	3.30 Å	N18-H38···O25	3.05 Å
N19-H39···O20	3.05 Å	N19-H40···O20	2.82 Å	N19-H39···O20	3.36 Å
N19-H40···O20	2.92 Å	O25-H46···O21	2.78 Å	N19-H40···O21	2.97 Å
O47-H48···O15	2.99 Å			O25-H46B···O25	3.13 Å
O47-H49···O21	2.76 Å			O25-H46A···O25	3.56 Å

Table 4-1 : Hydrogen bonds list of acrinol hydrate, anhydrous **A** and

The dehydration mechanism can be drawn from the crystal structures of hydrate and anhydrous **A**. Take it in to account the facts of similarity of crystal structures between hydrate and anhydrous **A** which can be seen in the existence of the arrangement of water molecule along *a* axis in hydrate form, as shown in Figure 4-6(c), the dehydration might be undergo through the *a* axis. Because the water remove can proceed through the *a* axis, the crystal packing can retain after dehydration, thus, the transformation can proceed with minor structural changes, such as the translation of ethacridine and the rotation of lactic acid in order to make the reasonable crystal packing and hydrogen bonds. The requirement of minor structural changes in dehydration process is very important information to explain the easy hydration of anyhdrous **A**, because, in another saying, the hydration of anhydrous **A** will also require minor structural changes, as well as dehydration process, and it can consider that it will occur easily.

4.4.4. Crystal Structure of Anhydrous B and the Mechanistic Aspects of Polymorphic Transformation Process

The crystal structure of anyhdrous **B** is shown in Figure 4-8. The structure is quite different from those of hydrate and anhydrous **B**. The similarity of the crystal structures between anhydrous **B** and hydrate(or anhydrous **A**) is the stacking of ethacridine and one dimensional arrangement of the lactic acid

molecule and the difference is the direction of the stacking arrangement of ethacridine molecule as can be seen from the comparison of Figure 4-6(a) (or (b)) and Figure 4-8(a). Although the directions of the stacking arrangement of ethacridine molecule are same in hydrate and anhydrous **A**, the directions are not same in anhydrous **B** and, finally, these differences result in the difference of space group (hydrate and anyhdrous **A** is $P\bar{1}$ and anhydrous **B** is $C2/c$).

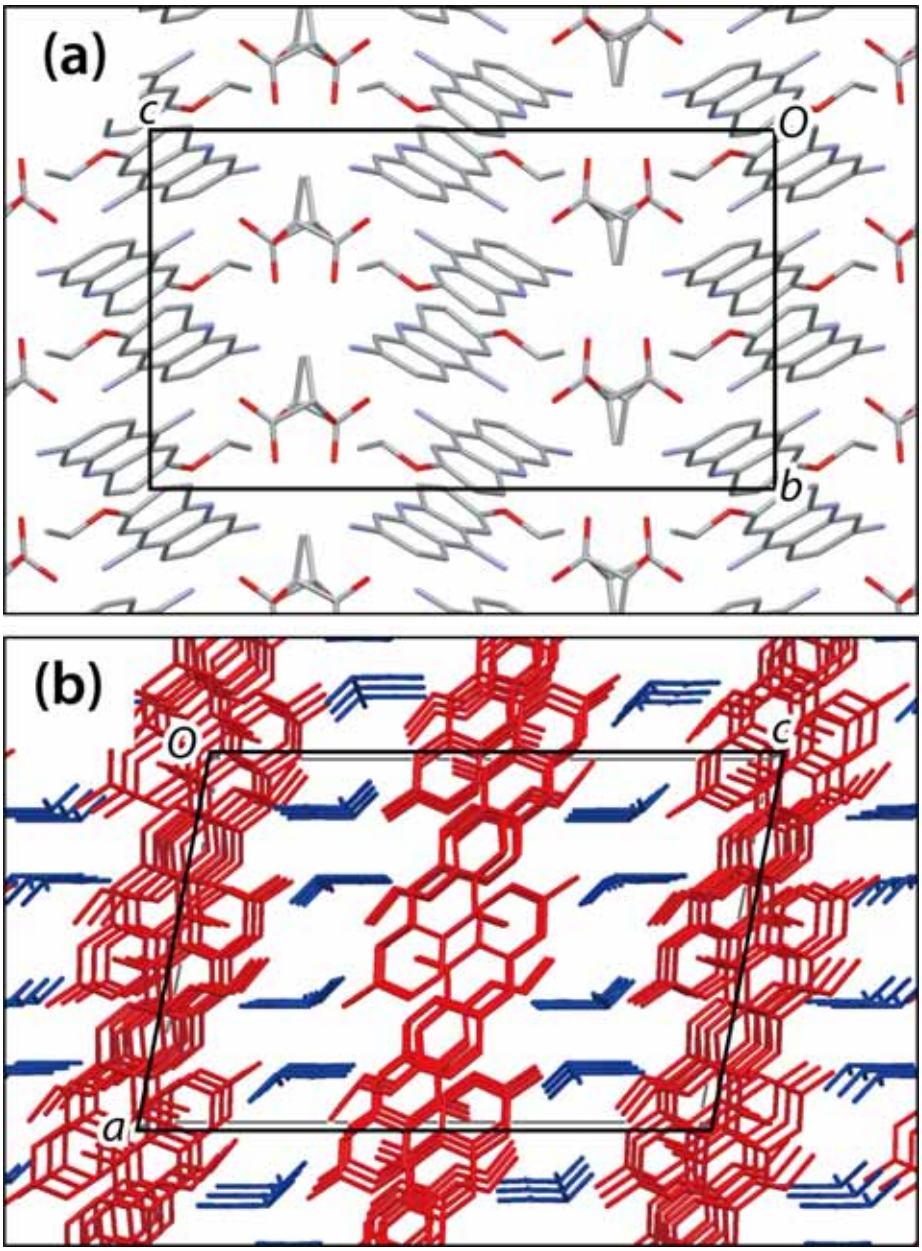

Figure 4-8 : Crystal structures of acrinol (a) anhydrous **B** view along *a* axis, (b) anhydrous **B** view along *b* axis.

The hydrogen bonds of anhydrous **B** are shown in Figure 4-7 c and are listed in Table 4-1. There are also similar hydrogen bonds with those of hydrate and anhydrous **A**, one N-$H^{+}\cdots O^{-}$ (N···O, 2.56Å); one N-H···O^{-} (N···O, 3.36Å), three N-H···O (N···O, 3.10Å, 3.05Å and 2.97Å) and two disordered O-H···O (O···O, 3.13Å and 3.56Å). The hydrogen bonding donors and acceptors are fully interacted each other, thus, it can be considered that this structure is sufficiently stabilized compare to anhydrous **A** in which the hydrogen bonding donors and acceptors are not fully occupied. The expectation of that anhydrous **B** is more stable than anhydrous **A** can be confirmed from the fact of the transformation of anhydrous **A** to **B** is exothermic transformation. Because the system lost internal energy in the transformation process, the resulted phase (anhydrous **B**) is more stable than initial state (anhydrous **B**). Actually the term of stability should consider the contribution of entropy, however, only the contribution of enthalpy has been considered here.

The reason of why anhydrous **B** does not easily return to hydrate can be explained from the difference of crystal structures. Because the polymorphic transformation from anhydrous **A** to **B** accompanied large structural change as discussed above, in turn, the hydration of anhydrous **B** requires large structural change. As a result, anhydrous **B** is stable for the humidity and the hydration occurred only in high humidity condition (RH 80%). The stability for the hydration such like anhydrous **B** is very useful property for pharmaceutical, because usually the hydration is one of the problems in the storage or processing. This result and structural consideration will be useful information for drug use.

4.4.5. Initial Dissolution Rate

The initial dissolution rates are shown in Figure 4-9. By liner least square fitting, the initial dissolution rates of hydrate, anhrdous **A** and **B** are calculated as follows; hydrate 7.8mg/ml min, anhydrous **A** 19.9mg/ml min and anhydrous **B** 39.8mg/ml min. Interestingly, the newly obtained anhydrous **B** has a highest initial dissolution rate which is five times faster than hydrate form. Such a large difference in the dissolution rates is very important and useful information in the practical use and these results clearly suggest the effectiveness of an investigation of alternative forms such as hydrates and polymorphs. In addition, the slowest initial dissolution rates of hydrate is consistent with the fact of that

the monohydrate form is usually obtained by recrystallization.

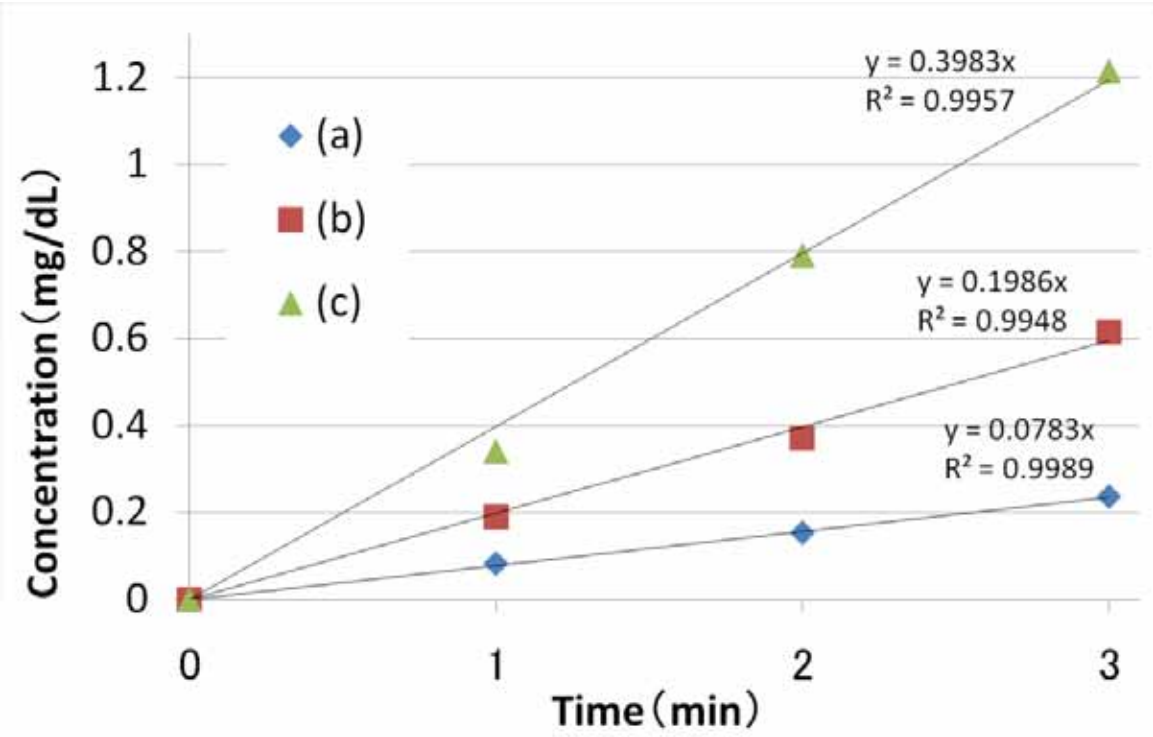

Figure 4-9 : Initial dissolution rates of acrinol (a) hydrate, (b) anhydrous **A**, (c) anhydrous **B**.

4.5. Concluding Remarks

In present work, new two anhydrous phases were found for acrinol. One is anhydrous **A** which was obtained by dehydration of acrinol hydrate and another is anhydrous **B** which was obtained by polymorphic transformation of anhydrous **A**. Interestingly, from DVS measurements, large difference in the hydration properties were found. Although the hydration of anhydrous **A** was occurred at low humidity condition (RH10%), the hydration of anhydrous **B** was occurred at high humidity condition (RH80%). In order to reveal the mechanistic aspects in the transformations and their hydration properties, crystal structures of anhydrous **A** and **B** were analyzed from powder X-ray diffraction data. The mechanistic aspects of the dehydration and polymorphic transformation were clearly drawn from resulted crystal structures and the difference in hydration properties were understood from the similarity of hydrate and anhydrous **A** and the large structural difference of hydrate and anhydrous **B**. As shown in this work, the technique of crystal structure determination from powder X-ray diffraction data can act a key role for understanding crystalline transformation such as dehydrations or polymorphic transformations. In addition to the understanding the transformation mechanisms, a large differences of the initial dissolution rate were found among acrinol hydrate, anhydrous **A** and **B**. The fastest dissolution rate was achieved for anhydrous **B** and which has five times faster than well used hydrate form. These results clearly suggest the effectiveness of an investigation of alternative forms such as hydrates and polymorphs.

Reference

(1) J. K. Haleblian, *J. Pharm. Sci.* **1975**, 64, 1269–1288.

(2) S. Data, D. J. W. Grant, *Nature Rev.* **2004**, 3, 42-57.

(3) K. R. Morrisa, U. J. Griesserb, C. J. Eckhardtc, J. G. Stowella, *Adv. Drug Deliv. Rev.* **2001**, 48, 91-114.

(4) R. K. Khankari, D. J. W. Grant, *Thermochim.Acta*, **1995**, 61-79.

(5) R. L. Te, U. J. Griesser, K. R. Morris, S. R. Byrn, J. G. Stowell, *Cryst. Growth & Des.*, **2003**, 3, 997-1004.

(6) K. Kobayashi, H. Fukuhara, T. Hata, Y. Ohashi, *Chem. Pharm. Bull.* **2003**, 51, 1356-1362.

(7) K. D. M. Harris, M. Tremayne, *Chem. Mater.* **1996**, 8, 2554-2570.

(8) K. D. M. Harris, M. Tremayne, B. M. Kariuki, *Angew. Chem. Int. Ed.* **2001**, 40, 1626-1651.

(9) V.V. Chernyshev, *Russian Chem. Bull.* **2001**, 50, 2273.

(10) W. I. F. David, K. Shankland, L. B. McCusker, C. Baerlocher, Ed.; Structure Determination from Powder Diffraction Data, OUP/IUCr, **2002**.

(11) A. Huq, P. W. Stephens, *J. Pharm. Sci.* **2003**, 92, 244-249.

(12) K. D. M. Harris, E. Y. Cheung, *Chem. Soc. Rev.* **2004**, 33, 526-538.

(13) M. Tremayne, *Phil. Trans. R. Soc.* **2004**, 362, 2691-2707.

(14) V. Favre-Nicolin, R. Cerny, *Z. Kristallogr.* **2004**, 219, 847-856.

(15) K. Shankland, A. J. Markvardsen, W. I. F. David, *Z. Kristallogr.* **2004**, 219, 857-865.

(16) V. Brodski, R. Peschar, H. Schenk, *J. Appl. Crystallogr.* **2005**, 38, 688-693.

(17) S. Karki, L. Fabian, T. Friscic, W. Jones, *Org. Lett.* **2007**, 9, 3133-3136.

(18) H. Tsue, M. Horiguchi, R. Tamura, K. Fujii, H. Uekusa, *J. Synth. Org. Chem. Japan* **2007**, 65, 1203-1212.

(19) W.I.F. David, K. Shankland, *Acta Crystallogr. Sect. A* **2008**, 64, 52-64.

(20) K. D. M. Harris, M. Tremayne, P. Lightfoot, P. G. Bruce, *J. Am. Chem. Soc.* **1994**, 116, 3543-3547.

(21) F. Guo, K. D. M. Harris, *J. Am. Chem. Soc.* **2005**, 127, 7314-7315.

(22) A. J. Mora, E. E. Avila, G. E. Delgado, A. N. Fitch, M. Brunelli, *Acta Cryst. B*,

2005,61 , 96-102.

(23) C. Platteau, J. Lefebvre, F. Affouard, J. F. Willart, P. Derollez, F. Mallet, *Acta Cryst. B*, **2005**, 61, 185-191..

(24) A. Hirano, S. Toyota, F. Toda, K.Fujii, H. Uekusa, *Angew. Chem. Int. Ed.* **2005**, 45 ,6013-6016.

(25) C. Guguta, H. Meekes, R. Gelder, *Cryst. Growth & Des.* **2006**, 6, 2686-2692.

(26) F. Guo, E. Y. Cheung, K. D. M. Harris, V. R. Pedireddi, *Cryst. Growth & Des.* **2006**, 6, 846-848.

(27) D. Albesa-Jové, Z. Pan, K. D. M. Harris, H. Uekusa, *Cryst. Growth & Des.***2008**, 8, 3641-3645.

(28) K.Fujii, Y. Ashida, H. Uekusa, A. Hirano, S. Toyota, F. Toda, Z. Pan, K. D. M. Harris, *Cryst. Growth & Des. in press.*

(29) S. Neudle, A. Aggarwal, *Acta Crystallogr. Sect. B* **1982**, 38, 2420-2424.

(30) A. Boultif, D. Louer, *J. Appl. Cryst.* **2004**, 37, 724-731.

(31) P. M. Wolff, *J. Appl. Cryst.* **1972**, 5, 243.

(32) G. S. Smith, R. L. Snyder, *J. Appl. Cryst.* **1979**, 12, 60-65.

(33) A. Le Bail, H. Duroy, J.L. Fourquet, *Mater. Res. Bull.*, **1988**, 23, 447-452.

(34) B. M. Kariuki, H. Serrano-González, R. L. Johnston, K. D. M. Harris, *Chem. Phys. Lett.*,**1997**, 280, 189-195.

(35) K. D. M. Harris, R. L. Johnston, B. M. Kariuki, *Acta Cryst. A*, **1998**, 54, 632-645.

(36) G. W. Turner, E. Tedesco, K. D. M. Harris, R. L. Johnston, B. M. Kariuki, *Chem. Phys. Lett.*, **2000**, 321, 183-190.

(37) S. Habershon, K. D. M. Harris, R. L. Johnston, *J. Comp. Chem.*, **2003**, 24, 1766-1774.

(38) E. Y. Cheung, E. E. McCabe, K. D. M. Harris, R. L. Johnston, E. Tedesco, K. M. P. Raja, P. Balaram, *Angew. Chem. Int. Ed.*, **2002**, 41, 494-496.

(39) Rietveld, H. M. 1969, J. Appl. Cryst. 1969, 2, 65-71.

(40) Larson, A. C.; Von Dreele, R. B. GSAS; Los Alamos Laboratory Report No. LA-UR-86-748; Los Alamos National Laboratory: Los Alamos, NM, 1987.

Chapter 5

General Conclusion

In this dissertation, the crystal-to-crystal pseudopolymorphic transformations, such as desolvation, solvation and solvent exchange phenomenon, were investigated by *ab initio* powder X-ray diffraction analysis technique. In all studies, the *ab initio* powder X-ray diffraction analysis technique acted the very important role, because these transformations could not reveal using traditional single crystal diffraction analysis.

In chapter 2, the unknown crystalline phase obtained by grinding of methanol solvate co-crystal of 5-methyl-2-pyridone and tirimesic acid was successfully revealed as hydrate phase by *ab initio* powder X-ray diffraction analysis. The result gave the idea that the transformations might be induced by solvent vapors, then, newly vapor induced crystalline transformations between co-crystal solvates are discovered and the mechanistic aspects are clearly revealed from the crystal structures. Furthermore, the differences of photoreactivities are revealed using the concept of reaction cavity.

In chapter 3, the three crystalline hydrates (dihydrate, monohydrate and anhydrous) of pharmaceutical lisinopril were determined by *ab initio* powder X-ray diffraction analysis, and the mechanistic aspects of two step dehydrations were clearly revealed. In addition to the dehydration mechanism, the expectation of the hydration mechanism was also speculated from the existence of vacant channel which can be considered as the reason of the instability of monohydrate and anhydrous phases for the humidity.

In chapter 4, new two anhydrous phases were found for pharmaceutical acrinol and the crystal structures of these phases were successfully determined by *ab initio* powder X-ray diffraction analysis. The mechanistic aspects of the dehydration and polymorphic transformations were clearly revealed from the structures. From the comparison of the crystal structures, it was also revealed

that the difference of the hydration properties comes from the structural similarity of anhydrous forms and hydrate form.

Clearly, the *ab initio* powder X-ray diffraction analysis technique is the powerful technique to investigate such transformations, because the technique has a potential to give the three dimensional information – “crystal structure” – from crystalline powder or polycrystalline materials which is generated by transformations. Thus, the technique enables us to establish the detailed structural changes and the relationship between properties and structures. The new strategies to investigate crystalline transformations were exhibited in the present dissertation. The strategy is expected to be used for many scenes in future.

Appendix : Crystallographic Data

Co-crystal hydrate of 5-methyl-2-pyridone and trimesic acid

Sample

Co-crystal hydrate of 5-methyl-2-pyridone and trimesic acid

Computing details

Program(s) used to refine structure: *GSAS*.

Crystal data

$C_{15}H_{15}NO_8$	$\alpha = 107.9100\ (16)^o$
$M_r = 337.28$	$\beta = 97.7464\ (16)^o$
Triclinic, $P\bar{1}$	$\gamma = 88.0882\ (10)^o$
$a = 10.5423\ (2)$ Å	$V = 772.59\ (4)$ Å^3
$b = 10.9487\ (3)$ Å	$Z = 2$
$c = 7.09939\ (11)$ Å	synchrotron radiation $\lambda = 1.2368$ Å

Data collection

$2\theta_{min} = 5.0$, $2\theta_{max} = 70.0^o$	Increment in $2\theta = 0.01^o$

Refinement

Least-squares matrix: full	163 parameters
$R_p = 0.036$	113 restraints
$R_{wp} = 0.052$	
$R_{exp} = 0.010$	$(\Delta/\sigma)_{max} = 0.04$
$S = 5.32$	

Profile function: CW Profile function number 2 with 18 terms Profile coefficients for Simpson's rule integration of pseudovoigt function C.J. Howard (1982). J. Appl. Cryst.,15,615-620. P. Thompson, D.E. Cox & J.B. Hastings (1987). J. Appl. Cryst.,20,79-83. #1(GU) = 125.278 #2(GV) = -21.681 #3(GW) = 3.937 #4(LX) = 0.394 #5(LY) = 18.193 #6(trns) = 0.000 #7(asym) = 0.3896 #8(shft) = -0.0699 #9(GP) = 0.000 #10(stec)= 0.00 #11(ptec)= 0.00 #12(sfec)= 0.00 #13(L11) = 0.000 #14(L22) = 0.000 #15(L33) = 0.031 #16(L12) = -0.001 #17(L13) = 0.004 #18(L23) = 0.013 Peak tails are ignored where the intensity is below 0.0010 times the peak Aniso. broadening axis 0.0 0.0 1.0

Fractional atomic coordinates and isotropic or equivalent isotropic displacement parameters (Å^2)

	x	*y*	*z*	U_{iso}*/U_{eq}
C1	0.7818 (6)	0.7031 (4)	−0.0005 (5)	0.0368 (11)*
C6	0.8848 (6)	0.7886 (6)	0.0621 (5)	0.0368 (11)*
C5	0.8671 (6)	0.9165 (5)	0.1669 (5)	0.0368 (11)*
C4	0.7438 (6)	0.9568 (5)	0.2049 (5)	0.0368 (11)*
C3	0.6410 (6)	0.8712 (5)	0.1421 (5)	0.0368 (11)*
C2	0.6593 (6)	0.7434 (5)	0.0386 (5)	0.0368 (11)*
C7	0.8041 (6)	0.5706 (5)	−0.1315 (4)	0.0368 (11)*
C9	0.9784 (5)	1.0063 (5)	0.2556 (5)	0.0368 (11)*
C8	0.5083 (5)	0.9129 (5)	0.1808 (4)	0.0368 (11)*
O1	0.9093 (6)	0.5375 (7)	−0.1796 (6)	0.0368 (11)*
O2	0.7024 (6)	0.4957 (7)	−0.1775 (4)	0.0368 (11)*
O5	0.9645 (7)	1.1109 (6)	0.3739 (6)	0.0368 (11)*
O6	1.0888 (6)	0.9579 (7)	0.2030 (5)	0.0368 (11)*
O3	0.4233 (6)	0.8398 (6)	0.1772 (6)	0.0368 (11)*
O4	0.5004 (7)	1.0380 (5)	0.2538 (4)	0.0368 (11)*
H6	0.7203 (13)	0.4156 (7)	−0.2505 (6)	0.0371 (13)*
H3	0.9683 (7)	0.7596 (11)	0.0346 (8)	0.0371 (13)*
H5	1.1535 (9)	1.0131 (13)	0.2663 (8)	0.0371 (13)*
H2	0.7298 (11)	1.0440 (6)	0.2759 (7)	0.0371 (13)*
H4	0.4247 (8)	1.0605 (13)	0.2993 (6)	0.0371 (13)*
H1	0.5893 (9)	0.6846 (9)	−0.0049 (8)	0.0371 (13)*
C10	0.7219 (6)	0.7704 (5)	0.5449 (5)	0.0368 (11)*
C11	0.6115 (6)	0.6913 (6)	0.4797 (5)	0.0368 (11)*
C12	0.6226 (6)	0.5650 (6)	0.3775 (5)	0.0368 (11)*
C13	0.7422 (7)	0.5100 (5)	0.3337 (5)	0.0368 (11)*
C14	0.8462 (6)	0.5886 (6)	0.3977 (5)	0.0368 (11)*
C15	0.7552 (8)	0.3699 (5)	0.2204 (6)	0.0368 (11)*
N1	0.8355 (6)	0.7155 (5)	0.5006 (5)	0.0368 (11)*
O7	0.7242 (7)	0.8898 (5)	0.6418 (6)	0.0368 (11)*
H7	0.5313 (8)	0.7289 (12)	0.5098 (7)	0.0371 (13)*
H8	0.5474 (8)	0.5130 (10)	0.3350 (6)	0.0371 (13)*
H9	0.9313 (7)	0.5623 (12)	0.3769 (7)	0.0371 (13)*
H10	0.9070 (8)	0.7676 (10)	0.5432 (6)	0.0371 (13)*
H11	0.759 (8)	0.3189 (18)	0.313 (3)	0.0371 (13)*
H12	0.833 (4)	0.357 (2)	0.156 (10)	0.0371 (13)*
H13	0.681 (5)	0.3426 (16)	0.118 (8)	0.0371 (13)*

O8	0.7439 (9)	0.2503 (11)	−0.3660 (15)	0.0368 (11)*
H14	0.711 (3)	0.220 (9)	−0.271 (7)	0.0371 (13)*
H15	0.823 (2)	0.215 (6)	−0.401 (3)	0.0371 (13)*

Geometric parameters (Å, °)

C1—C6	1.3903 (23)	O4—C8	1.3112 (23)
C1—C2	1.3871 (23)	O4—H4	0.9000 (12)
C1—C7	1.4937 (23)	C10—C11	1.4131 (23)
C6—H3	0.9500 (12)	C11—C12	1.3589 (23)
C5—C6	1.3890 (23)	C11—H7	0.9500 (12)
C5—C9	1.4955 (23)	C12—C13	1.4107 (23)
C4—C5	1.3922 (23)	C12—H8	0.9501 (12)
C4—H2	0.9500 (12)	C13—C14	1.3551 (23)
C3—C4	1.3900 (23)	C13—C15	1.5094 (23)
C3—C8	1.4920 (23)	C14—H9	0.9499 (12)
C2—C3	1.3866 (23)	C15—H11	0.9804 (12)
C2—H1	0.9499 (12)	C15—H12	0.9801 (12)
O1—C7	1.2150 (23)	C15—H13	0.9801 (12)
O2—C7	1.3150 (23)	N1—C10	1.3529 (23)
O2—H6	0.8999 (12)	N1—C14	1.3653 (23)
O5—C9	1.2119 (23)	N1—H10	0.9201 (12)
O6—C9	1.3152 (23)	O7—C10	1.2752 (23)
O6—H5	0.8999 (12)	O8—H14	0.9427 (12)
O3—C8	1.2135 (23)	O8—H15	0.9423 (12)
C6—C1—C2	121.0 (4)	C8—O4—H4	110.7 (7)
C6—C1—C7	117.9 (4)	O6—H5—O7^{i}	174.0 (7)
C2—C1—C7	120.6 (4)	C11—C10—N1	117.5 (4)
C1—C6—C5	120.5 (4)	C11—C10—O7	125.7 (5)
C1—C6—H3	120.1 (6)	N1—C10—O7	116.8 (5)
C5—C6—H3	119.4 (6)	C10—C11—C12	119.7 (4)
C6—C5—C4	118.3 (4)	C10—C11—H7	118.1 (6)
C6—C5—C9	121.2 (4)	C12—C11—H7	122.1 (6)
C4—C5—C9	120.1 (4)	C11—C12—C13	121.6 (4)
C5—C4—C3	121.1 (4)	C11—C12—H8	118.7 (6)
C5—C4—H2	119.5 (5)	C13—C12—H8	119.7 (6)
C3—C4—H2	119.4 (5)	C12—C13—C14	117.2 (4)
C4—C3—C2	120.4 (4)	C12—C13—C15	121.9 (5)
C4—C3—C8	121.7 (4)	C14—C13—C15	120.9 (5)
C2—C3—C8	117.9 (4)	C13—C14—N1	121.3 (4)

C1—C2—C3	118.7 (4)	C13—C14—H9	124.6 (6)
C1—C2—H1	120.6 (6)	N1—C14—H9	114.1 (6)
C3—C2—H1	120.7 (6)	C13—C15—H11	109.5 (9)
C1—C7—O1	121.2 (5)	C13—C15—H12	109.5 (19)
C1—C7—O2	113.5 (4)	C13—C15—H13	109.2 (19)
O1—C7—O2	125.2 (5)	H11—C15—H12	109.8 (13)
C5—C9—O5	120.8 (4)	H11—C15—H13	109.7 (16)
C5—C9—O6	114.1 (4)	H12—C15—H13	109.0 (7)
O5—C9—O6	125.0 (4)	C10—N1—C14	122.6 (4)
C3—C8—O3	123.7 (5)	C10—N1—H10	117.1 (6)
C3—C8—O4	112.0 (4)	C14—N1—H10	120.3 (6)
O3—C8—O4	123.3 (5)	H14—O8—H15	114.6 (35)
C7—O2—H6	111.2 (7)		
C9—O6—H5	111.0 (7)		

Lisinopril dihydrate

Sample

Lisinopril dihydrate

Computing details

Program(s) used to refine structure: *GSAS*.

Crystal data

$C_{21}H_{35}N_3O_7$	c = 14.30517 (14) Å
M_r = 441.52	β = 113.1447 (6)º
Monoclinic, $P2_1$	V = 1139.73 (2) Å^3
a = 14.66066 (14) Å	Z = 2
b = 5.91012 (6) Å	synchrotron radiation λ = 1.20854 Å

Data collection

$2\theta_{min}$ = 4.52, $2\theta_{max}$ = 72.99º	Increment in 2θ = 0.01º

Refinement

Least-squares matrix: full	244 parameters
R_p = 0.044	191 restraints
R_{wp} = 0.058	
R_{exp} = 0.012	$(\Delta/\sigma)_{max}$ = 0.68
S = 5.65	

Profile function: CW Profile function number 2 with 18 terms Profile coefficients for Simpson's rule integration of pseudovoigt function C.J. Howard (1982). J. Appl. Cryst.,15,615-620. P. Thompson, D.E. Cox & J.B. Hastings (1987). J. Appl. Cryst.,20,79-83. #1(GU) = 61.131 #2(GV) = -15.447 #3(GW) = 0.502 #4(LX) = 3.542 #5(LY) = 3.798 #6(trns) = 0.000 #7(asym) = 0.4251 #8(shft) = -0.0005 #9(GP) = 0.000 #10(stec)= 10.74 #11(ptec)= -1.64 #12(sfec)= 0.00 #13(L11) = 0.000 #14(L22) = 0.004 #15(L33) = 0.000 #16(L12) = 0.000 #17(L13) = 0.000 #18(L23) = 0.000 Peak tails are ignored where the intensity is below 0.0010 times the peak Aniso. broadening axis 0.0 0.0 1.0

Fractional atomic coordinates and isotropic or equivalent isotropic displacement parameters (Å^2)

	x	*y*	*z*	U_{iso}*/U_{eq}
C1	0.7757 (3)	0.0	0.8469 (2)	0.0441 (7)*
C2	0.8581 (4)	−0.1405 (6)	0.8930 (2)	0.0441 (7)*
C3	0.9517 (3)	−0.0686 (11)	0.90186 (17)	0.0441 (7)*
C4	0.9632 (2)	0.1435 (11)	0.8649 (3)	0.0441 (7)*
C5	0.8809 (3)	0.2842 (6)	0.8188 (3)	0.0441 (7)*
C6	0.7871 (2)	0.2124 (3)	0.80981 (17)	0.0441 (7)*
C7	0.6725 (3)	−0.0799 (8)	0.8372 (3)	0.0441 (7)*
C8	0.6060 (3)	−0.1141 (14)	0.7267 (3)	0.0441 (7)*
C9	0.50229 (17)	−0.2047 (11)	0.7160 (2)	0.0441 (7)*
C10	0.50890 (13)	−0.4203 (10)	0.77722 (19)	0.0441 (7)*
O11	0.49748 (15)	−0.4156 (12)	0.8623 (2)	0.0441 (7)*
O12	0.5256 (2)	−0.5905 (11)	0.7383 (3)	0.0441 (7)*
N13	0.4446 (3)	−0.0265 (11)	0.7488 (3)	0.0441 (7)*
C14	0.3364 (2)	0.0101 (11)	0.6863 (2)	0.0441 (7)*
C15	0.3063 (3)	0.0733 (15)	0.5769 (3)	0.0441 (7)*
C16	0.1976 (3)	0.0828 (14)	0.5244 (4)	0.0441 (7)*
C17	0.1677 (4)	0.1963 (12)	0.4137 (3)	0.0441 (7)*
C18	0.1528 (3)	0.4371 (11)	0.4178 (5)	0.0441 (7)*
N19	0.0547 (4)	0.4863 (10)	0.4254 (4)	0.0441 (7)*
C20	0.28635 (17)	−0.2080 (10)	0.69911 (13)	0.0441 (7)*
O21	0.2951 (3)	−0.3847 (11)	0.65364 (19)	0.0441 (7)*
N22	0.2453 (2)	−0.2203 (10)	0.76657 (19)	0.0441 (7)*
C23	0.2566 (5)	−0.0662 (10)	0.8516 (4)	0.0441 (7)*
C24	0.2296 (5)	−0.2003 (11)	0.9243 (4)	0.0441 (7)*
C25	0.1808 (4)	−0.3924 (12)	0.8786 (4)	0.0441 (7)*
C26	0.2038 (2)	−0.4455 (9)	0.7845 (3)	0.0441 (7)*
C27	0.10894 (17)	−0.5100 (8)	0.6936 (3)	0.0441 (7)*
O28	0.0718 (3)	−0.3853 (9)	0.6198 (3)	0.0441 (7)*
O29	0.0733 (2)	−0.7059 (8)	0.7029 (4)	0.0441 (7)*
H30	0.8503 (6)	−0.2847 (6)	0.9182 (3)	0.0536 (11)*
H31	1.0077 (4)	−0.1638 (14)	0.93315 (18)	0.0536 (11)*
H32	1.0270 (3)	0.1923 (14)	0.8710 (4)	0.0536 (11)*
H33	0.8888 (5)	0.4284 (6)	0.7936 (4)	0.0536 (11)*
H34	0.7311 (3)	0.3077 (6)	0.77853 (18)	0.0536 (11)*

H35	0.6433 (3)	0.0343 (16)	0.8667 (6)	0.0536 (11)*
H36	0.6791 (5)	−0.2231 (12)	0.8738 (4)	0.0536 (11)*
H37	0.6368 (3)	−0.223 (2)	0.6965 (5)	0.0536 (11)*
H38	0.5975 (5)	0.0305 (19)	0.6907 (5)	0.0536 (11)*
H39	0.4638 (3)	−0.2482 (14)	0.6452 (3)	0.0536 (11)*
H40	0.5038 (2)	−0.5596 (13)	0.8885 (3)	0.0536 (11)*
H41	0.4749 (3)	0.0994 (11)	0.7585 (6)	0.0536 (11)*
H42	0.3124 (3)	0.1377 (10)	0.7141 (3)	0.0536 (11)*
H43	0.3323 (7)	−0.039 (2)	0.5435 (5)	0.0536 (11)*
H44	0.3341 (7)	0.222 (2)	0.5727 (5)	0.0536 (11)*
H45	0.1703 (6)	0.174 (2)	0.5646 (6)	0.0536 (11)*
H46	0.1705 (7)	−0.0709 (19)	0.5166 (6)	0.0536 (11)*
H47	0.1062 (6)	0.1269 (13)	0.3662 (4)	0.0536 (11)*
H48	0.2208 (6)	0.1691 (17)	0.3897 (6)	0.0536 (11)*
H49	0.1534 (7)	0.5078 (17)	0.3561 (9)	0.0536 (11)*
H50	0.2067 (4)	0.5005 (15)	0.4773 (10)	0.0536 (11)*
H51	0.0179 (6)	0.3671 (13)	0.409 (4)	0.0536 (11)*
H52	0.0647 (10)	0.527 (8)	0.4868 (9)	0.0536 (11)*
H53	0.2119 (11)	0.0636 (12)	0.8271 (9)	0.0536 (11)*
H54	0.3255 (7)	−0.014 (2)	0.8841 (7)	0.0536 (11)*
H55	0.1866 (11)	−0.1095 (15)	0.9475 (13)	0.0536 (11)*
H56	0.2900 (9)	−0.2412 (18)	0.9828 (4)	0.0536 (11)*
H57	0.2027 (10)	−0.5188 (11)	0.9267 (6)	0.0536 (11)*
H58	0.1092 (4)	−0.370 (3)	0.8576 (7)	0.0536 (11)*
H59	0.2555 (3)	−0.5617 (10)	0.8019 (7)	0.0536 (11)*
H60	0.0168 (2)	−0.7347 (9)	0.6462 (5)	0.0536 (11)*
O61	0.5132 (8)	−0.3194 (16)	1.0624 (5)	0.0441 (7)*
H62	0.542 (5)	−0.435 (8)	1.111 (3)	0.0536 (11)*
H63	0.512 (5)	−0.366 (5)	0.9983 (14)	0.0536 (11)*
O64	0.5171 (6)	−0.6002 (17)	0.5353 (6)	0.0441 (7)*
H65	0.491 (6)	−0.741 (9)	0.505 (7)	0.0536 (11)*
H66	0.519 (4)	−0.596 (10)	0.6026 (12)	0.0536 (11)*

Geometric parameters (Å, °)

C1—C2	1.3992 (19)	C16—C17	1.6136 (20)
C1—C6	1.3983 (19)	C16—H45	0.9800 (5)
C1—C7	1.538 (5)	C16—H46	0.9800 (5)
C2—C3	1.3936 (19)	C17—H47	0.9800 (5)

C2—H30	0.9500 (5)	C17—H48	0.9800 (5)
C3—C4	1.3960 (19)	C18—N19	1.5125 (20)
C3—H31	0.9500 (5)	C18—H49	0.9800 (5)
C4—C5	1.3989 (19)	C18—H50	0.9800 (5)
C4—H32	0.9500 (5)	N19—H51	0.8616 (20)
C5—C6	1.3953 (19)	N19—H52	0.8664 (20)
C5—H33	0.9500 (5)	C20—O21	1.2634 (20)
C6—H34	0.9500 (5)	C20—N22	1.3252 (19)
C7—C8	1.5104 (20)	N22—C23	1.4756 (19)
C7—H35	0.9800 (5)	N22—C26	1.526 (5)
C7—H36	0.9800 (5)	C23—C24	1.4796 (20)
C8—C9	1.5613 (19)	C23—H53	0.9800 (5)
C8—H37	0.9800 (5)	C23—H54	0.9801 (5)
C8—H38	0.9800 (5)	C24—C25	1.3641 (20)
C9—C10	1.5281 (20)	C24—H55	0.9800 (5)
C9—N13	1.5357 (20)	C24—H56	0.9800 (5)
C9—H39	0.9800 (5)	C25—C26	1.5438 (19)
C10—O11	1.2926 (20)	C25—H57	0.9800 (5)
C10—O12	1.2200 (20)	C25—H58	0.9800 (5)
O11—H40	0.9200 (5)	C26—N22	1.526 (5)
O11—H63	1.896 (7)	C26—C27	1.5323 (19)
N13—C14	1.4994 (19)	C26—H59	0.9799 (5)
N13—H41	0.8500 (5)	C27—O28	1.2257 (20)
C14—C15	1.4977 (20)	C27—O29	1.2981 (20)
C14—C20	1.5290 (20)	O29—H60	0.9200 (5)
C14—H42	0.9800 (5)	O64—H65	0.9502 (11)
C15—C16	1.4713 (19)	O64—H66	0.9501 (11)
C15—H43	0.9800 (5)		
C15—H44	0.9800 (5)		
C2—C1—C6	120.09 (12)	C15—C16—H45	109.42 (12)
C2—C1—C7	119.80 (19)	C15—C16—H46	109.42 (15)
C6—C1—C7	120.11 (20)	C17—C16—H45	109.38 (19)
C1—C2—C3	119.95 (11)	C17—C16—H46	109.39 (22)
C1—C2—H30	120.04 (9)	H45—C16—H46	109.41 (14)
C3—C2—H30	120.02 (9)	C16—C17—C18	110.94 (22)
C2—C3—C4	120.00 (10)	C16—C17—H47	109.18 (13)
C2—C3—H31	119.99 (9)	C16—C17—H48	109.19 (15)

C4—C3—H31	120.00 (9)	C18—C17—H47	109.17 (12)
C3—C4—C5	120.14 (10)	C18—C17—H48	109.18 (17)
C3—C4—H32	119.92 (9)	H47—C17—H48	109.16 (13)
C5—C4—H32	119.94 (9)	C17—C18—N19	110.78 (21)
C4—C5—C6	119.92 (11)	C17—C18—H49	109.21 (13)
C4—C5—H33	120.05 (9)	C17—C18—H50	109.21 (13)
C6—C5—H33	120.03 (9)	N19—C18—H49	109.19 (17)
C1—C6—C5	119.90 (11)	N19—C18—H50	109.22 (13)
C1—C6—H34	120.05 (9)	H49—C18—H50	109.22 (12)
C5—C6—H34	120.04 (9)	C18—N19—H51	109.7 (13)
C1—C7—C8	110.08 (16)	C18—N19—H52	109.9 (4)
C1—C7—H35	109.33 (18)	H51—N19—H52	109.6 (7)
C1—C7—H36	109.34 (16)	C14—C20—O21	119.00 (22)
C8—C7—H35	109.36 (11)	C14—C20—N22	120.67 (20)
C8—C7—H36	109.35 (16)	O21—C20—N22	119.77 (22)
H35—C7—H36	109.36 (11)	C20—N22—C23	129.04 (22)
C7—C8—C9	110.61 (18)	C20—N22—C26	119.71 (22)
C7—C8—H37	109.23 (13)	C23—N22—C26	108.85 (17)
C7—C8—H38	109.23 (15)	N22—C23—C24	105.90 (16)
C9—C8—H37	109.26 (15)	N22—C23—H53	110.19 (18)
C9—C8—H38	109.26 (17)	N22—C23—H54	110.19 (13)
H37—C8—H38	109.23 (11)	C24—C23—H53	110.15 (20)
C8—C9—C10	112.95 (21)	C24—C23—H54	110.14 (13)
C8—C9—N13	111.55 (23)	H53—C23—H54	110.20 (12)
C8—C9—H39	109.51 (12)	C23—C24—C25	110.17 (33)
C10—C9—N13	108.33 (25)	C23—C24—H55	109.32 (32)
C10—C9—H39	104.74 (32)	C23—C24—H56	109.34 (14)
N13—C9—H39	109.51 (11)	C25—C24—H55	109.34 (14)
C9—C10—O11	121.29 (23)	C25—C24—H56	109.34 (15)
C9—C10—O12	113.87 (23)	H55—C24—H56	109.32 (11)
O11—C10—O12	124.84 (24)	C24—C25—C26	109.46 (20)
C10—O11—H40	109.49 (11)	C24—C25—H57	109.47 (11)
C9—N13—C14	119.83 (22)	C24—C25—H58	109.47 (14)
C9—N13—H41	109.49 (20)	C26—C25—H57	109.47 (21)
C14—N13—H41	109.49 (14)	C26—C25—H58	109.49 (12)
N13—C14—C15	117.86 (22)	H57—C25—H58	109.47 (15)
N13—C14—C20	104.57 (23)	N22—C26—C25	101.97 (25)

N13—C14—H42	109.48 (11)	N22—C26—C27	111.30 (24)
C15—C14—C20	112.17 (24)	N22—C26—H59	109.50 (14)
C15—C14—H42	103.1 (4)	C25—C26—C27	110.78 (20)
C20—C14—H42	109.53 (14)	C25—C26—H59	109.47 (16)
C14—C15—C16	110.94 (20)	C27—C26—H59	113.23 (35)
C14—C15—H43	109.17 (23)	C26—C27—O28	121.92 (22)
C14—C15—H44	109.16 (21)	C26—C27—O29	113.71 (22)
C16—C15—H43	109.18 (14)	O28—C27—O29	124.37 (23)
C16—C15—H44	109.17 (18)	C27—O29—H60	109.51 (11)
H43—C15—H44	109.19 (12)	H62—O61—H63	109.6 (17)
C15—C16—C17	109.81 (19)	H65—O64—H66	109.5 (26)

Lisinopril monohydrate

Sample

Lisinopril monohydrate

Computing details

Program(s) used to refine structure: *GSAS*.

Crystal data

$C_7H_{11}NO_2$	c = 14.2254 (3) Å
M_r = 141.17	β = 112.8796 (13)º
Monoclinic, $P2_1$	V = 1136.58 (5) Å^3
a = 14.6677 (3) Å	Z = 2
b = 5.91243 (11) Å	synchrotron radiation λ = 1.200253 Å

Data collection

$2\theta_{min}$ = 3.0, $2\theta_{max}$ = 79.02º	Increment in 2θ = 0.01º

Refinement

R_p = 0.034	232 parameters
R_{wp} = 0.049	185 restraints
R_{exp} = 0.024	
S = 2.36	$(\Delta/\sigma)_{max}$ = 0.08
Least-squares matrix: full	Profile function: CW Profile function number 2 with 18 terms Profile coefficients for Simpson's rule integration of pseudovoigt function C.J. Howard (1982). J. Appl. Cryst.,15,615-620. P. Thompson, D.E. Cox & J.B. Hastings (1987). J. Appl. Cryst.,20,79-83. #1(GU) = 102.403 #2(GV) = -15.612 #3(GW) = 1.125 #4(LX) = 3.505 #5(LY) = 6.436 #6(trns) = 0.000 #7(asym) = 0.3874 #8(shft) = 0.0000 #9(GP) = 0.000 #10(stec)= 13.03 #11(ptec)= -1.69 #12(sfec)= 0.00 #13(L11) = 0.000 #14(L22) = 0.000 #15(L33) = 0.000 #16(L12) = -0.002 #17(L13) = 0.000 #18(L23) = -0.001 Peak tails are ignored where the intensity is below 0.0010 times the peak Aniso. broadening axis 0.0 0.0 1.0

Fractional atomic coordinates and isotropic or equivalent isotropic displacement parameters (Å2)

	x	*y*	*z*	U_{iso}*/U_{eq}
C1	0.7680 (5)	0.0	0.8410 (3)	0.0372 (15)*
C2	0.8492 (6)	−0.1433 (7)	0.8872 (4)	0.0372 (15)*
C3	0.9439 (5)	−0.0738 (14)	0.8979 (3)	0.0372 (15)*
C4	0.9575 (5)	0.1390 (14)	0.8624 (5)	0.0372 (15)*
C5	0.8764 (5)	0.2822 (7)	0.8162 (5)	0.0372 (15)*
C6	0.7816 (5)	0.2127 (2)	0.8055 (3)	0.0372 (15)*
C7	0.6622 (3)	−0.0767 (10)	0.8288 (3)	0.0372 (15)*
C8	0.5981 (3)	−0.114 (2)	0.7176 (3)	0.0372 (15)*
C9	0.49649 (19)	−0.2113 (17)	0.7072 (3)	0.0372 (15)*
C10	0.50775 (19)	−0.4226 (15)	0.7729 (3)	0.0372 (15)*
O11	0.4965 (2)	−0.4152 (18)	0.8590 (3)	0.0372 (15)*
O12	0.5278 (3)	−0.5919 (17)	0.7356 (5)	0.0372 (15)*
N13	0.4416 (3)	−0.0339 (15)	0.7433 (4)	0.0372 (15)*
C14	0.3341 (3)	0.0022 (15)	0.6825 (2)	0.0372 (15)*
C15	0.3031 (4)	0.0440 (19)	0.5711 (3)	0.0372 (15)*
C16	0.2003 (4)	0.120 (3)	0.5280 (7)	0.0372 (15)*
C17	0.1748 (7)	0.216 (2)	0.4146 (4)	0.0372 (15)*
C18	0.1496 (8)	0.452 (2)	0.4090 (12)	0.0372 (15)*
N19	0.0501 (10)	0.481 (3)	0.4161 (13)	0.0372 (15)*
C20	0.2864 (2)	−0.2150 (14)	0.69875 (15)	0.0372 (15)*
O21	0.2952 (3)	−0.3952 (15)	0.65587 (17)	0.0372 (15)*
N22	0.2460 (2)	−0.2216 (12)	0.76628 (15)	0.0372 (15)*
C23	0.2612 (8)	−0.0646 (14)	0.8509 (6)	0.0372 (15)*
C24	0.2258 (9)	−0.1855 (16)	0.9213 (6)	0.0372 (15)*
C25	0.1795 (5)	−0.3805 (15)	0.8773 (5)	0.0372 (15)*
C26	0.2054 (3)	−0.4362 (12)	0.7844 (4)	0.0372 (15)*
C27	0.1113 (3)	−0.5026 (11)	0.6938 (5)	0.0372 (15)*
O28	0.0756 (3)	−0.3802 (13)	0.6192 (5)	0.0372 (15)*
O29	0.0750 (4)	−0.6966 (11)	0.7049 (8)	0.0372 (15)*
H30	0.8400 (8)	−0.2879 (7)	0.9113 (5)	0.043 (2)*
H31	0.9990 (6)	−0.1711 (18)	0.9293 (3)	0.043 (2)*
H32	1.0218 (5)	0.1862 (19)	0.8696 (6)	0.043 (2)*
H33	0.8857 (7)	0.4267 (7)	0.7921 (6)	0.043 (2)*
H34	0.7266 (5)	0.3101 (5)	0.7741 (3)	0.043 (2)*

H35	0.6323 (3)	0.040 (2)	0.8566 (9)	0.043 (2)*
H36	0.6669 (5)	−0.2181 (16)	0.8664 (4)	0.043 (2)*
H37	0.6309 (4)	−0.220 (3)	0.6881 (6)	0.043 (2)*
H38	0.5881 (6)	0.031 (3)	0.6811 (7)	0.043 (2)*
H39	0.4575 (3)	−0.249 (2)	0.6357 (3)	0.043 (2)*
H40	0.5060 (4)	−0.5573 (19)	0.8876 (4)	0.043 (2)*
H41	0.4718 (4)	0.0918 (15)	0.7517 (6)	0.043 (2)*
H42	0.3106 (4)	0.1302 (14)	0.7108 (3)	0.043 (2)*
H43	0.3093 (11)	−0.096 (2)	0.5373 (6)	0.043 (2)*
H44	0.3456 (5)	0.161 (3)	0.5604 (5)	0.043 (2)*
H45	0.1909 (12)	0.240 (4)	0.5708 (8)	0.043 (2)*
H46	0.1565 (7)	−0.007 (4)	0.5250 (12)	0.043 (2)*
H47	0.1188 (13)	0.131 (3)	0.3661 (7)	0.043 (2)*
H48	0.2325 (12)	0.196 (4)	0.3967 (10)	0.043 (2)*
H49	0.1467 (15)	0.515 (3)	0.3441 (17)	0.043 (2)*
H50	0.2001 (11)	0.533 (2)	0.4655 (19)	0.043 (2)*
H51	0.023 (2)	0.351 (4)	0.41 (2)	0.043 (2)*
H52	0.0579 (15)	0.55 (4)	0.473 (9)	0.043 (2)*
H53	0.2225 (15)	0.0736 (15)	0.8257 (13)	0.043 (2)*
H54	0.3316 (10)	−0.028 (3)	0.8855 (10)	0.043 (2)*
H55	0.1793 (15)	−0.089 (2)	0.937 (2)	0.043 (2)*
H56	0.2823 (15)	−0.221 (3)	0.9845 (5)	0.043 (2)*
H57	0.2017 (10)	−0.5042 (16)	0.9269 (8)	0.043 (2)*
H58	0.1078 (5)	−0.362 (3)	0.8547 (8)	0.043 (2)*
H59	0.2569 (4)	−0.5527 (13)	0.8034 (7)	0.043 (2)*
H60	0.0188 (4)	−0.7267 (12)	0.6481 (9)	0.043 (2)*
O61	0.5017 (14)	−0.354 (3)	1.0654 (12)	0.0372 (15)*
H62	0.544 (6)	−0.44 (2)	1.121 (5)	0.043 (2)*
H63	0.503 (7)	−0.409 (8)	1.003 (2)	0.043 (2)*

Geometric parameters (Å, °)

C1—C2	1.3999 (14)	C15—H44	0.9800 (4)
C1—C6	1.3985 (14)	C16—C17	1.6105 (15)
C1—C7	1.561 (7)	C16—H45	0.9800 (4)
C2—C3	1.3999 (14)	C16—H46	0.9800 (4)
C2—H30	0.9500 (4)	C17—C18	1.4403 (15)
C3—C4	1.3984 (14)	C17—H47	0.9800 (4)
C3—H31	0.9500 (4)	C17—H48	0.9800 (4)

C4—C5	1.3987 (14)	C18—N19	1.5102 (15)
C4—H32	0.9500 (4)	C18—H49	0.9800 (4)
C5—C6	1.4001 (14)	C18—H50	0.9800 (4)
C5—H33	0.9500 (4)	N19—H51	0.8600 (4)
C6—H34	0.9500 (4)	N19—H52	0.8600 (4)
C7—C8	1.5100 (15)	C20—O21	1.2589 (15)
C7—H35	0.9800 (4)	C20—N22	1.3100 (15)
C7—H36	0.9800 (4)	N22—C23	1.4673 (15)
C8—C9	1.5513 (15)	N22—C26	1.467 (6)
C8—H37	0.9800 (4)	C23—C24	1.4793 (15)
C8—H38	0.9800 (4)	C23—H53	0.9800 (4)
C9—C10	1.5296 (15)	C23—H54	0.9800 (4)
C9—N13	1.5273 (15)	C24—C25	1.3611 (15)
C9—H39	0.9800 (4)	C24—H55	0.9800 (4)
C10—O11	1.2993 (15)	C24—H56	0.9800 (4)
C10—O12	1.2214 (15)	C25—C26	1.5453 (14)
O11—H40	0.9200 (4)	C25—H57	0.9800 (4)
N13—C14	1.4896 (15)	C25—H58	0.9800 (4)
N13—H41	0.8500 (4)	C26—C27	1.5285 (15)
C14—C15	1.4899 (15)	C26—H59	0.9800 (4)
C14—C20	1.5225 (15)	C27—O28	1.2214 (15)
C14—H42	0.9800 (4)	C27—O29	1.2996 (15)
C15—C14	1.4899 (15)	O29—H60	0.9200 (4)
C15—C16	1.4602 (15)	O61—H62	0.9505 (15)
C15—H43	0.9800 (4)	O61—H63	0.9504 (15)
C2—C1—C6	119.92 (9)	C17—C16—H45	109.52 (30)
C2—C1—C7	120.25 (16)	C17—C16—H46	109.52 (20)
C6—C1—C7	119.83 (16)	H45—C16—H46	109.52 (13)
C1—C2—C3	120.05 (8)	C16—C17—C18	110.54 (34)
C1—C2—H30	119.98 (7)	C16—C17—H47	109.25 (18)
C3—C2—H30	119.97 (7)	C16—C17—H48	109.26 (20)
C2—C3—C4	119.99 (8)	C18—C17—H47	109.25 (11)
C2—C3—H31	120.01 (7)	C18—C17—H48	109.25 (27)
C4—C3—H31	120.00 (6)	H47—C17—H48	109.26 (19)
C3—C4—C5	119.98 (7)	C17—C18—N19	109.92 (30)
C3—C4—H32	120.01 (7)	C17—C18—H49	109.38 (27)
C5—C4—H32	120.01 (7)	C17—C18—H50	109.38 (18)

C4—C5—C6	120.04 (8)	N19—C18—H49	109.38 (24)
C4—C5—H33	119.98 (6)	N19—C18—H50	109.38 (18)
C6—C5—H33	119.98 (7)	H49—C18—H50	109.38 (13)
C1—C6—C5	120.02 (8)	C18—N19—H51	109 (7)
C1—C6—H34	119.99 (6)	C18—N19—H52	109.5 (29)
C5—C6—H34	120.00 (7)	H51—N19—H52	109.5 (23)
C1—C7—C8	110.16 (16)	C14—C20—O21	120.03 (18)
C1—C7—H35	109.33 (20)	C14—C20—N22	120.11 (17)
C1—C7—H36	109.33 (20)	O21—C20—N22	119.38 (17)
C8—C7—H35	109.33 (9)	C20—N22—C23	127.96 (18)
C8—C7—H36	109.33 (18)	C20—N22—C26	119.01 (20)
H35—C7—H36	109.34 (9)	C23—N22—C26	110.22 (18)
C7—C8—C9	109.67 (14)	N22—C23—C24	105.58 (17)
C7—C8—H37	109.44 (10)	N22—C23—H53	110.22 (23)
C7—C8—H38	109.43 (15)	N22—C23—H54	110.22 (12)
C9—C8—H37	109.44 (16)	C24—C23—H53	110.22 (26)
C9—C8—H38	109.43 (20)	C24—C23—H54	110.23 (10)
H37—C8—H38	109.43 (9)	H53—C23—H54	110.27 (13)
C8—C9—C10	111.97 (19)	C23—C24—C25	109.9 (4)
C8—C9—N13	109.00 (20)	C23—C24—H55	109.4 (4)
C8—C9—H39	109.49 (9)	C23—C24—H56	109.38 (12)
C10—C9—N13	107.57 (21)	C25—C24—H55	109.37 (15)
C10—C9—H39	109.26 (23)	C25—C24—H56	109.37 (17)
N13—C9—H39	109.49 (8)	H55—C24—H56	109.37 (9)
C9—C10—O11	121.68 (18)	C24—C25—C26	109.25 (22)
C9—C10—O12	113.02 (18)	C24—C25—H57	109.51 (10)
O11—C10—O12	125.30 (18)	C24—C25—H58	109.51 (14)
C10—O11—H40	109.50 (8)	C26—C25—H57	109.52 (21)
C9—N13—C14	118.77 (20)	C26—C25—H58	109.52 (9)
C9—N13—H41	109.48 (15)	H57—C25—H58	109.51 (14)
C14—N13—H41	109.49 (12)	N22—C26—C25	102.57 (24)
N13—C14—C15	117.20 (20)	N22—C26—C27	111.67 (21)
N13—C14—C20	103.67 (21)	N22—C26—H59	109.50 (12)
N13—C14—H42	109.47 (9)	C25—C26—C27	109.51 (19)
C15—C14—C20	109.48 (21)	C25—C26—H59	109.51 (13)
C15—C14—H42	107.36 (30)	C27—C26—H59	113.51 (30)
C20—C14—H42	109.49 (11)	C26—C27—O28	121.44 (17)

C14—C15—C16	109.64 (20)	C26—C27—O29	113.74 (18)
C14—C15—H43	109.44 (26)	O28—C27—O29	124.82 (18)
C14—C15—H44	109.43 (19)	C27—O29—H60	109.50 (8)
C16—C15—H43	109.44 (10)	H62—O61—H63	109.8 (21)
C16—C15—H44	109.44 (19)		
H43—C15—H44	109.44 (13)		
C15—C16—C17	109.23 (24)		
C15—C16—H45	109.52 (16)		
C15—C16—H46	109.52 (26)		

Lisinopril anhydrous

Sample

Lisinopril anhydrous

Computing details

Program(s) used to refine structure: *GSAS*.

Crystal data

$C_{21}H_{31}N_3O_5$	c = 14.2291 (3) Å
M_r = 405.49	β = 120.6209 (9)º
Monoclinic, $P2_1$	V = 1104.84 (4) Å^3
a = 15.1769 (3) Å	Z = 2
b = 5.94511 (8) Å	synchrotron radiation λ = 1.1977 Å

Data collection

$2\theta_{min}$ = 4.01, $2\theta_{max}$ = 77.13º	Increment in 2θ = 0.01º

Refinement

Least-squares matrix: full	244 parameters
R_p = 0.044	191 restraints
R_{wp} = 0.058	
R_{exp} = 0.012	$(\Delta/\sigma)_{max}$ = 0.68
S = 5.65	

Profile function: CW Profile function number 2 with 18 terms Profile coefficients for Simpson's rule integration of pseudovoigt function C.J. Howard (1982). J. Appl. Cryst.,15,615-620. P. Thompson, D.E. Cox & J.B. Hastings (1987). J. Appl. Cryst.,20,79-83. #1(GU) = 61.131 #2(GV) = -15.447 #3(GW) = 0.502 #4(LX) = 3.542 #5(LY) = 3.798 #6(trns) = 0.000 #7(asym) = 0.4251 #8(shft) = -0.0005 #9(GP) = 0.000 #10(stec)= 10.74 #11(ptec)= -1.64 #12(sfec)= 0.00 #13(L11) = 0.000 #14(L22) = 0.004 #15(L33) = 0.000 #16(L12) = 0.000 #17(L13) = 0.000 #18(L23) = 0.000 Peak tails are ignored where the intensity is below 0.0010 times the peak Aniso. broadening axis 0.0 0.0 1.0

Fractional atomic coordinates and isotropic or equivalent isotropic displacement parameters (Å^2)

	x	*y*	*z*	U_{iso}*/U_{eq}
C1	−0.7325 (5)	0.0	0.2160 (5)	0.0108 (11)*
C2	−0.7504 (5)	0.2066 (8)	0.2480 (5)	0.0108 (11)*
C3	−0.8480 (6)	0.2659 (11)	0.2221 (7)	0.0108 (11)*
C4	−0.9289 (4)	0.1185 (17)	0.1636 (6)	0.0108 (11)*
C5	−0.9116 (5)	−0.0891 (17)	0.1314 (5)	0.0108 (11)*
C6	−0.8137 (7)	−0.1491 (10)	0.1574 (6)	0.0108 (11)*
C7	−0.6238 (7)	−0.0516 (14)	0.2494 (6)	0.0108 (11)*
C8	−0.6136 (5)	−0.1344 (19)	0.1572 (6)	0.0108 (11)*
C9	−0.5079 (5)	−0.2395 (17)	0.2010 (5)	0.0108 (11)*
C10	−0.5153 (4)	−0.4544 (15)	0.1397 (3)	0.0108 (11)*
O12	−0.5543 (6)	−0.6165 (18)	0.1616 (6)	0.0108 (11)*
O11	−0.4809 (5)	−0.4508 (19)	0.0716 (4)	0.0108 (11)*
N13	−0.4563 (6)	−0.0802 (18)	0.1619 (6)	0.0108 (11)*
C14	−0.3484 (5)	−0.0194 (16)	0.2376 (5)	0.0108 (11)*
C15	−0.3267 (6)	0.037 (2)	0.3513 (7)	0.0108 (11)*
C16	−0.2202 (6)	0.125 (2)	0.4226 (9)	0.0108 (11)*
C17	−0.2101 (7)	0.223 (3)	0.5350 (8)	0.0108 (11)*
C18	−0.1574 (9)	0.4398 (19)	0.5667 (12)	0.0108 (11)*
N19	−0.0649 (8)	0.440 (3)	0.5511 (9)	0.0108 (11)*
C20	−0.2893 (5)	−0.2263 (15)	0.2334 (3)	0.0108 (11)*
O21	−0.2966 (6)	−0.4104 (17)	0.2733 (5)	0.0108 (11)*
N22	−0.2339 (5)	−0.2137 (17)	0.1841 (6)	0.0108 (11)*
C23	−0.2468 (9)	−0.0528 (17)	0.0986 (10)	0.0108 (11)*
C24	−0.1951 (9)	−0.1518 (18)	0.0447 (10)	0.0108 (11)*
C25	−0.1423 (7)	−0.337 (2)	0.1014 (9)	0.0108 (11)*
C26	−0.1848 (4)	−0.4133 (16)	0.1758 (6)	0.0108 (11)*
C27	−0.0955 (3)	−0.4890 (13)	0.2869 (5)	0.0108 (11)*
O28	−0.0675 (6)	−0.3823 (16)	0.3719 (7)	0.0108 (11)*
O29	−0.0543 (4)	−0.6742 (15)	0.2805 (7)	0.0108 (11)*
H30	−0.6952 (6)	0.3077 (12)	0.2881 (6)	0.0051 (13)*
H31	−0.8600 (8)	0.4083 (11)	0.2437 (10)	0.0051 (13)*
H32	−0.9962 (5)	0.160 (2)	0.1454 (9)	0.0051 (13)*
H33	−0.9670 (7)	−0.190 (2)	0.0915 (6)	0.0051 (13)*
H34	−0.8016 (9)	−0.2922 (11)	0.1365 (9)	0.0051 (13)*
H35	−0.5975 (8)	−0.167 (2)	0.3067 (9)	0.0051 (13)*

H36	−0.5828 (8)	0.0854 (19)	0.2787 (10)	0.0051 (13)*
H37	−0.6217 (8)	−0.008 (3)	0.1093 (9)	0.0051 (13)*
H38	−0.6665 (5)	−0.247 (2)	0.1157 (10)	0.0051 (13)*
H39	−0.4711 (6)	−0.240 (2)	0.2811 (5)	0.0051 (13)*
H40	−0.4898 (7)	−0.590 (2)	0.0398 (5)	0.0051 (13)*
H41	−0.4919 (8)	0.0388 (19)	0.1375 (10)	0.0051 (13)*
H42	−0.3305 (8)	0.1123 (15)	0.2093 (7)	0.0051 (13)*
H43	−0.3355 (15)	−0.098 (3)	0.3847 (13)	0.0051 (13)*
H44	−0.3757 (8)	0.152 (4)	0.3458 (9)	0.0051 (13)*
H45	−0.2069 (15)	0.246 (3)	0.3845 (16)	0.0051 (13)*
H46	−0.1708 (10)	0.003 (4)	0.4402 (13)	0.0051 (13)*
H47	−0.1720 (17)	0.115 (3)	0.5941 (12)	0.0051 (13)*
H48	−0.2789 (10)	0.242 (5)	0.5242 (18)	0.0051 (13)*
H49	−0.1343 (15)	0.469 (3)	0.6436 (15)	0.0051 (13)*
H50	−0.2049 (12)	0.559 (3)	0.522 (2)	0.0051 (13)*
H51	−0.0453 (8)	0.285 (3)	0.547 (2)	0.0051 (13)*
H52	−0.0825 (14)	0.519 (4)	0.4831 (17)	0.0051 (13)*
H53	−0.2152 (18)	0.0917 (16)	0.132 (2)	0.0051 (13)*
H54	−0.3197 (10)	−0.032 (4)	0.0454 (15)	0.0051 (13)*
H55	−0.1475 (15)	−0.042 (3)	0.044 (3)	0.0051 (13)*
H56	−0.2461 (17)	−0.194 (3)	−0.0303 (6)	0.0051 (13)*
H57	−0.1516 (16)	−0.458 (2)	0.0503 (16)	0.0051 (13)*
H58	−0.0693 (6)	−0.301 (5)	0.1466 (13)	0.0051 (13)*
H59	−0.2360 (6)	−0.5317 (17)	0.1390 (13)	0.0051 (13)*
H60	−0.0014 (4)	−0.7129 (16)	0.3487 (9)	0.0051 (13)*

Geometric parameters (Å, °)

C1—C2	1.385 (5)	C15—H44	0.9803 (14)
C1—C6	1.397 (5)	C16—C17	1.635 (5)
C1—C7	1.498 (10)	C16—H45	0.9801 (14)
C2—C3	1.377 (5)	C16—H46	0.9801 (14)
C2—H30	0.9499 (14)	C17—C18	1.460 (5)
C3—C4	1.388 (5)	C17—H47	0.9801 (14)
C3—H31	0.9499 (14)	C17—H48	0.9800 (14)
C4—C5	1.387 (5)	C18—N19	1.529 (5)
C4—H32	0.9499 (14)	C18—H49	0.9803 (14)
C5—C6	1.384 (5)	C18—H50	0.9800 (14)
C5—H33	0.9499 (14)	N19—H51	0.9800 (14)
C6—H34	0.9494 (14)	N19—H52	0.9807 (14)

C7—C8	1.480 (5)	C20—O21	1.263 (5)
C7—H35	0.9797 (14)	C20—N22	1.344 (5)
C7—H36	0.9799 (14)	N22—C23	1.480 (5)
C8—C9	1.528 (5)	N22—C26	1.438 (10)
C8—H37	0.9798 (14)	C23—C24	1.471 (5)
C8—H38	0.9797 (14)	C23—H53	0.9799 (14)
C9—C10	1.518 (5)	C23—H54	0.9801 (14)
C9—N13	1.505 (5)	C24—C25	1.361 (5)
C9—H39	0.9800 (14)	C24—H55	0.9801 (14)
C10—O12	1.251 (5)	C24—H56	0.9802 (14)
C10—O11	1.314 (5)	C25—C26	1.562 (5)
O11—H40	0.9199 (14)	C25—H57	0.9801 (14)
N13—C14	1.475 (5)	C25—H58	0.9801 (14)
N13—H41	0.8499 (14)	C26—N22	1.438 (10)
C14—C15	1.516 (5)	C26—C27	1.535 (5)
C14—C20	1.541 (5)	C26—H59	0.9800 (14)
C14—H41	1.932 (6)	C27—O28	1.233 (5)
C14—H42	0.9800 (14)	C27—O29	1.292 (5)
C15—C16	1.498 (5)	O29—H60	0.9199 (14)
C15—H43	0.9801 (14)		
C2—C1—C6	119.90 (26)	C15—C16—C17	108.5 (5)
C2—C1—C7	116.5 (4)	C15—C16—H45	109.64 (29)
C6—C1—C7	123.6 (4)	C15—C16—H46	109.7 (4)
C1—C2—C3	120.20 (23)	C17—C16—H45	109.7 (5)
C1—C2—H30	119.89 (23)	C17—C16—H46	109.7 (4)
C3—C2—H30	119.91 (22)	H45—C16—H46	109.64 (29)
C2—C3—C4	120.07 (24)	C16—C17—C18	112.3 (7)
C2—C3—H31	119.95 (21)	C16—C17—H47	108.9 (4)
C4—C3—H31	119.97 (24)	C16—C17—H48	108.9 (4)
C3—C4—C5	120.13 (22)	C18—C17—H47	108.89 (22)
C3—C4—H32	119.95 (20)	C18—C17—H48	108.9 (5)
C5—C4—H32	119.92 (20)	H47—C17—H48	108.9 (4)
C4—C5—C6	119.92 (22)	C17—C18—N19	110.8 (6)
C4—C5—H33	120.04 (23)	C17—C18—H49	109.2 (4)
C6—C5—H33	120.04 (22)	C17—C18—H50	109.21 (31)
C1—C6—C5	119.77 (24)	N19—C18—H49	109.21 (32)
C1—C6—H34	120.21 (23)	N19—C18—H50	109.2 (4)
C5—C6—H34	120.01 (21)	H49—C18—H50	109.16 (32)
C1—C7—C8	112.5 (5)	C18—N19—H51	109.5 (9)

C1—C7—H35	108.90 (33)	C18—N19—H52	109.6 (5)
C1—C7—H36	108.84 (32)	H51—N19—H52	109.5 (5)
C8—C7—H35	108.84 (31)	C14—C20—O21	119.2 (4)
C8—C7—H36	108.84 (35)	C14—C20—N22	120.4 (4)
H35—C7—H36	108.91 (22)	O21—C20—N22	120.3 (4)
C7—C8—C9	109.7 (4)	C20—N22—C23	127.5 (4)
C7—C8—H37	109.28 (35)	C20—N22—C26	119.0 (4)
C7—C8—H38	109.84 (35)	C23—N22—C26	108.8 (4)
C9—C8—H37	109.28 (34)	N22—C23—C24	106.7 (4)
C9—C8—H38	109.44 (30)	N22—C23—H53	110.1 (4)
H37—C8—H38	109.33 (22)	N22—C23—H54	110.01 (28)
C8—C9—C10	110.8 (4)	C24—C23—H53	110.0 (5)
C8—C9—N13	103.2 (4)	C24—C23—H54	109.98 (25)
C8—C9—H39	109.42 (26)	H53—C23—H54	110.05 (26)
C10—C9—N13	102.5 (4)	C23—C24—C25	109.0 (7)
C10—C9—H39	119.9 (5)	C23—C24—H55	109.5 (8)
N13—C9—H39	109.53 (24)	C23—C24—H56	109.58 (25)
C9—C10—O12	114.3 (5)	C25—C24—H55	109.55 (31)
C9—C10—O11	118.0 (4)	C25—C24—H56	109.60 (32)
O12—C10—O11	127.7 (5)	H55—C24—H56	109.54 (33)
C10—O11—H40	109.52 (29)	C24—C25—C26	108.3 (5)
C9—N13—C14	118.5 (5)	C24—C25—H57	109.69 (24)
C9—N13—H41	109.4 (5)	C24—C25—H58	109.70 (31)
C14—N13—H41	109.47 (30)	C26—C25—H57	109.7 (5)
N13—C14—C15	113.0 (4)	C26—C25—H58	109.72 (28)
N13—C14—C20	103.1 (5)	H57—C25—H58	109.70 (31)
N13—C14—H42	109.43 (24)	N22—C26—C25	103.2 (5)
C15—C14—C20	113.9 (5)	N22—C26—C27	112.3 (5)
C15—C14—H42	107.8 (7)	N22—C26—H59	109.50 (29)
C20—C14—H42	109.48 (31)	C25—C26—C27	109.3 (4)
C14—C15—C16	111.9 (5)	C25—C26—H59	109.5 (4)
C14—C15—H43	109.0 (6)	C27—C26—H59	112.6 (7)
C14—C15—H44	109.0 (4)	C26—C27—O28	122.8 (4)
C16—C15—H43	108.99 (25)	C26—C27—O29	112.5 (5)
C16—C15—H44	109.0 (4)	O28—C27—O29	124.7 (5)
H43—C15—H44	108.97 (29)	C27—O29—H60	109.49 (24)

Acrinol anhydrous A

Sample

Acrinol anhydrous A

Computing details

Program(s) used to refine structure: *GSAS*.

Crystal data

$C_{18}H_{21}N_3O_4$	$\alpha = 102.4356\ (19)^o$
$M_r = 343.38$	$\beta = 103.177\ (3)^o$
Triclinic, $P\bar{1}$	$\gamma = 98.648\ (3)^o$
$a = 8.0467\ (3)$ Å	$V = 833.92\ (3)$ Å^3
$b = 9.3558\ (2)$ Å	$Z = 2$
$c = 11.9151\ (2)$ Å	synchrotron radiation $\lambda = 1.19712$ Å

Data collection

$2\theta_{min} = 4.01$, $2\theta_{max} = 77.13^o$	Increment in $2\theta = 0.01^o$

Refinement

Least-squares matrix: full	85 parameters
$R_p = 0.043$	151 restraints
$R_{wp} = 0.058$	
$R_{exp} = 0.018$	$(\Delta/\sigma)_{max} = 0.05$
$S = 3.45$	

Profile function: CW Profile function number 2 with 18 terms Profile coefficients for Simpson's rule integration of pseudovoigt function C.J. Howard (1982). J. Appl. Cryst.,15,615-620. P. Thompson, D.E. Cox & J.B. Hastings (1987). J. Appl. Cryst.,20,79-83. #1(GU) = 414.614 #2(GV) = -10.965 #3(GW) = 3.344 #4(LX) = 0.837 #5(LY) = 21.327 #6(trns) = 0.000 #7(asym) = -0.2559 #8(shft) = 0.0697 #9(GP) = 0.000 #10(stec)= 0.00 #11(ptec)= 0.00 #12(sfec)= 0.00 #13(L11) = 0.023 #14(L22) = 0.006 #15(L33) = 0.000 #16(L12) = 0.000 #17(L13) = -0.002 #18(L23) = 0.001 Peak tails are ignored where the intensity is below 0.0010 times the peak Aniso. broadening axis 0.0 0.0 1.0

Fractional atomic coordinates and isotropic or equivalent isotropic displacement parameters (Å^2)

	x	*y*	*z*	U_{iso}*/U_{eq}
C1	−0.1431 (2)	0.6870 (3)	0.3921 (3)	0.0631 (8)*
C2	−0.19855 (15)	0.8104 (2)	0.36116 (9)	0.0631 (8)*
C3	−0.2299 (2)	0.9224 (3)	0.4506 (3)	0.0631 (8)*
C4	−0.2875 (2)	1.0534 (3)	0.4257 (3)	0.0631 (8)*
C5	−0.3151 (2)	1.1586 (3)	0.5211 (3)	0.0631 (8)*
C6	−0.37259 (14)	1.29201 (18)	0.50322 (10)	0.0631 (8)*
C7	−0.39936 (8)	1.39361 (9)	0.59462 (16)	0.0631 (8)*
C8	−0.37053 (18)	1.3697 (3)	0.7124 (2)	0.0631 (8)*
C9	−0.31435 (14)	1.23999 (19)	0.73230 (10)	0.0631 (8)*
C10	−0.2871 (2)	1.1361 (3)	0.6382 (2)	0.0631 (8)*
N11	−0.23264 (14)	1.01154 (19)	0.65976 (10)	0.0631 (8)*
C12	−0.2052 (2)	0.9089 (3)	0.5693 (2)	0.0631 (8)*
C13	−0.14438 (14)	0.78384 (18)	0.59785 (9)	0.0631 (8)*
C14	−0.11289 (8)	0.67500 (10)	0.51204 (16)	0.0631 (8)*
O15	−0.0992 (3)	0.5684 (4)	0.3209 (3)	0.0631 (8)*
C16	−0.09704 (10)	0.56573 (16)	0.19914 (15)	0.095 (4)*
C17	−0.10800 (10)	0.40374 (13)	0.13712 (8)	0.095 (4)*
N18	−0.30924 (7)	1.07189 (8)	0.31582 (10)	0.0631 (8)*
N19	−0.39892 (7)	1.47481 (8)	0.80147 (8)	0.0631 (8)*
O20	−0.4272 (7)	0.7724 (5)	0.8042 (5)	0.0841 (15)*
O21	−0.1787 (5)	0.9482 (7)	0.8695 (6)	0.0841 (15)*
C22	−0.3073 (5)	0.8686 (4)	0.8829 (3)	0.0841 (15)*
C23	−0.3257 (2)	0.88769 (16)	1.01031 (19)	0.0841 (15)*
C24	−0.44971 (13)	0.76035 (12)	1.01984 (7)	0.0841 (15)*
O25	−0.1635 (3)	0.9063 (4)	1.0947 (3)	0.0841 (15)*
H26	−0.21113	0.82201	0.28002	0.0707 (10)*
H27	−0.39179	1.31252	0.42451	0.0707 (10)*
H28	−0.43814	1.48421	0.58061	0.0707 (10)*
H29	−0.29243	1.22266	0.81212	0.0707 (10)*
H30	−0.1268	0.77292	0.67947	0.0707 (10)*
H31	−0.07337	0.5887	0.53501	0.0707 (10)*
H32	0.01195	0.62806	0.19849	0.109 (5)*
H33	−0.19723	0.60091	0.1588	0.109 (5)*
H34	−0.09423	0.39708	0.05665	0.109 (5)*

H35	−0.2218	0.34375	0.13171	0.109 (5)*
H36	−0.01512	0.36544	0.18262	0.109 (5)*
H37	−0.39087	1.11426	0.28709	0.0707 (10)*
H38	−0.27767	1.01166	0.26305	0.0707 (10)*
H39	−0.3817	1.46201	0.87568	0.0707 (10)*
H40	−0.4349	1.55676	0.78581	0.0707 (10)*
H41	−0.22917	0.99032	0.73206	0.0707 (10)*
H42	−0.37174	0.97811	1.03125	0.0959 (18)*
H43	−0.56916	0.76841	0.9829	0.0959 (18)*
H44	−0.42554	0.66649	0.97778	0.0959 (18)*
H45	−0.43427	0.76432	1.10484	0.0959 (18)*
H46	−0.08809	0.96863	1.08194	0.0959 (18)*

Geometric parameters (Å, °)

C1—C2	1.3897 (28)	C13—H30	0.9801 (10)
C1—C14	1.4262 (30)	C14—H31	0.9802 (10)
C1—O15	1.3871 (34)	O15—C16	1.4501 (33)
C2—C3	1.4208 (32)	C16—C17	1.5161 (18)
C2—H26	0.9801 (10)	C16—H32	0.9800 (9)
C3—C4	1.4380 (32)	C16—H33	0.9800 (9)
C3—C12	1.4186 (31)	C17—H34	0.9799 (9)
C4—C5	1.4177 (32)	C17—H35	0.9801 (9)
C4—N18	1.3329 (31)	C17—H36	0.9799 (8)
C5—C6	1.4356 (30)	N18—H37	0.8603 (9)
C5—C10	1.4283 (32)	N18—H38	0.8606 (9)
C6—C7	1.3634 (25)	N19—H39	0.9000 (9)
C6—H27	0.9801 (10)	N19—H40	0.9001 (8)
C7—C8	1.4412 (27)	O20—C22	1.259 (4)
C7—H28	0.9800 (10)	O21—C22	1.243 (4)
C8—C9	1.4044 (26)	C22—C23	1.5337 (32)
C8—N19	1.3689 (29)	C23—C24	1.4765 (22)
C9—C10	1.3984 (31)	C23—O25	1.4155 (28)
C9—H29	0.9801 (10)	C23—H42	0.9801 (9)
C10—N11	1.3591 (30)	C24—H43	0.9831 (8)
N11—C12	1.3636 (31)	C24—H44	0.9830 (9)
N11—H41	0.9201 (10)	C24—H45	0.9836 (9)
C12—C13	1.4115 (30)	O25—H46	0.8400 (10)
C13—C14	1.3761 (24)		

C2—C1—C14	120.72 (22)	C1—C14—C13	120.00 (15)
C2—C1—O15	128.37 (26)	C1—C14—H31	121.49 (17)
C14—C1—O15	110.78 (23)	C13—C14—H31	118.47 (16)
C1—C2—C3	118.77 (18)	C1—O15—C16	121.02 (29)
C1—C2—H26	120.60 (18)	O15—C16—C17	106.06 (15)
C3—C2—H26	120.58 (19)	O15—C16—H32	109.99 (12)
C2—C3—C4	122.10 (24)	O15—C16—H33	110.90 (16)
C2—C3—C12	120.76 (25)	C17—C16—H32	110.07 (12)
C4—C3—C12	117.14 (26)	C17—C16—H33	109.74 (12)
C3—C4—C5	117.74 (26)	H32—C16—H33	110.00 (10)
C3—C4—N18	119.10 (25)	C16—C17—H34	109.42 (10)
C5—C4—N18	123.15 (24)	C16—C17—H35	109.54 (8)
C4—C5—C6	120.99 (25)	C16—C17—H36	109.62 (9)
C4—C5—C10	121.48 (27)	H34—C17—H35	109.41 (9)
C6—C5—C10	117.53 (25)	H34—C17—H36	109.39 (9)
C5—C6—C7	121.27 (15)	H35—C17—H36	109.45 (9)
C5—C6—H27	120.20 (18)	C4—N18—H37	120.04 (16)
C7—C6—H27	118.52 (17)	C4—N18—H38	120.08 (16)
C6—C7—C8	120.66 (14)	H37—N18—H38	114.58 (13)
C6—C7—H28	119.99 (16)	C8—N19—H39	120.03 (13)
C8—C7—H28	119.35 (16)	C8—N19—H40	120.00 (12)
C7—C8—C9	119.20 (18)	H39—N19—H40	119.97 (12)
C7—C8—N19	118.61 (18)	O20—C22—O21	128.1 (4)
C9—C8—N19	122.19 (18)	O20—C22—C23	114.6 (4)
C8—C9—C10	119.91 (17)	O21—C22—C23	117.3 (4)
C8—C9—H29	120.28 (17)	C22—C23—C24	111.84 (21)
C10—C9—H29	119.80 (18)	C22—C23—O25	112.18 (19)
C5—C10—C9	121.43 (25)	C22—C23—H42	107.98 (18)
C5—C10—N11	119.78 (23)	C24—C23—O25	109.18 (14)
C9—C10—N11	118.79 (21)	C24—C23—H42	107.70 (15)
C10—N11—C12	119.72 (17)	O25—C23—H42	107.78 (21)
C10—N11—H41	119.83 (19)	C23—C24—H43	108.82 (10)
C12—N11—H41	119.91 (19)	C23—C24—H44	108.99 (9)
C3—C12—N11	124.14 (25)	C23—C24—H45	108.49 (11)
C3—C12—C13	118.77 (24)	H43—C24—H44	109.78 (9)
N11—C12—C13	117.08 (20)	H43—C24—H45	110.40 (9)
C12—C13—C14	120.94 (14)	H44—C24—H45	110.32 (9)

C12—C13—H30	119.69 (17)	C23—O25—H46	109.43 (21)
C14—C13—H30	119.36 (17)		

Acrinol anhydrous B

Sample

Acrinol anhydrous B

Computing details

Program(s) used to refine structure: *GSAS*.

Crystal data

$C_{18}H_{21.00}N_3O_4$	c = 20.9323 (8) Å
M_r = 343.38	β = 100.936 (3)º
Monoclinic, *C*2/*c*	V = 3408.38 (17) Å^3
a = 14.0496 (5) Å	Z = 8
b = 11.80399 (19) Å	CuKα$_1$ radiation λ = 1.5406 Å

Data collection

$2\theta_{min}$ = 5.02, $2\theta_{max}$ = 69.93º	Increment in 2θ = 0.02º

Refinement

R_p = 0.033	83 parameters
R_{wp} = 0.045	153 restraints
R_{exp} = 0.013	
S = 3.61	$(\Delta/\sigma)_{max}$ = 0.07
Least-squares matrix: full	Profile function: CW Profile function number 3 with 19 terms Pseudovoigt profile coefficients as parameterized in P. Thompson, D.E. Cox & J.B. Hastings (1987). J. Appl. Cryst.,20,79-83. Asymmetry correction of L.W. Finger, D.E. Cox & A. P. Jephcoat (1994). J. Appl. Cryst.,27,892-900. #1(GU) = 479.806 #2(GV) = -2.528 #3(GW) = 2.949 #4(GP) = 0.000 #5(LX) = 3.510 #6(LY) = 14.186 #7(S/L) = 0.0182 #8(H/L) = 0.0204 #9(trns) = 0.00 #10(shft)= 0.0000 #11(stec)= 0.00 #12(ptec)= 0.00 #13(sfec)= 0.00 #14(L11) = 0.000 #15(L22) = 0.000 #16(L33) = 0.000 #17(L12) = 0.000 #18(L13) = 0.000 #19(L23) = 0.000 Peak tails are ignored where the intensity is below 0.0010 times the peak Aniso. broadening axis 0.0 0.0 1.0

Fractional atomic coordinates and isotropic or equivalent isotropic displacement parameters (Å^2)

	x	*y*	*z*	U_{iso}*/U_{eq}	Occ. (<1)
C1	0.3231 (2)	0.42919 (14)	0.97122 (15)	0.0823 (11)*	
C2	0.23238 (16)	0.38026 (6)	0.95508 (5)	0.0823 (11)*	
C3	0.1659 (3)	0.38846 (15)	0.99840 (14)	0.0823 (11)*	
C4	0.0698 (2)	0.33945 (14)	0.98491 (14)	0.0823 (11)*	
C5	0.0081 (2)	0.35227 (15)	1.03163 (15)	0.0823 (11)*	
C6	−0.08785 (14)	0.30764 (5)	1.02350 (5)	0.0823 (11)*	
C7	−0.14342 (8)	0.32234 (8)	1.06953 (8)	0.0823 (11)*	
C8	−0.1071 (2)	0.38359 (11)	1.12817 (12)	0.0823 (11)*	
C9	−0.01442 (15)	0.42799 (5)	1.13754 (5)	0.0823 (11)*	
C10	0.0427 (3)	0.41267 (13)	1.08999 (13)	0.0823 (11)*	
N11	0.13387 (15)	0.45797 (6)	1.10132 (5)	0.0823 (11)*	
C12	0.1943 (2)	0.44678 (14)	1.05729 (13)	0.0823 (11)*	
C13	0.28160 (14)	0.51069 (6)	1.06760 (5)	0.0823 (11)*	
C14	0.34451 (8)	0.50267 (8)	1.02497 (8)	0.0823 (11)*	
O15	0.3878 (3)	0.44017 (18)	0.93021 (16)	0.0823 (11)*	
C16	0.36862 (8)	0.36849 (9)	0.87362 (8)	0.093 (4)*	
C17	0.45252 (8)	0.38391 (7)	0.83868 (5)	0.093 (4)*	
N18	0.04322 (6)	0.28082 (6)	0.93024 (5)	0.0823 (11)*	
N19	−0.16199 (7)	0.39845 (5)	1.17436 (4)	0.1189 (11)*	
O21	0.1619 (3)	0.5826 (5)	0.2030 (4)	0.146 (2)*	
O20	0.16466 (12)	0.7500 (6)	0.1498 (3)	0.146 (2)*	
C22	0.16349 (10)	0.6889 (4)	0.19860 (18)	0.146 (2)*	
C23	0.16422 (7)	0.74709 (19)	0.26395 (10)	0.146 (2)*	
C24	0.14071 (6)	0.86794 (11)	0.25399 (4)	0.146 (2)*	
O25	0.10007 (9)	0.68858 (10)	0.29766 (12)	0.146 (2)*	
H26	0.21236	0.34373	0.91262	0.0938 (14)*	
H27	−0.11236	0.25787	0.98656	0.0938 (14)*	
H28	−0.20578	0.28307	1.06514	0.0938 (14)*	
H29	0.00856	0.4777	1.17477	0.0938 (14)*	
H30	0.30062	0.55449	1.10777	0.0938 (14)*	
H31	0.40763	0.54064	1.03501	0.0938 (14)*	
H32	0.36477	0.28926	0.88689	0.103 (6)*	
H33	0.30811	0.39064	0.84481	0.103 (6)*	

H34	0.45367	0.321	0.80829	0.103 (6)*	
H35	0.51345	0.38528	0.87052	0.103 (6)*	
H36	0.44479	0.45548	0.81453	0.103 (6)*	
H37	−0.01506	0.24656	0.92186	0.0938 (14)*	
H38	0.07974	0.28352	0.89929	0.0938 (14)*	
H39	−0.138	0.43714	1.21092	0.0938 (14)*	
H40	−0.22233	0.36962	1.1684	0.0938 (14)*	
H41	0.15655	0.49328	1.14043	0.199 (6)*	
H42	0.22989	0.74133	0.28989	0.171 (3)*	
H43	0.11794	0.89779	0.29211	0.171 (3)*	
H44	0.19884	0.90934	0.24799	0.171 (3)*	
H45	0.08984	0.87693	0.21522	0.171 (3)*	
H46A	0.12045	0.62231	0.30617	0.171 (3)*	0.5
H46B	0.04321	0.69296	0.27625	0.171 (3)*	0.5

Geometric parameters (Å, °)

C1—C2	1.3813 (30)	O15—C1	1.370 (4)
C1—C14	1.4074 (32)	O15—C16	1.439 (4)
C1—O15	1.370 (4)	C16—C17	1.5116 (19)
C2—C3	1.4226 (33)	C16—H32	0.9799 (9)
C2—H26	0.9800 (10)	C16—H33	0.9800 (9)
C3—C4	1.4477 (33)	C17—H34	0.9800 (9)
C3—C12	1.4022 (33)	C17—H35	0.9801 (9)
C4—C5	1.4324 (34)	C17—H36	0.9799 (9)
C4—N18	1.3287 (32)	N18—H37	0.9002 (9)
C5—C6	1.4269 (32)	N18—H38	0.9000 (9)
C5—C10	1.4183 (33)	N19—H39	0.9000 (9)
C6—C7	1.3615 (25)	N19—H40	0.9000 (9)
C6—H27	0.9800 (10)	O21—C22	1.259 (4)
C7—C8	1.4325 (28)	O20—C22	1.253 (4)
C7—H28	0.9800 (10)	C22—C23	1.5289 (34)
C8—C9	1.3827 (27)	C23—C22	1.5289 (34)
C8—N19	1.3575 (31)	C23—C24	1.4701 (23)
C9—C10	1.4034 (33)	C23—O25	1.4244 (23)
C9—H29	0.9799 (10)	C23—H42	0.9800 (8)
C10—N11	1.3671 (32)	C24—H43	0.9800 (9)
N11—C12	1.3724 (32)	C24—H44	0.9800 (9)
N11—H41	0.9200 (10)	C24—H45	0.9800 (9)

C12—C13	1.4215 (32)	O25—H46A	0.8404 (10)
C13—C14	1.3732 (25)	O25—H46B	0.8402 (10)
C13—H30	0.9801 (10)		
C14—H31	0.9801 (10)		
		C1—C14—H31	120.06 (18)
C2—C1—C14	120.05 (24)	C13—C14—H31	119.79 (17)
C2—C1—O15	125.28 (28)	C1—O15—C16	114.67 (30)
C14—C1—O15	112.08 (24)	O15—C16—C17	106.63 (19)
C1—C2—C3	120.14 (19)	O15—C16—H32	109.86 (12)
C1—C2—H26	119.90 (18)	O15—C16—H33	110.78 (15)
C3—C2—H26	119.85 (19)	C17—C16—H32	110.01 (13)
C2—C3—C4	123.34 (25)	C17—C16—H33	109.58 (13)
C2—C3—C12	118.86 (26)	H32—C16—H33	109.94 (11)
C4—C3—C12	117.80 (27)	C16—C17—H34	109.47 (10)
C3—C4—C5	119.20 (27)	C16—C17—H35	109.48 (9)
C3—C4—N18	118.37 (24)	C16—C17—H36	109.47 (9)
C5—C4—N18	122.40 (24)	H34—C17—H35	109.52 (9)
C4—C5—C6	124.03 (26)	H34—C17—H36	109.40 (10)
C4—C5—C10	119.24 (27)	H35—C17—H36	109.50 (9)
C6—C5—C10	116.73 (25)	C4—N18—H37	119.87 (15)
C5—C6—C7	121.60 (16)	C4—N18—H38	119.75 (14)
C5—C6—H27	119.87 (18)	H37—N18—H38	119.83 (13)
C7—C6—H27	118.16 (17)	C8—N19—H39	119.97 (13)
C6—C7—C8	120.79 (14)	C8—N19—H40	119.99 (13)
C6—C7—H28	119.72 (17)	H39—N19—H40	120.04 (12)
C8—C7—H28	119.07 (17)	O21—C22—O20	129.5 (5)
C7—C8—C9	119.05 (19)	O21—C22—C23	112.3 (5)
C7—C8—N19	121.16 (19)	O20—C22—C23	118.2 (4)
C9—C8—N19	119.79 (18)	C22—C23—C24	110.22 (23)
C8—C9—C10	120.00 (17)	C22—C23—O25	109.15 (21)
C8—C9—H29	119.94 (18)	C22—C23—H42	108.08 (16)
C10—C9—H29	119.65 (18)	C24—C23—O25	113.24 (13)
C5—C10—C9	121.82 (26)	C24—C23—H42	107.97 (16)
C5—C10—N11	120.18 (24)	O25—C23—H42	108.04 (16)
C9—C10—N11	118.00 (21)	C23—C24—H43	109.43 (12)
C10—N11—C12	121.63 (18)	C23—C24—H44	109.37 (10)
C10—N11—H41	119.12 (18)	C23—C24—H45	109.36 (10)

C12—N11—H41	119.15 (19)	H43—C24—H44	109.50 (10)
C3—C12—N11	121.95 (25)	H43—C24—H45	109.62 (9)
C3—C12—C13	119.13 (24)	H44—C24—H45	109.54 (9)
N11—C12—C13	118.22 (21)	C23—O25—H46A	109.51 (19)
C12—C13—C14	120.55 (14)	C23—O25—H46B	109.44 (17)
C12—C13—H30	119.81 (17)	H46A—O25—H46B	114.95 (15)
C14—C13—H30	119.31 (17)		
C1—C14—C13	119.71 (16)		